

RICE UNIVERSITY

**Sedimentological Investigations of Paleo-Ice Sheet Dynamics in  
West Antarctica**

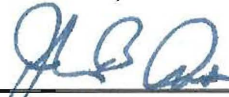
by

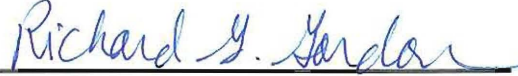
**Alexandra Ellen Kirshner**

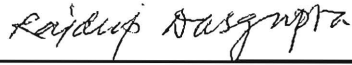
A THESIS SUBMITTED  
IN PARTIAL FULFILLMENT OF THE  
REQUIREMENTS FOR THE DEGREE


**Doctor of Philosophy**

APPROVED, THESIS COMMITTEE

  
\_\_\_\_\_  
John B. Anderson, Chair  
W. Maurice Ewing Professor of  
Oceanography, Earth Sciences

  
\_\_\_\_\_  
Richard G. Gordon  
Keck Professor of Geophysics, Earth  
Science Department Chair

  
\_\_\_\_\_  
Rajdeep Dasgupta  
Assistant Professor, Earth Sciences

  
\_\_\_\_\_  
Christopher Hight  
Associate Professor, Architecture

HOUSTON, TEXAS  
March 2013

## ABSTRACT

### **Sedimentological Investigations of Paleo-Ice Sheet Dynamics in West Antarctica**

by

**Alexandra Ellen Kirshner**

Modern Pine Island and Thwaites Glaciers, which both drain into Pine Island Bay (PIB), are some of the fastest moving portions of the cryosphere and may be the most unstable ice streams in Antarctica. I examined over 133 cores to conduct a detailed sedimentological facies analysis. These data, augmented by new radiocarbon and  $^{210}\text{Pb}$  dates, and bathymetric data, are used to reconstruct the post-LGM deglacial history of PIB and to gain a better understanding of the causes of ice sheet retreat.

My results record a clear retreat stratigraphy in PIB composed of, from top to base; terrigenous sandy silt (plumite), pebbly sandy mud (ice-proximal glacimarine), and till. Initial retreat from the outer continental shelf began shortly after the LGM and before 16.4 k cal yr BP, in response to rising sea level. Bedforms in outer PIB document episodic retreat in the form of back-stepping grounding zone wedges and are associated with proximal glacimarine sediments. A sub-ice shelf facies is observed in central PIB that spans ~12.3–10.6 k cal yr BP. Widespread impingement of warm water onto the continental shelf caused an abrupt change from sub-ice shelf sedimentation to distal glacimarine sedimentation dominated by dispersal of terrigenous silt between 7.8 and 7.0 k cal yr BP. The uppermost sediments in PIB were hydrodynamically sorted by meltwater



plumes. Inner PIB contains several large basins that are linked by channels. The most recent release of sediment coincides with rapid retreat of the grounding line, and has an order of magnitude greater flux relative to the entire unit, indicating episodic sedimentation. This is the first identification of a meltwater-derived deposit in Antarctica and demonstrates that punctuated meltwater-intensive glacial retreat occurred at least three times throughout the Holocene in this region.

Quartz sand grains were used to conduct an analysis of mode of transport for sediments in the Antarctic Peninsula region from the Eocene to present to record the onset of glaciation. Glacial transport imparts a unique suite of microtextures on quartz grains from high shear-stresses. Eocene samples are free of glacial influence. Late Eocene samples show the inception of glacially derived high-stress microtextures, marking the onset of alpine glaciation. Oligocene grains are similar to the late Eocene samples. Middle Miocene microtextures are characteristic of transport from far-field large ice sheets, originating from ice rafting from the West Antarctic Ice Sheet. The Pliocene and Pleistocene samples indicate the existence of the northern Antarctic Peninsula Ice Sheet at this time, consistent with other proxies.

# Acknowledgments

To begin with, I would like to extend my gratitude to John B. Anderson. You have been a wonderful advisor and mentor throughout this entire process. Your excitement about Antarctic science is contagious and has motivated me to be the scientist that I am today. I feel honored to be one of your students and to have worked with such a brilliant scientist. Thank you.

Many colleagues aided in the collection of data and in scientific discussion. In particular, thank you to Julia Wellner for being a second advisor, by including me in your lab group, and for being a positive encouragement of my work.

This dissertation bears only my name, but has greatly benefitted from many scientists whom I am lucky to work with, Thank you all for including me into the Antarctic Earth Science community. Thank you to Brandon Dugan for being my self-imposed graduate student advisor and mentor throughout this work. Additionally, I extend my gratitude to my thesis committee members: Richard Gordon, Rajdeep Dasgupta and Christopher Hight for taking interest in my work.

Thank you to Davin Wallace and Dale Sawyer for helping to develop my teaching skills and trusting that I would be able to successfully teach my first class.

Thank you to everyone who helped collected the data for this thesis. In particular to Rodrigo Fernandez, Becky Minzoni and Travis Stollendorf for braving the cold and wet of Pine Island Bay as well as the captain and crew of the Icebreaker Oden, and the entire onboard scientific party on expedition OSO0910. Thanks to Charlotte Sjunneskog and

Steven Petrushak from the Antarctic Marine Research Facility at Florida State University for the help on site and for sending me boxes and boxes of sediment. Thank you to Carolyn Branecky for your interest in my research and hard work. Your excitement kept me motivated

Funding for this dissertation was provided through the National Science Foundation, Office of Polar Programs, BP, Exxon Mobil, Society of Independent Professional Earth Scientists, The Douglas and Martha Lou Broussard, and the Houston Geological Society.

The Rice University Earth Science Department has been a wonderful community over the past few years. In particular: Jacob Siegel, Lacey Pyle, Emily Chin, Davin Wallace and Hugh Daigle.

This work was not purely an academic effort. The support of my friends and family allowed me to stay motivated throughout this process. Thanks to the Institute for being my Houston home. Thanks to Angela Schafer and Steph Mair for listening to me on the phone and meeting up with me at all corners of the world. My family has always been a source of motivation. They have always been supportive and proud of my accomplishments. Thank you Mom, Dad, Jordan and Brent.

Lastly, I would like to thank my fiancé Eli Witus for his infinite love and support in all facets of my life.

# Contents

<b>Acknowledgments</b> .....	<b>iv</b>
<b>Contents</b> .....	<b>vi</b>
<b>List of Figures</b> .....	<b>ix</b>
<b>List of Tables</b> .....	<b>xi</b>
<b>Introduction</b> .....	<b>xii</b>
<b>Cenozoic Glacial History of the Northern Antarctic Peninsula: A Micromorphological Investigation of Quartz Sand Grains</b> .....	<b>1</b>
2.1 Introduction .....	2
2.2 Geologic Setting.....	4
2.3 Methods.....	5
2.4 Results .....	8
2.4.1 Eocene.....	8
2.4.1.1 Eocene La Meseta Formation, Seymour Island. ....	8
2.4.1.2 Late Eocene Offshore James Ross Basin.....	10
2.4.2 Late Oligocene and Middle Miocene .....	12
2.4.2.1 Late Oligocene Joinville Plateau.....	12
2.4.2.2 Middle Miocene.....	14
2.4.3 Pliocene.....	15
2.4.3.1 Early Pliocene.....	15
2.4.3.2 Late early Pliocene.....	17
2.4.4 Pleistocene .....	17
2.4.4.1 Offshore Joinville Plateau.....	17
2.4.4.2 Late Pleistocene till.....	18
2.5 Discussion .....	18
2.6 Conclusion.....	23
<b>Post-LGM deglaciation in Pine Island Bay, West Antarctica</b> .....	<b>25</b>
3.1 Introduction .....	26
3.2 Regional setting and existing data.....	30
3.3 Materials and methods .....	35
3.4 Results .....	39
3.4.1 Stratigraphic succession and facies distribution .....	39

3.4.1.1	Unit 1.....	40
3.4.1.1.1	Subunit 1-A.....	43
3.4.1.1.2	Subunit 1-B.....	44
3.4.1.1.3	Subunit 1-C.....	45
3.4.1.2	Unit 2.....	45
3.4.1.2.1	Subunit 2-A.....	46
3.4.1.2.2	Subunit 2-B.....	47
3.4.1.2.3	Subunit 2-C.....	47
3.4.1.2.4	Subunit 2-D.....	47
3.4.1.3	Unit 3.....	48
3.4.1.4	Unit 4.....	48
3.4.1.5	Unit 5.....	49
3.4.2	Radiocarbon analysis.....	49
3.5	Discussion.....	53
3.5.1	Depositional environment/sedimentary facies model.....	53
3.5.2	Deglacial history.....	57
3.5.3	Mechanisms of glacial retreat.....	62
3.6	Conclusions.....	66
<b>Meltwater Intensive Glacial Retreat in Polar Environments and Investigation of Associated Sediments: example from Pine Island Bay, West Antarctica.....</b>		<b>68</b>
4.1	Introduction.....	69
4.1.1	Geologic Setting.....	73
4.1.1.1	Geomorphology.....	74
4.1.1.2	Regional Oceanography.....	74
4.1.1.3	Sedimentology.....	77
4.1.1.4	Marine Record of Deglaciation.....	78
4.2	Materials and Methods.....	79
4.2.1	Sediment Characterization.....	79
4.2.2	Multibeam Swath Bathymetry Mapping and Analysis.....	83
4.2.3	Hydraulic Analysis.....	85
4.2.4	Dating Methods.....	85
4.2.5	Sediment Flux Calculation.....	86
4.3	Results.....	87
4.3.1	Sedimentology of Unit 1.....	87
4.3.1.1	Core Lithology and Physical Characteristics.....	89

4.3.1.2	Detailed Quantitative Grain Size Distributions .....	92
4.3.1.3	Grain Attributes.....	96
4.3.1.3.1	Grain Shape.....	96
4.3.1.3.2	Micromorphology .....	98
4.3.1.4	Bulk Composition .....	101
4.3.2	Thickness of Unit 1.....	104
4.3.3	Bathymetric Data Analysis .....	105
4.3.3.1	Subglacial Water Storage and Capacity .....	106
4.3.3.2	Organization of Channel Systems.....	108
4.3.4	Age Constraints and Rate of deposition of Unit 1 .....	110
4.3.5	Sediment Flux in Pine Island Bay .....	113
4.4	Discussion .....	116
4.4.1	Sediment and Facies Analysis .....	116
4.4.1.1	Sedimentology, Deposition, and Transport.....	116
4.4.1.2	Grain Characteristics as an Indication of Transport.....	117
4.4.1.3	Sediment Composition and Source Region .....	118
4.4.2	Bathymetry .....	119
4.4.3	Style of Deposition .....	119
4.4.4	Transport Mechanism .....	121
4.4.5	Sediment Delivery .....	122
4.4.6	Pine Island Bay compared to other glacial systems.....	123
4.5	Conclusions .....	124
	<b>Conclusions.....</b>	<b>127</b>
	<b>References.....</b>	<b>129</b>
	<b>Appendix A.....</b>	<b>153</b>
	<b>Appendix B.....</b>	<b>159</b>

# List of Figures

<b>Figure 2-1 Geographic map of northern Antarctic Peninsula.....</b>	<b>4</b>
<b>Figure 2-2 Examples of microtextures examined in this study.....</b>	<b>7</b>
<b>Figure 2-3 Representative samples from the Eocene La Meseta Formation.....</b>	<b>9</b>
<b>Figure 2-4 Occurrence of microtextures by age of samples.....</b>	<b>11</b>
<b>Figure 2-5 Representative samples from the late Eocene, late Oligocene, and the middle Miocene. ....</b>	<b>13</b>
<b>Figure 2-6 Samples from Pleistocene till, Joinville Plateau, and Pliocene.....</b>	<b>16</b>
<b>Figure 2-7 Overall stratigraphy, grain surface textures, and glacial history of the James Ross Basin. ....</b>	<b>21</b>
<b>Figure 3-1 Study area map of the Amundsen Sea Embayment.....</b>	<b>29</b>
<b>Figure 3-2 Bathymetry of outer PIB acquired aboard I/B Oden. ....</b>	<b>31</b>
<b>Figure 3-3 Example core for each geomorphic region .....</b>	<b>40</b>
<b>Figure 3-4 Representative grain size curves for each subunit. ....</b>	<b>42</b>
<b>Figure 3-5 Plot of mean grain size and degree of sorting for all samples analyzed..</b>	<b>44</b>
<b>Figure 3-6 Stratigraphic cross section of depositional facies in Pine Island Bay constructed along axis of trough.....</b>	<b>53</b>
<b>Figure 3-7 Reconstructed cross section from continental shelf edge to the modern grounding location through the Pine Island Trough at significant intervals of the Pine Island Glacier retreat history.....</b>	<b>56</b>
<b>Figure 3-8 LGM to Present Ice Sheet reconstruction for the Amundsen Sea Embayment.....</b>	<b>58</b>
<b>Figure 4-1 Bathymetry map of the Amundsen Sea with inset maps showing locations of Pine Island Bay .....</b>	<b>72</b>
<b>Figure 4-2 Idealized retreat stratigraphy in Pine Island Bay using representative cores along north-south transect .....</b>	<b>77</b>

<b>Figure 4-3 Ice stream profiles from Kamb Ice Stream (formerly Ice Stream C) and Thwaites Glacier .....</b>	<b>84</b>
<b>Figure 4-4 Stratigraphy of Unit 1 in focus cores.....</b>	<b>89</b>
<b>Figure 4-5 Grain size frequency curves for samples of Unit 1.....</b>	<b>92</b>
<b>Figure 4-6 Photograph of core NBP99-02 TC/PC 46 . Average grain size data of the logarithmic grain diameter vs core depth.....</b>	<b>95</b>
<b>Figure 4-7 Relative frequency of microtextures observed on quartz grains .....</b>	<b>100</b>
<b>Figure 4-8 A. Thickness of Unit 1 in centimeters versus core latitude.....</b>	<b>104</b>
<b>Figure 4-9 Meltwater depressions and channels in inner PIB.....</b>	<b>106</b>
<b>Figure 4-10 Hydraulic analysis of Pine Island Glacier.....</b>	<b>109</b>



# List of Tables

<b>Table 3-1 Radiocarbon constraints on West Antarctic Ice Sheet retreat following the Last Glacial Maximum .....</b>	<b>33</b>
<b>Table 3-2 Attribute table of physical properties for cores collected in Pine Island Bay.....</b>	<b>39</b>
<b>Table 3-3 Information for sediment core sites for eastern Amundsen Sea Embayment.....</b>	<b>52</b>
<b>Table 4-1 Average roughness and elongation values yielded by Fourier analysis of grain shapes for Pine Island Bay sediments. ....</b>	<b>98</b>
<b>Table 4-2 X-ray diffraction data for select cores within Pine Island Bay.....</b>	<b>103</b>
<b>Table 4-3 Total volume of water stored in cavities on the inner shelf .....</b>	<b>107</b>
<b>Table 4-4 Table of excess <sup>210</sup>Pb measured on sediment cores from within Pine Island Bay.....</b>	<b>115</b>

# Introduction

Remote sensing measurements have identified that the West Antarctic and Antarctic Peninsula Ice Sheets are currently in a state of retreat. However, the long-term glacial history of the Antarctic Ice Sheets is fragmentary. An accurate understanding of how the Antarctic Ice Sheets behaved in the past will lead to increased predictability of ice sheet behavior. This includes understanding the role and interaction of different deglacial mechanisms including: buoying by eustatic sea-level rise, under-pinning by subglacial meltwater, thermal erosion by impinging oceanic waters, thermal isolation by opening of oceanic gateways, and warming climate. Hypothetically, all of these mechanisms leave a geological record.

This dissertation focuses on two separate geographic areas and very different time frames, including 1) Eocene to Pleistocene sediments from Seymour Island and the adjacent continental shelf, Antarctic Peninsula and 2) Last Glacial Maximum to present sediments in Pine Island Bay, West Antarctica. The history of glacial onset and retreat in

both areas are important in continent-wide paleoclimate and ice sheet reconstructions and as input for numerical models for testing ice sheet response to various external forcings. Despite difference in location and age of sediments, similar sedimentologic and geomorphic data were collected and interpreted in both regions.

The second chapter in this dissertation documents the climate demise in the Antarctic Peninsula region and the growth of the Antarctic Peninsula Ice Sheet. This study is a part of a larger collaboration that resulted in an AGU volume on the "Tectonic, Climatic, and Cryospheric Evolution of the Antarctic Peninsula". The larger work is a multi-proxy investigation of sediments and geophysical data that range in age from Eocene to Pleistocene and provide a record of the onset of glaciation regionally. My contribution to this collaborative work was to examine surface textures on quartz grains to identify transport mechanism. Glacial transport, owing to its high shear-stress regime, imparts a unique suite of microtextures on quartz grains. This analysis provided a basis for differentiating non-glacial, alpine glacial and ice sheet conditions.

Prior to this dissertation, understanding of ice sheet retreat within Pine Island Bay following the Last Glacial Maximum was based on seven radiocarbon dates and only fragmentary seafloor geomorphic evidence. The third chapter in this dissertation includes detailed sedimentological facies analysis of sediment 133 cores, the addition of 23 new radiocarbon dates, and new bathymetric data from Pine Island Bay. These combined data were used to reconstruct the post-LGM deglacial history of Pine Island Bay, which is published in *Quaternary Science Reviews*. The mechanisms controlling ice sheet retreat varied throughout post-LGM, and include: buoying by eustatic sea-level rise, thermal erosion from warm waters and under-penning by subglacial meltwater.

The fourth chapter in this dissertation expands on findings from chapter three and is a more detailed examination of the most recent sediments in Pine Island Bay. This research characterizes the uppermost sediments as a plumite deposit. This is the first detailed study of a meltwater-derived facies in Antarctica, and has yielded the first evidence that subglacial meltwater was an important contributor to ice sheet instability in the past. There is also strong evidence that the current rapid retreat of Pine Island Glacier is a meltwater intensive event.

# **Cenozoic Glacial History of the Northern Antarctic Peninsula: A Micromorphological Investigation of Quartz Sand Grains<sup>1</sup>**

Glacial transport, owing to its high shear-stress regime, imparts a unique suite of microtextures on quartz grains. Here we examine surface textures of quartz sand grains from expedition SHALDRIL I and II and from an outcrop on Seymour Island, Antarctic Peninsula. The samples range in age from Eocene to Pleistocene and provide a record of

---

<sup>1</sup> This chapter has been edited, reformatted and reprinted from Tectonic, Climatic, and Cryospheric Evolution of the Antarctic Peninsula/ John B. Anderson and Julia S. Wellner , editors, special publication; 63 Kirshner, A. E. and Anderson, J.B., Cenozoic Glacial History of the Northern Antarctic Peninsula: A Micromorphologic Investigation of Quartz Sand Grains, Doi: 10.1029/SP063, ISBN: 978-0-87590-734-5, Copyright 2011. Reproduced with permission of American Geophysical Union

the onset of glaciation regionally. The Eocene La Meseta Formation, Seymour Island, is void of any high-stress microtextures, supporting earlier interpretations that this unit is free of glacial influence. The inception of glacially derived high-stress microtextures and a very low occurrence of subparallel linear fractures on quartz grains begins in the late Eocene, marking the onset of alpine glaciation. Oligocene grains exhibit a continued presence of glacially derived microtextures, with a similar style to the late Eocene sediments. The morphological character changes in the middle Miocene. The middle Miocene microtextures are characteristic of transport from large ice sheets, displaying an increase in high-stress microtextures such as grooves, deep troughs, and crescentic gouges, an elevated degree of physical weathering, and an increased abundance of subparallel linear fractures. This is due to larger transit distances by ice rafting from the West Antarctic Ice Sheet. The Pliocene and Pleistocene samples contain abundant glacial microtextures, consistent with other evidence for the existence of the northern Antarctic Peninsula Ice Sheet at this time.

## **2.1 Introduction**

It has long been established that quartz grains are recorders of environmental history (Krinsley and Doornkamp, 1973; Bull, 1981; Marshall, 1987; Mahaney, 2002), as their robust nature allows for the signature of transportation to be imprinted onto their surface. This has led to an extensive body of literature based on analysis of such features using scanning electron microscopy (SEM). Recognition of past episodes of glacial erosion and transport is possible by identifying a suite of microtextures that are unique to

sustained high-stress conditions (Krinsley and Margolis, 1969; Mahaney and Kalm, 1995, 2000; Mahaney, 2002; Sweet and Soreghan, 2010).

The scientific aim of SHALDRIL was to investigate the long-term climate record of the Antarctic Peninsula region (Anderson et al., 2011). A number of sites were drilled which span the late Eocene to Pleistocene. In this chapter, we report results from an investigation of the micromorphology of quartz grains from the SHALDRIL site sediments in conjunction with Eocene sediments from neighboring Seymour Island in order to document major stages in Cenozoic glacial history of the northern Antarctic Peninsula region.

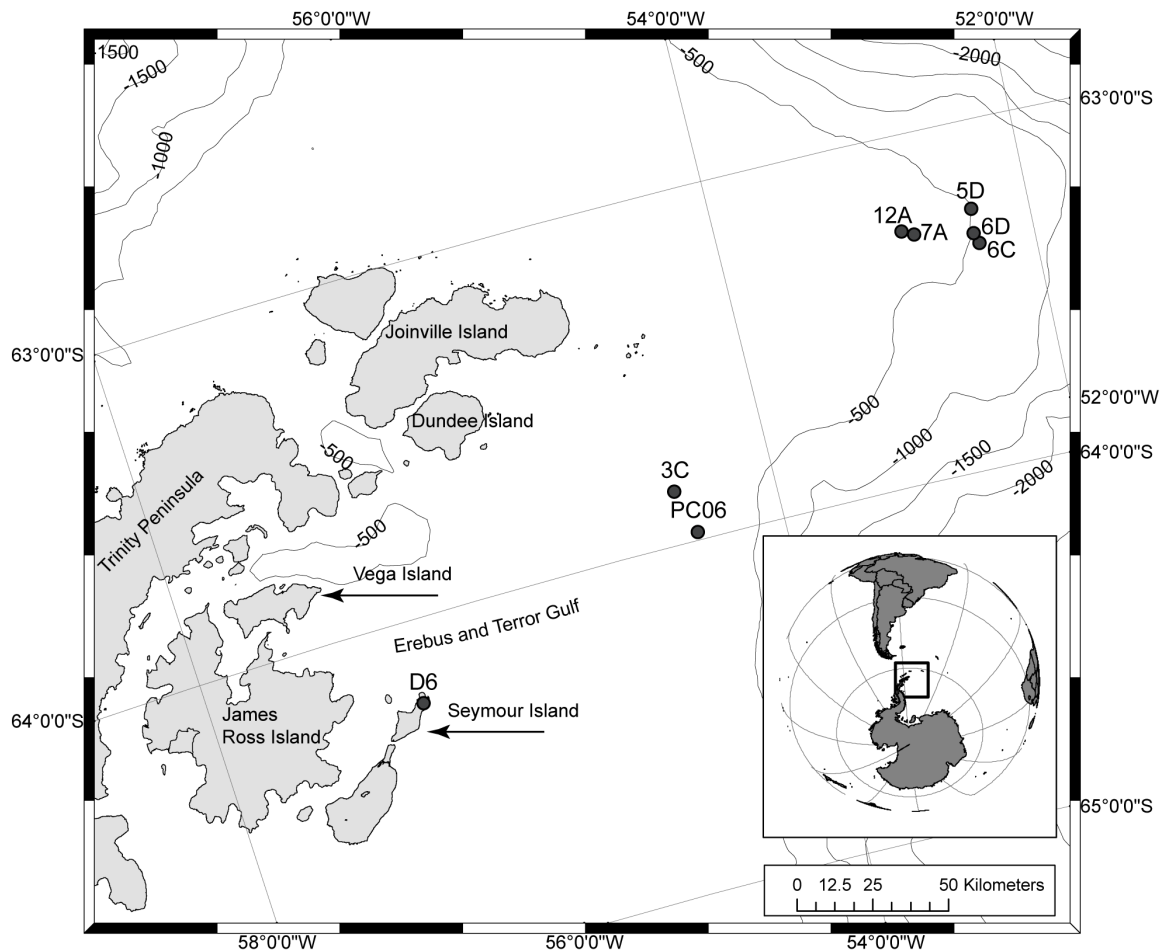


**Figure 2-1 Geographic map of northern Antarctic Peninsula with locations of core sites. Bathymetric contours based on ETOPO2 (Smith and Sandwell, 1997) (see [http://topex.ucsd.edu/marine\\_topo/mar\\_topo.html](http://topex.ucsd.edu/marine_topo/mar_topo.html)). Circles mark core sites (PC06, 3C, 12A, 7A, 5D, 6D, and 6C) and outcrop area (D6).**

## 2.2 Geologic Setting

This study area is located between 63°S to 65°S and 58°W to 52°W and includes Seymour Island, the northern James Ross Basin, and the southern flank of the Joinville Plateau, south of Joinville Island (Figure 2-1). Samples from Seymour Island were taken



from the Eocene La Meseta Formation, in particular, the youngest Submeseta unit. This sandy unit has been interpreted as preglacial, based on an absence of dropstones or other evidence for glaciation (Marensi et al., 2002). The northern James Ross Basin sites include Pleistocene till that occurs just below the seafloor, in a region of spectacular glacial geomorphic features (Heroy and Anderson, 2005), and an uppermost Eocene muddy sand unit sampled at SHALDRIL Site 3C (Figure 1-1). The Joinville Plateau sites (12A, 7A, 5D, 6D, and 6C) sampled a thick sedimentary wedge along the southern flank of the plateau and recovered sediments that range in age from late Oligocene to Pleistocene. These sites occur in an area that is influenced by contour currents from the Weddell Gyre (Maldonado et al., 2005; Wellner et al., 2011).

### **2.3 Methods**

A total of 10 sand grains per sample from 19 stratigraphic intervals were examined in detail for surface morphological characterization (Stickley et al., 2009). This includes 40 grains from the Holocene/Pleistocene, 20 grains from the Pleistocene, 20 grains from the early Pliocene, 20 grains from the middle Miocene, 20 grains from the late Oligocene, 30 grains from the late Eocene, and 30 grains from the Eocene. Rock samples from Seymour Island were provided by the United States Polar Rock Repository (D6-03, D6-05, D6-07). These samples were collected in 1986 and were noted to have been collected from pristine outcrops of unconsolidated sand. All other samples were acquired from drill core and piston cores.

Throughout the sample preparation, care was taken to preserve sample morphology and avoid generating any surface features, following the procedures of

Mahaney et al. (1988). Samples were prepared by first immersing approximately 0.5 g of bulk sediment into a mixture of sodium hexametaphosphate and reverse osmosis water for 24 h in order to deflocculate clays. Following disaggregation, the samples were gently wet-sieved through a 63  $\mu\text{m}$  sieve. The sand-sized particles were then split, and quartz grains were selected using a dissecting microscope. The separated quartz grains were mounted onto SEM sample mounts with carbon tape. The mounted specimens were then sputtered-coated with approximately 20 nm of a conductive material (gold or carbon) and examined using a FEI Quanta 400 high-resolution field emission scanning electron microscope in high-vacuum mode. The composition of each grain was verified as pure  $\text{SiO}_2$  with energy-dispersive X-ray spectroscopy.

Textural features were identified based on the criteria and examples from Mahaney (2002). Microtextures were recorded as not-present (barren), low abundance (faint or scarce occurrence), medium abundance (present), and high abundance (exceptional occurrence). Fifteen different features were assessed in groups based on the process of microtexture formation (Sweet and Soreghan, 2010). The groups include polygenetic features comprised of fracture faces, subparallel linear fractures, conchoidal fractures, arc-shaped steps, linear steps, sharp angular features; sustained high-stress features consisting of crescentic gouges, straight grooves, curved grooves, deep troughs, and mechanically upturned plates; percussion features of v-shaped percussion cracks and edge rounding; chemical dissolution/diagenesis features such as dissolution etching; and diagenetic physical weathering resulting in a weathered surface. Examples of some of the most diagnostic features are illustrated in Figure 2-2.

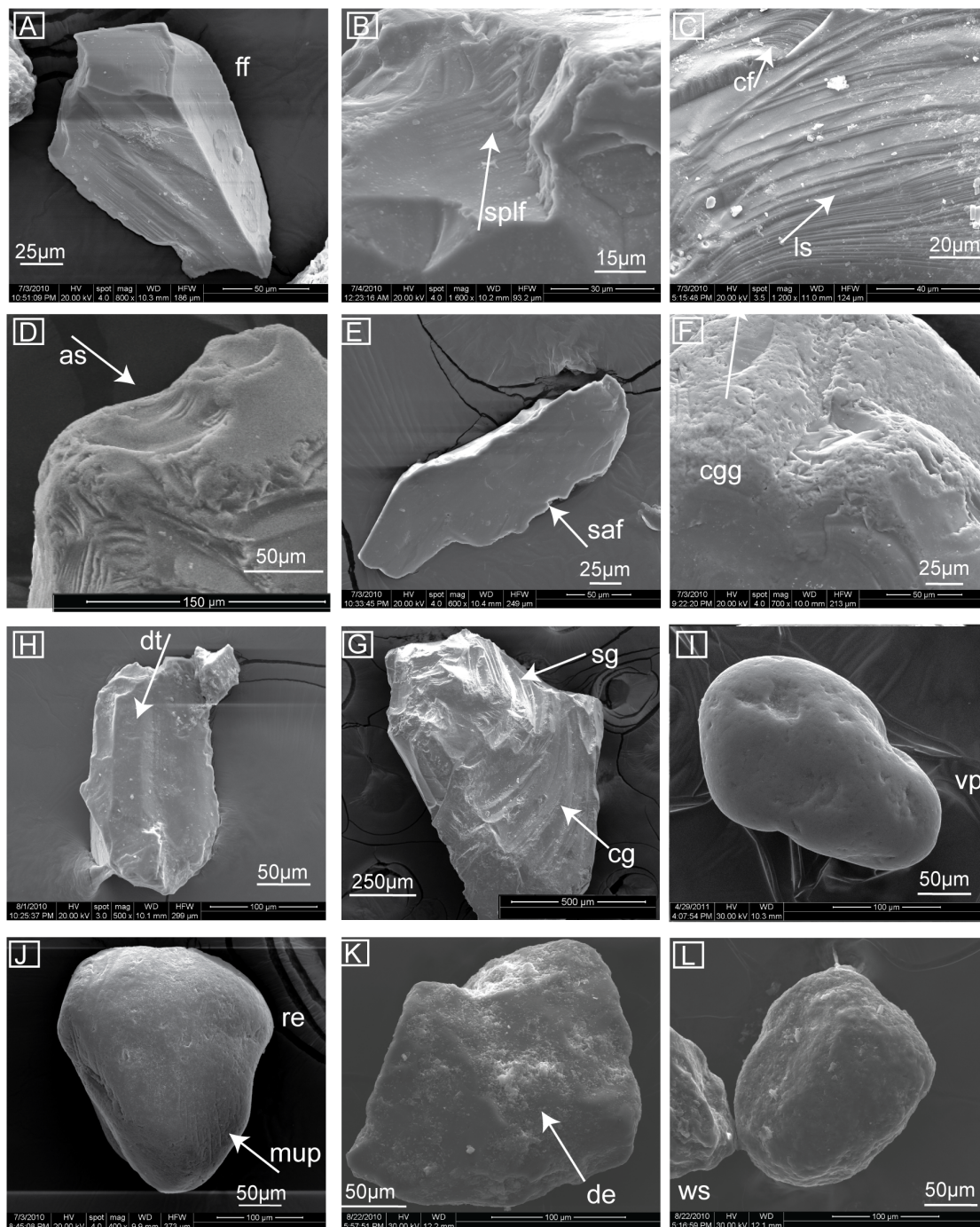


**Figure 2-2 Examples of microtextures examined in this study including (a) fracture faces (ff ), (b) subparallel linear fractures (splf ), (c) (top left) conchoidal fractures (cf ) and (right) linear steps (ls), (d) arc steps (as), (e) sharp angular features (saf ), (f) crescentic gouges (cgg), (g) (top) straight grooves (sg) and**

**(bottom) curved grooves (cg), (h) deep trough (dt), (i) v-shaped percussion pits (vp), (j) mechanically upturned plates (mp) and rounded edges (re), (k) dissolution etching (de), and (l) weathered surface (ws).**

## **2.4 Results**

### **2.4.1 Eocene**

#### **2.4.1.1 Eocene La Meseta Formation, Seymour Island.**

The Eocene La Meseta Formation sites (D6-3m, D6-5m, and D6-7m, Figure 2-3) are characterized by a general low abundance of microtextures. The most prevalent features are those associated with weathering and diagenesis, including weathered surfaces, dissolution etching, and edge rounding, which all occur in medium abundances. Over two thirds of the grains are rounded. Sustained high-impact features are present in low (crescentic gouges) to zero abundance (straight and curved grooves, deep troughs, and mechanically upturned plates) (Figure 2-4).

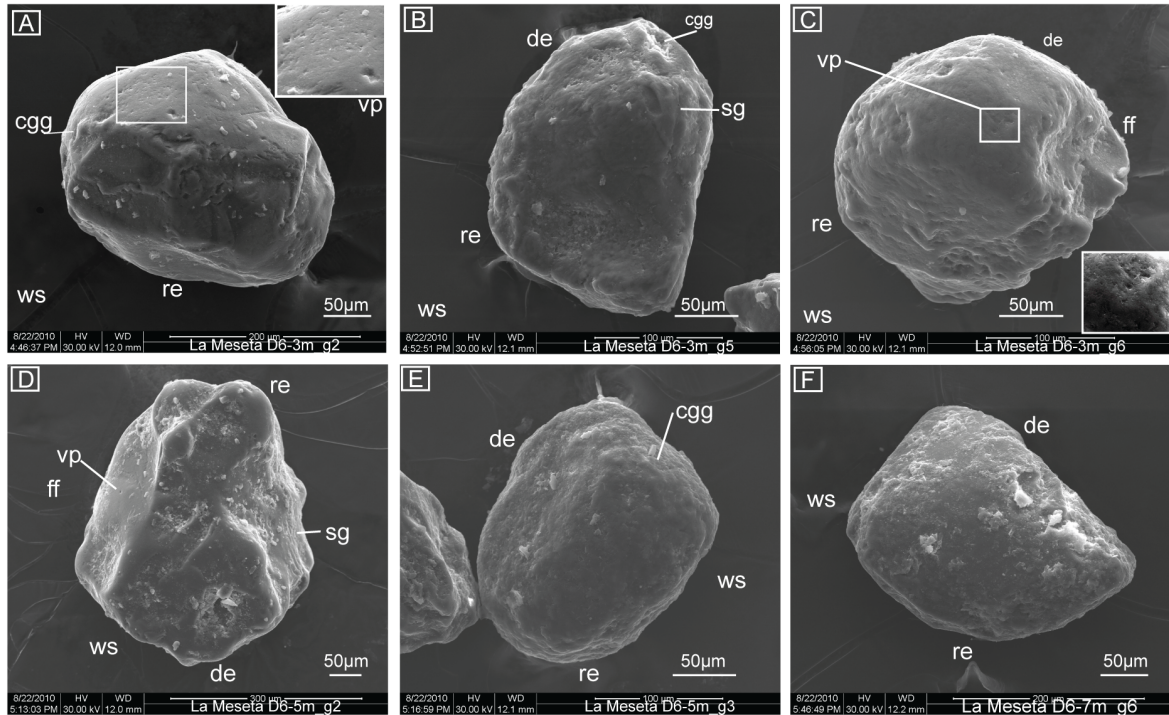


**Figure 2-3 Representative samples from the Eocene La Meseta Formation.**

(a) Sample D6-3m, a weathered grain that is very rounded with rounded edges (re), weathered surface (ws), weathered crescentic gouges (cgg), and v-shaped impact pits (vp). (b) D6-3m grain with crescentic gouges (cgg), straight grooves (sg), dissolution etching (de), rounded edges (re), and weathered surface (ws). (c) V-shaped impact pits (vp) and fracture faces (ff) on grain D6-3m, along with weathering features, including dissolution etching (de), rounded edges (re), and weathered surface (ws). (d) Sample D6-5m is highly weathered with v-shaped impact pits (vp), fracture faces (ff), straight grooves (sg), dissolution etching (de), rounded edges (re), and weathered surface (ws). (e) This highly weathered grain from sample D6-5m displays many weathering features including dissolution etching (de), rounded edges (re), weathered surface (ws), and weathering features superimposed on crescentic gouges (cgg, arrow). (f) Sample D6-7m is a highly weathered grain characterized by dissolution etching (de), rounded edges (re), and weathered surface (ws).

#### **2.4.1.2 Late Eocene Offshore James Ross Basin.**

Late Eocene sand grains from SHALDRIL Site 3C (3C-3\_8-9cm, 3C-3\_114-115cm, and 3C-7\_47-48cm, Figure 2-5) are fresh, with over half angular grains and a large majority of the grains displaying angular edge features. The most common microtexture is fracture faces, which occurs at medium frequency. The subsequent most abundant features include a medium to low abundance of linear steps and sharp angular features. The samples contain low abundances of the sustained high-impact features, including, in order of abundance, straight grooves, crescentic gouges, deep troughs, and curved grooves. There is a low occurrence of subparallel linear fractures (Figure 2-4).

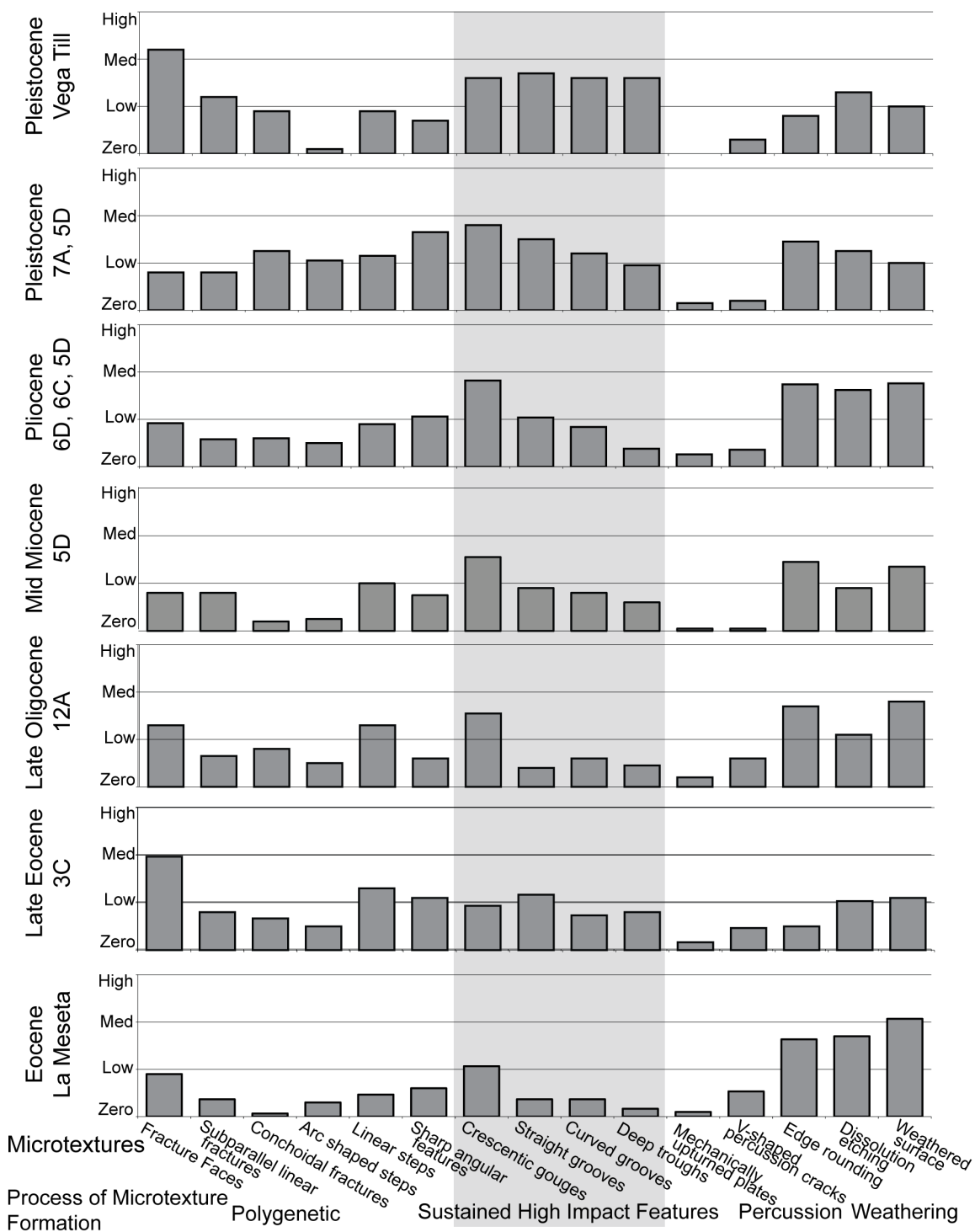


**Figure 2-4 Occurrence of microtextures by age of samples.**

**The x axis is 15 identifiable microtextures, and the y axis is relative abundance of features based on classification of Mahaney (2002). Feature classification is zero, low, medium, and high abundances. Processes of microtexture formation are from**

**the work of Sweet and Soreghan (2010). Gray area highlights sustained high-impact features formed during glacial transport. Graphs are representative of entire intervals of time and are averaged within units.**

## **2.4.2 Late Oligocene and Middle Miocene**

### **2.4.2.1 Late Oligocene Joinville Plateau.**

Late Oligocene samples from Site 12A-2 (12A-2\_67-68cm and 12A-2\_225-226cm, Figure 2-5) contain semiangular grains with rounded edges. Edge rounding is the most common feature, occurring in medium abundance in over half of the grains. Microtextures appear to have a later phase of physical weathering, based on dulling and rounding of features and edges. There are low/medium abundances of crescentic gouges and curved grooves, both with rounded feature edges (Figure 2-4).



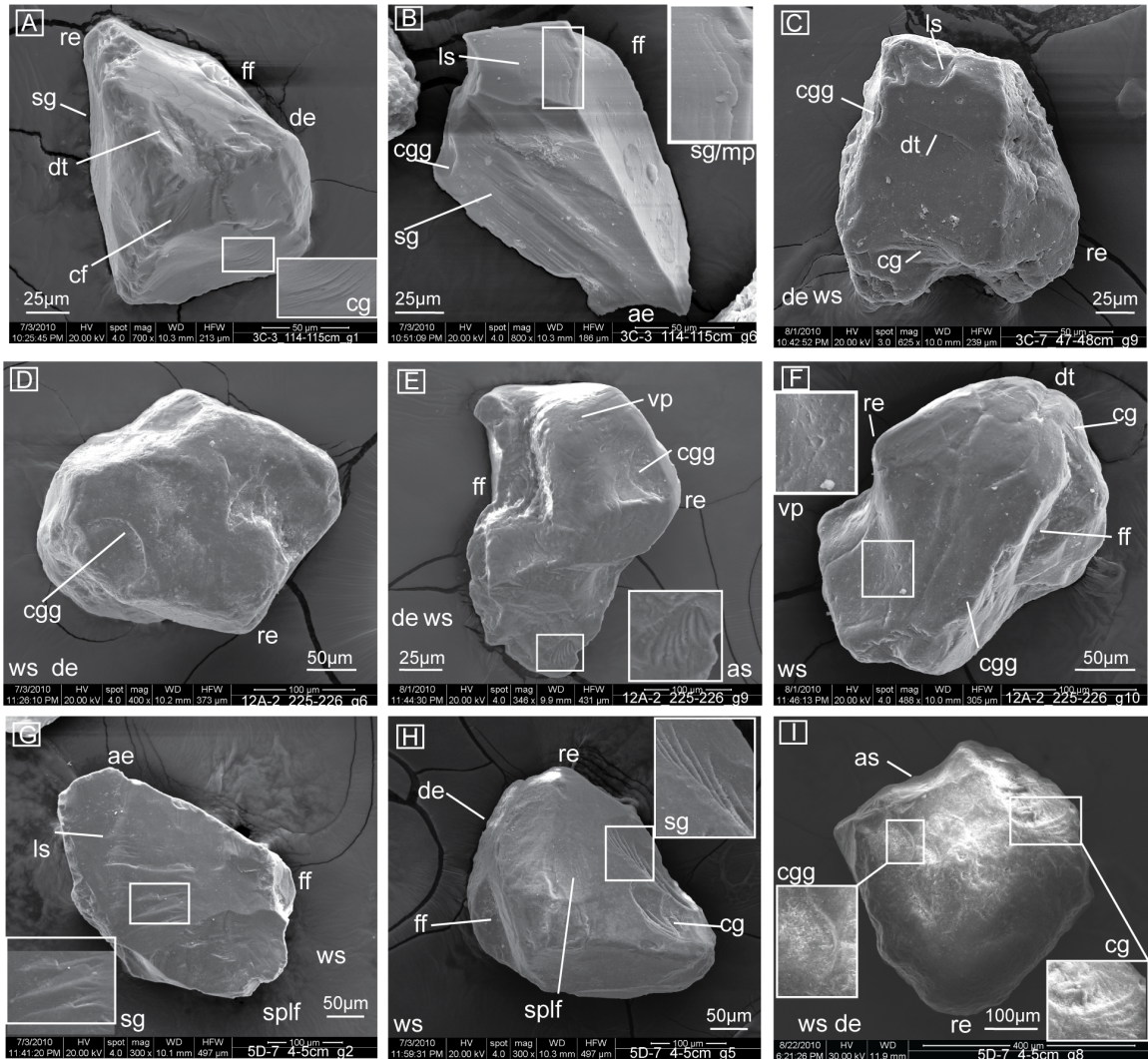


**Figure 2-5 Representative samples from the late Eocene, late Oligocene, and the middle Miocene.**

Representative samples from the (top) late Eocene, (middle) late Oligocene, and (bottom) the middle Miocene. (a) Late Eocene sample 3C-3\_114-115cm contains straight and curved grooves (sg and cg), deep troughs (dt), fracture faces (ff), and conchoidal fractures (cf). The grain is slightly weathered, showing rounded edges (re) and dissolution etching (de). (b) Extremely fresh and angular late Eocene grain from sample 3C-3\_114-115cm with angular edges (ae), fracture faces (ff), linear steps (ls), crescentic gouges (cgg), straight grooves (sg), and mechanically upturned plates (mp). (c) Grain from late Eocene sample 3C-7\_47-48cm displays rounded edges (re), weathered surface (ws), dissolution etching (de), deep troughs (dt), crescentic gouges (cgg), curved grooves (cg), and linear steps (ls). (d) Grain from

late Oligocene sample 12A-2\_225-226cm illustrating crescentic gouges (cgg) that are overprinted by weathering features such as weathered surface (ws), rounded edges (re), and dissolution etching (de). (e) Late Oligocene 12A-2\_225-226cm grain showing fracture faces (ff), v-impact pits (vp), arc steps (as), crescentic gouges (cgg), rounded edges (re), dissolution etching (de), and a weathered surface (ws). (f) Late Oligocene sample 12A-2\_225-226cm grain illustrating crescentic gouges (cgg), curved grooves (cg), deep troughs (dt), and overprinting by weathering features including rounded edges (re). Grains from this site also contain v-impact pits (vp) and fracture faces (ff). (g) Grain from mid-Miocene sample 5D-7\_4-5cm with straight grooves (sg), linear steps (ls), fracture faces (ff), subparallel linear fractures (splf), angular edges (ae), and weathered surface (ws). (h) Grain from mid-Miocene sample 5D-7\_4-5cm has straight and curved grooves (sg and cg), subparallel linear fractures (splf), fracture faces (ff), rounded edges (re), dissolution etching (de), and a weathered surface (ws). (i) Grain from mid-Miocene sample 5D-7\_4-5cm illustrating weathered surfaces (ws), faint dissolution etching (de), and rounded edges (re), which overprint earlier stage crescentic gouges (cgg), curved grooves (cg), and arc shaped steps (as)

#### 2.4.2.2 Middle Miocene.

Middle Miocene samples from Site 5D (5D-6\_1-2cm, 5D-7\_4-5cm, and 5D-10\_44-45cm, Figure 2-5) are angular to subangular with rounded edges. The most abundant features, in medium abundances, are crescentic gouges, weathered surfaces, and edge rounding. The majority of grains display features of dissolution etching. Other attributes include fracture faces, subparallel linear fractures, linear steps, sharp angular features, straight and curved grooves, and deep troughs. Most of the impact features have subsequently been rounded, resulting in rounded edges and low relief.

### **2.4.3 Pliocene**

#### **2.4.3.1 Early Pliocene.**

The early Pliocene samples from SHALDRIL sites 6C and 5D (6C- 6\_46-47cm, 5D-2\_26-27cm, and 5D-4\_27-28cm, Figure 2-6) consist of a wide range of grain shapes, averaging slightly more than half rounded grains and slightly less than half angular grains. Rounded edges are common and appear in a majority of the grains. Most grains show evidence of silica precipitation, edge rounding, dissolution etching, and weathered surfaces. Crescentic gouges are the most common feature, occurring in medium abundance. There are low abundances of fracture faces, linear steps, sharp angular features, and straight grooves.

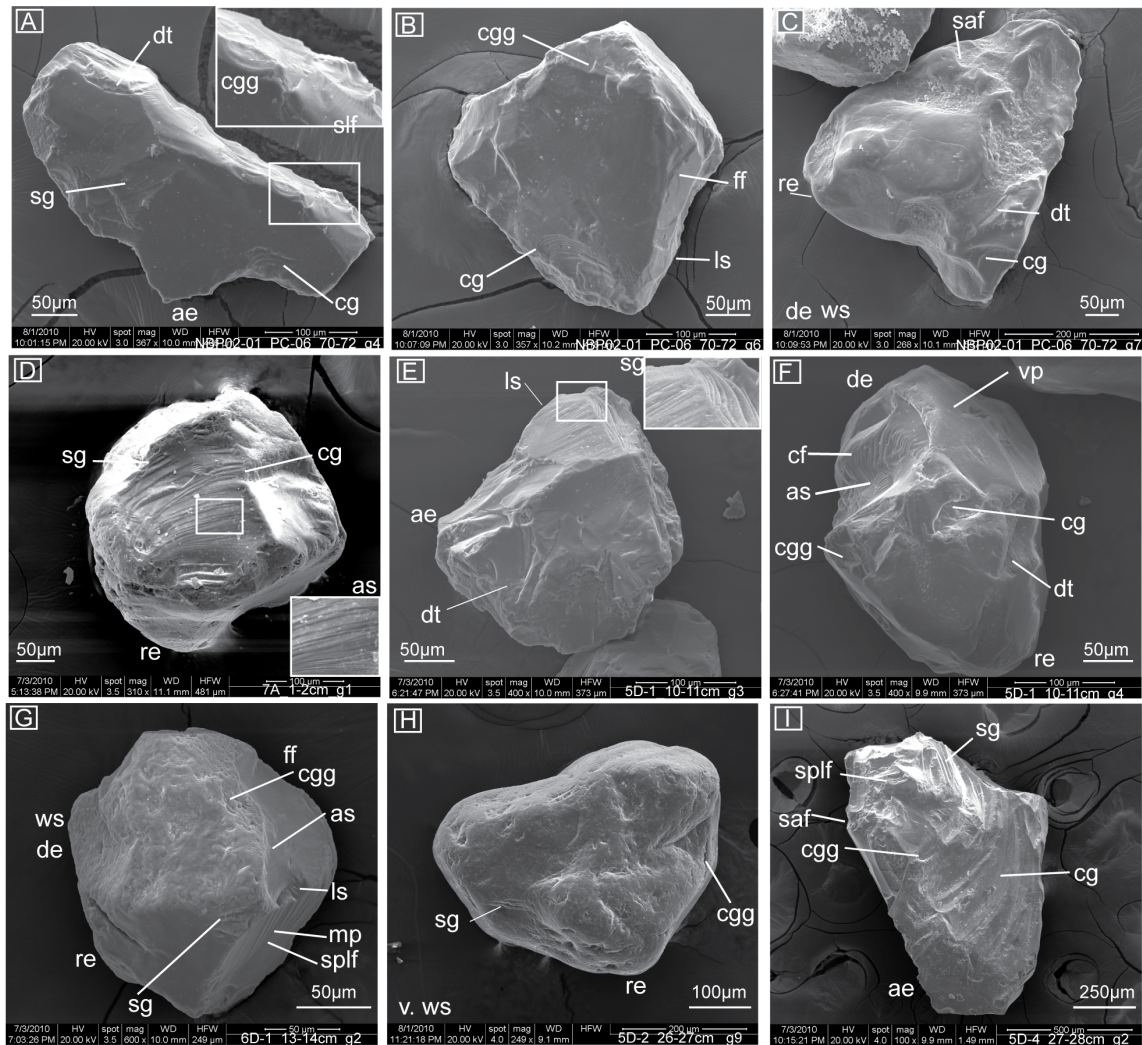


**Figure 2-6 Samples from Pleistocene till, Joinville Plateau, and Pliocene**

Samples from (top) Pleistocene till, from Joinville Plateau, (middle) sites 7A and 5D, and (bottom) Pliocene. (a) Sample NBP02-01\_PC-06\_70-72cm displays curved grooves (cg), straight grooves (sg), crescentic gouges (cgg), deep troughs (dt), and subparallel linear fractures (splf) and is fresh with little/no weathering and angular edges (ae). (b) Grain from Pleistocene sample NBP02-01\_PC-06\_70-72cm illustrating crescentic gouges (cgg), curved grooves (cg), fracture faces (ff), and linear steps (ls). (c) Pleistocene NBP02-01\_PC-06\_70-72cm grain with deep troughs (dt), curved grooves (cg), rounded edges (re), dissolution etching (de), sharp angular features (saf), and a weathered surface (ws). (d) Grain from Pleistocene SHALDRIL sample 7A\_1-2cm showing rounded edges (re), abundant curved grooves (cg), straight grooves (sg), and arc shaped steps (as). (e) Grain from Pleistocene sample

**5D-1\_10-11cm is very fresh with angular edges (ae), straight grooves (sg), deep troughs (dt), and linear steps (ls). (f) Sample 5D- 1\_10-11cm contains deep troughs (dt), curved grooves (cg), crescentic gouges (cgg), v-impact pits (vp), conchoidal fractures (cf), arc steps (as), dissolution etching (de), and rounded edges (re). (g) Grain from Pliocene sample 6D-1\_13-14cm with rounded edges (re), a weathered surface (ws), and dissolution etching (de). The grain also contains fracture faces (ff), straight grooves (sg), crescentic gouges (cgg), arc steps (as), linear steps (ls), mechanically upturned plates (mp), and subparallel linear features (splf). (h) Grains from early Pliocene sample 5D-2\_26-27cm have rounded edges (re), a very weathered surface (ws), relict straight grooves (sg), and weathered crescentic gouges (cgg). (i) This Pliocene 5D-4\_27-28cm sample is extremely fresh with angular edges (ae), crescentic gouges (cgg), curved and straight grooves (cg and sg), sharp angular features (saf), and subparallel linear features (splf).**

#### **2.4.3.2 Late early Pliocene.**

Late early Pliocene deposits from SHALDRIL sites 6D and 6C (6D-1\_13-14cm and 6C-2\_61-62cm, Figure 2-6) contain a range of grain shapes, with most grains displaying a high degree of angularity and low degree of rounding. The most abundant microtextures are crescentic gouges. There is a low abundance of fracture faces, subparallel linear and conchoidal fractures, linear steps, sharp angular features, and straight and curved grooves. The features are commonly very fresh, with individual grains having sharp edges.

#### **2.4.4 Pleistocene**

##### **2.4.4.1 Offshore Joinville Plateau.**

The Pleistocene samples from SHALDRIL sites 5D and 7A (7A\_1-2cm and 5D-1\_10-11cm, Figure 2-6) display a broad scope of grain shapes with a wide range of length to width ratios. The grain edges range in degree of rounding from rounded to quite

angular. The most abundant microtextures (medium abundance) include crescentic gouges, sharp angular features, and straight and curved grooves. There is a low abundance of fracture faces, subparallel linear and conchoidal fractures, arc-shaped and linear steps, curved grooves, and deep troughs.

#### **2.4.4.2 Late Pleistocene till.**

The Pleistocene till from piston core NBP02-01-PC06 (70–72cm, Figure 2-6) contains mostly highly angular grains, with individual grains having a high aspect ratio. Edges vary between fresh to weathered and rounded. There is a medium abundance of straight and curved grooves, fracture faces, crescentic gouges, and deep troughs on the majority of grains. There is a low frequency of weathered surfaces, dissolution etching, and edge rounding.

## **2.5 Discussion**

Sustained high-impact features are created through extreme shear stress during glacial transport and include crescentic gouges, straight and curved grooves, deep troughs and mechanically upturned plates (Mahaney et al., 1996; Sweet and Soreghan, 2010), (Figure 2-3, Figure 2-5, Figure 2-6). In this study, Pleistocene tills provide a baseline for glacially transported grains. Generally, the features observed most commonly in tills, in order of abundance, are (1) subparallel linear and conchoidal fractures; (2) sharp angular features, straight grooves, and deep troughs; and (3) curved grooves, low relief crescentic gouges, arc steps, linear steps, mechanically upturned plates, lattice shatters, and fracture features. The relative abundance of subparallel linear fractures can be related to the



amount of stress incurred during transport. Smaller glaciers and ice caps transport sediment in a lower stress regime and impart a lower relative abundance of subparallel linear fractures as opposed to large ice sheets which transport grains with higher stresses and have higher abundances of subparallel linear fractures (Mahaney, 2002).

The oldest sediments examined for this study are from the Eocene La Meseta Formation, which historically has been interpreted as a nonglacial deposit, void of any ice-rafted debris or any other evidence for glaciation (e.g., Marensie et al., 2002), (Figure 2-7). This interpretation is supported by this investigation, which has yielded no compelling evidence for glaciation at this time. The samples examined from the La Meseta Formation contain a low abundance of crescentic gouges and no other sustained high-stress microtextures (Figure 2-3 and Figure 2-4). Thus, the La Meseta Formation provides a preglacial baseline with which to compare samples from younger strata in the region.

SHALDRIL cores that sampled the late Eocene (Site 3C) consist of poorly sorted muddy/silty very fine sand with few subangular-subrounded pebbles. The age of the sampled interval has been constrained to 37–34 Ma based on diatom biostratigraphy and Sr dating (Bohaty et al., 2011). The samples from this core are characterized by a medium abundance of sustained high-impact microtextures, in contrast to the Seymour Island samples which are relatively void of such features (Figure 2-5). The samples also contain zero to low abundance of subparallel linear fractures and are characterized by high angularity. The dramatic difference in sand grain surface textures between the Eocene La Meseta samples and the SHALDRIL Site 3C (late Eocene) samples indicates that the onset of glaciation in the northern Antarctic Peninsula occurred at the end of the

Eocene, likely restricted to alpine glaciation. This is based on sharp-edged microtextures and low abundance of subparallel linear fractures (Mahaney, 2002). These findings are consistent with palynological results, which indicate a significant change in the vegetation of the area at this time (Warny and Askin, 2011(a), 2011(b)) and seismic stratigraphic analyses that show no evidence of ice having grounded on the continental shelf (Smith and Anderson, 2010). This corresponds to the beginning of a large positive oxygen isotopic excursion (Zachos et al., 2001) and fall in sea level (Miller et al., 2005) marking the transition from greenhouse to icehouse conditions (Figure 2-7).



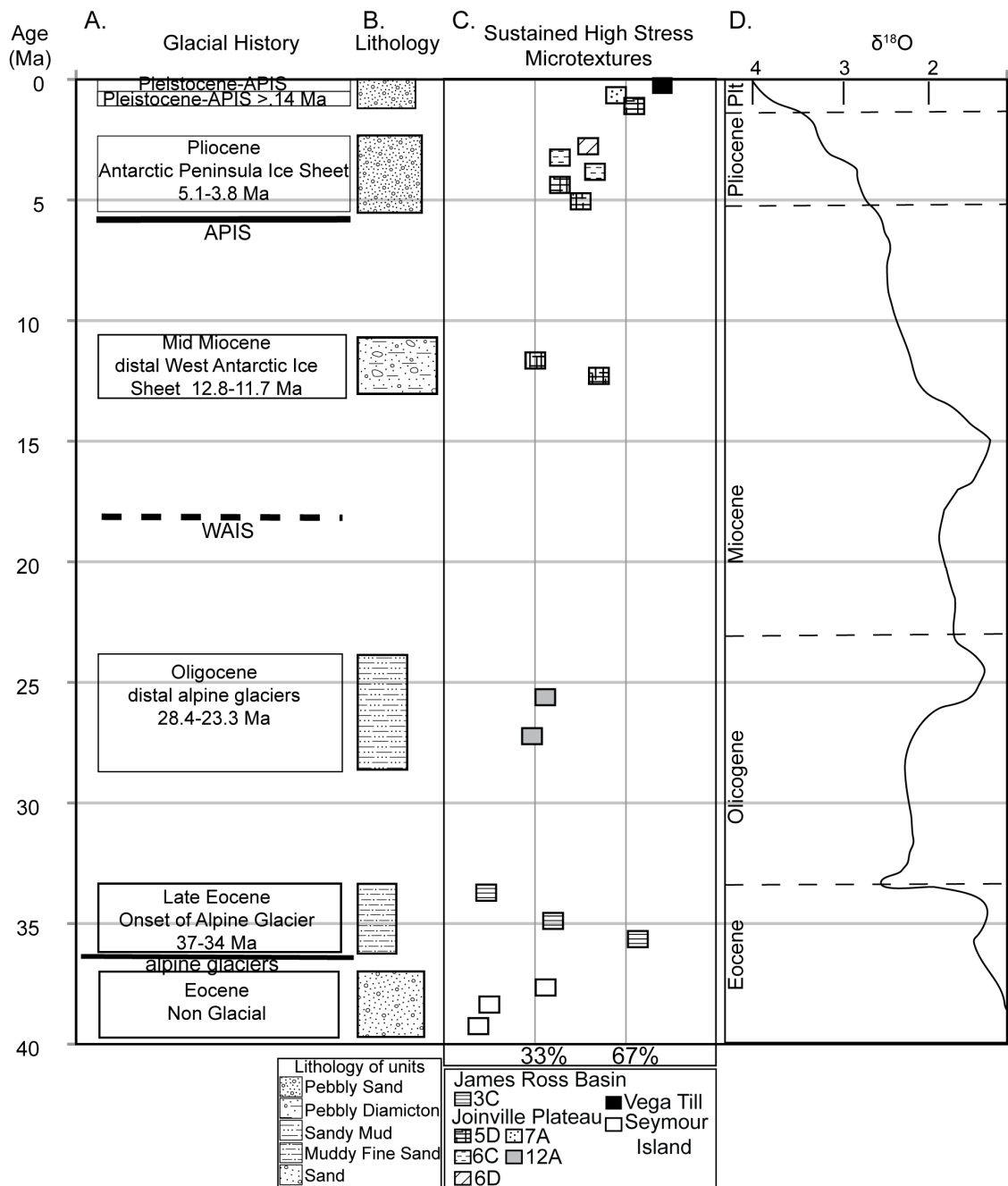


**Figure 2-7 Overall stratigraphy, grain surface textures, and glacial history of the James Ross Basin.**

(a) Age constraints on glacial evolution of the West Antarctic Ice Sheet (WAIS) and Antarctic Peninsula Ice Sheet (APIS) (Anderson et al., 2011). (b) Lithostratigraphic column of units sampled. (c) Plot of frequency of sustained high-stress microtextures based on the work of Sweet and Soreghan (2010). Frequency of particular features

**was calculated over the entire sample interval using the presence or absence of that feature and taking the mean. The relative frequency of sustained high-stress microtextures was calculated by averaging all five high-stress features for the specific sample. (d) Modified  $\delta^{18}\text{O}$  curve from the work of Zachos et al. (2001).**

The upper Oligocene deposits sampled by SHALDRIL Site 12A consist of dark gray sandy mud to muddy sand that contains clay lenses, burrows, and rare dropstones. This deposit is interpreted as representing a distal deltaic or shoreface environment (Wellner et al., 2011). Sand grains from the upper Oligocene display a presence, but a lower abundance, of glacially derived microtextures compared to Site 3C deposits, along with a high degree of physical weathering. A lower abundance of glacially derived microtextures may be a function of the distal location of this site in comparison to Site 3C. This is consistent with palynological evidence for a colder climate during the Oligocene than existed in the Eocene (Warny and Askin, 2011(a), 2011(b)).

The middle Miocene deposits recovered at SHALDRIL Site 5D sampled pebbly gray diamicton, interpreted as glacial marine sediment (Wellner et al., 2011) and thus indicate more extreme glacial conditions than previously existed in the region. The palynomorphs present at this site also indicate colder conditions relative to the late Oligocene, with limited land taxa and dominantly sea-ice species offshore (Warny and Askin, 2011(a), 2011(b)). The microtextures of grains from Site 5D show an increased abundance of high-impact features relative to the late Oligocene samples from Site 12A (Figure 2-4 and Figure 2-5). Individual grains display sustained high-impact features, but have a high degree of rounding (Figure 2-7). These glacial grains have medium to high abundances of physical weathering features and were likely transported by contour currents after being delivered to the drill site by icebergs drifting under the influence of

the Weddell Gyre. This is consistent with inferred expansion of the West Antarctic Ice Sheet (WAIS) onto the southwestern Weddell Sea continental shelf in the middle Miocene (Smith and Anderson, 2010).

The early Pliocene section recovered at sites 6C and 6D consists of pebbly glacimarine sediments. The sand grains from these sediments contain a mixture of well-rounded contour current-transported grains and glacially transported grains. The oldest deposits from Site 6C include very dark greenish gray, medium to coarse sand, and poorly sorted diamicton. Sand grains show a clear increase in the abundance of sustained high-stress microtextures (Figure 2-4), consistent with other evidence for extreme glacial conditions at this time, culminating in initial advance of the Antarctic Peninsula Ice Sheet (APIS) onto the Joinville Plateau (Smith and Anderson, 2011).

Pleistocene samples contain the highest abundance of sustained high-impact surface features (Figure 2-7), which is consistent with evidence for an expanding and contracting APIS during the Pleistocene. The SHALDRIL Pleistocene samples are only slightly lower in abundance of sustained high-impact features relative to the late Pleistocene till samples from piston cores.

## **2.6 Conclusion**

During the late Eocene, there was onset of alpine glaciation in the northern Antarctic Peninsula. The occurrence of glacial surface features records the continued presence of alpine glaciers during the late Oligocene, which is consistent with palynological evidence for significantly cooler conditions relative to the late Eocene.

Samples from mid-Miocene deposits include ice-rafted grains from distant sources, likely West Antarctica, that were probably transported to the study area by icebergs drifting under the influence of the Weddell Gyre. Samples from early Pliocene strata show an increase in the abundance of high-impact features and record the early development of the APIS. Pleistocene till samples display the highest abundance of glacially influenced microtextures and record the extreme glacial conditions that have characterized the region since the early Pliocene.

## Post-LGM deglaciation in Pine Island Bay, West Antarctica<sup>2</sup>

To date, understanding of ice sheet retreat within Pine Island Bay (PIB) following the Last Glacial Maximum (LGM) was based on seven radiocarbon dates and only fragmentary seafloor geomorphic evidence. During the austral summer 2009–2010, restricted sea ice cover allowed for the collection of 27 sediment cores from the outer PIB trough region. Combining these cores with data from prior cruises, over 133 cores have been used to conduct a detailed sedimentological facies analysis. These results,

---

<sup>2</sup> This chapter has been edited, reformatted and reprinted from *Quaternary Science Reviews*, Vol 38 Kirshner, A. E., Anderson, J.B, Jakobsson, M., O'Regan,M., Majewski, W., Nitsche, F., Post-LGM deglaciation in Pine Island Bay, West Antarctica, Doi:10.1016/j.quascirev.2012.01.017, Copyright 2012. Reproduced with permission of Elsevier

augmented by 23 new radiocarbon dates, are used to reconstruct the post-LGM deglacial history of PIB.

Our results record a clear retreat stratigraphy in PIB composed of, from top to base; terrigenous sandy silt (distal glacimarine), pebbly sandy mud (ice-proximal glacimarine), and till. Initial retreat from the outer-continental shelf began shortly after the LGM and before 16.4 k cal yr BP, as a likely response to rising sea level. Bedforms in outer PIB document episodic retreat in the form of back-stepping grounding zone wedges and are associated with proximal glacimarine sediments. A sub-ice shelf facies is observed in central PIB and spans ~12.3–10.6 k cal yr BP. It is possible that widespread impingement of warm water onto the continental shelf caused an abrupt and widespread change from sub-ice shelf sedimentation to distal glacimarine sedimentation dominated by widespread dispersal of terrigenous silt between 7.8 and 7.0 k cal yr BP. The final phase of retreat ended before ~1.3 k cal yr BP, when the grounding line migrated to a location near the current ice margin.

### **3.1 Introduction**

In 2011, T. Hughes eloquently summarized the necessity in thoroughly understanding the deglacial cycle of ice sheets. “Ice sheets are the only components of Earth’s climate system that can rapidly self-destruct, and thereby terminate a cycle of Quaternary glaciation (Denton and Hughes, 1981 and Hughes, 1998). How ice sheets self-destruct is unclear, but it seems to be linked to a rapid and progressive loss of ice-bed coupling, especially coupling beneath and beyond ice streams that causes rapid

gravitational collapse of marine portions of ice sheets (MacAyeal, 1992, 1993) followed by rapid disintegration of the resulting floating ice shelves (MacAyeal et al., 2003; Hulbe et al., 2004) and rapid migration of calving bays up stagnating ice streams into the collapsed ice sheet (Thomas, 1977 and Hughes, 2002), thereby carving out its accumulation zone so it can never recover (Hughes, 1977).”

Here we focus on the marine-based ice sheet in Pine Island Bay and the large Pine Island Glacier (PIG) ice stream, which have configurations conducive to rapid disintegration and show the greatest signs of inherent instability (Hughes, 1981). More importantly, the ice sheet is grounded below sea level on a landward-sloping seafloor, making it intrinsically dynamic (Weertman, 1976, Hughes, 1977 and Mercer, 1978). Glacial modeling supports this claim, suggesting that this portion of the ice sheet is inherently unstable (Schoof, 2007a and Schoof, 2007b). Corroborative to the hypothesized and modeled instability, focused research during the last 30 years has identified PIG as being one of the most dynamic portions of the cryosphere. It has experienced rapid ice-shelf thinning (Shepherd et al., 2001, Rignot et al., 2002 and Wingham et al., 2009); negative mass balance (Thomas et al., 2004 and Rignot et al., 2008); glacial flow acceleration (Rignot, 2006); and grounding line retreat of 1200 m over a 4-year period from 1994 to 1998 (Rignot, 1998). This extreme record of modern change has prompted authors to suggest that the PIG could potentially collapse over the millennial time-span of human civilization (e.g. Katz and Worster, 2010 and Hughes, 2011), raising eustatic sea-level up to ~1.5 m (Vaughan, 2008).

Currently, Circumpolar Deep Water (CDW) is documented as impinging into the Pine Island Trough, a large feature deeply incised into the continental shelf (Jacobs et al.,

1996 and Jacobs et al., 2011). Enhanced basal melting due to the presence of CDW thermally eroding the Pine Island Glacier has been identified as a potential culprit for the rapid nature of modern retreat. However, the question remains whether the changes measured in PIG represent the normal, transient behavior in the deglacial history or whether other mechanisms of retreat contributed previously to the deglacial cycle. In other words, are ongoing changes unprecedented in the context of the long-term, post-LGM deglaciation? To identify the mechanism(s) responsible for retreat of this ice sheet we must understand both the timing and style of deglaciation in the wider Amundsen Sea Embayment (ASE). Here we present constraints on the post-LGM retreat in PIB, eastern ASE, establish a framework to test whether current rates are exceptional, and provide insight into the mechanisms that allow for marine ice sheets to self-destruct. Complementary to the results from the sediment cores presented here is a paper by Jakobsson et al. (2012) providing the detailed glacial morphology of the outer Pine Island Trough and estimated formation time for the largest grounding zone wedge in PIB that indicates a long pause during the general post-LGM ice stream retreat.



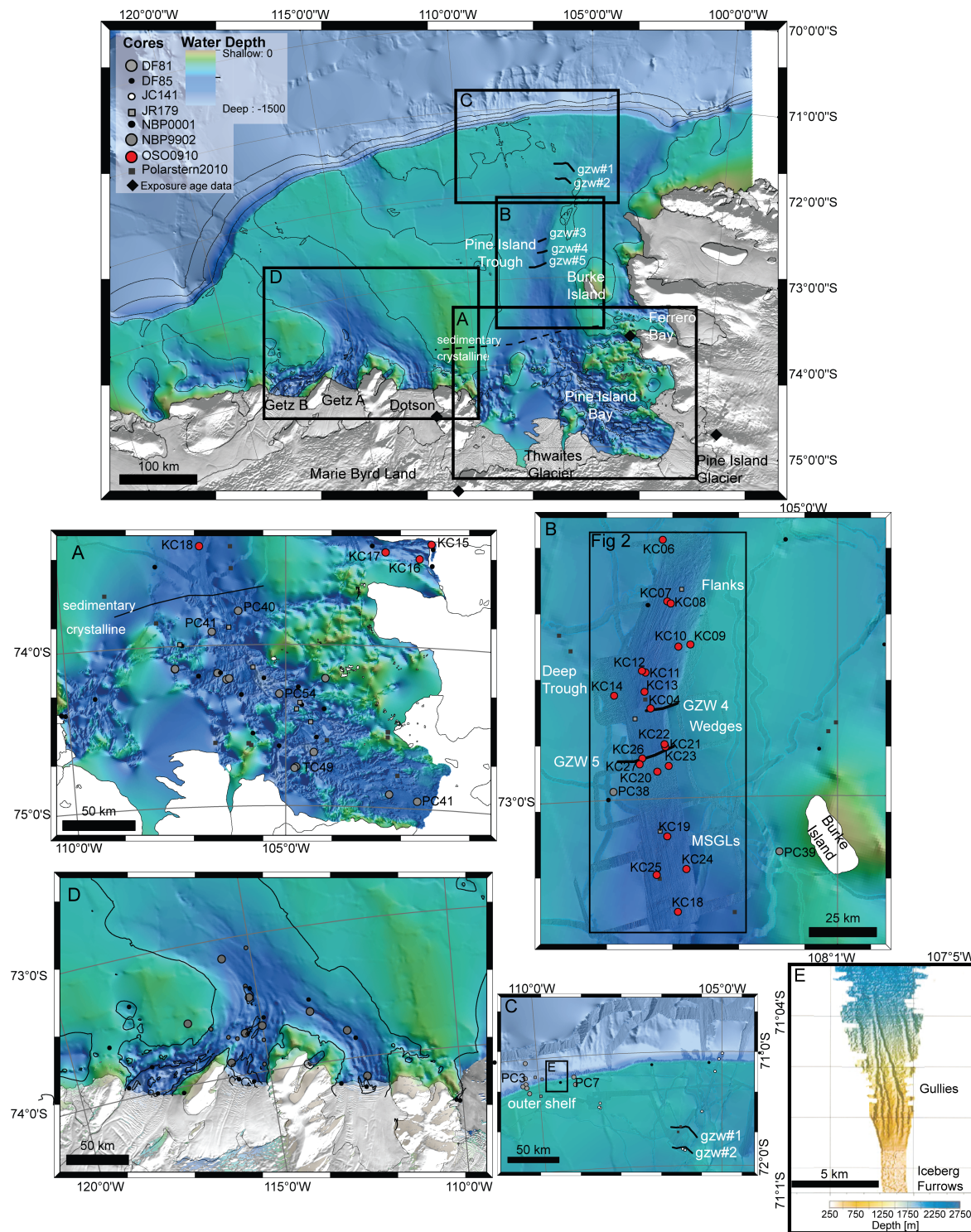


Figure 3-1 Study area map of the Amundsen Sea Embayment

**displaying geomorphic regions and core locations in UTM zone 13S projection. Core and exposure age site symbols include: OSO0910-red circles, NBP99-02-gray circles, and JCR 179-gray squares. Grounding zone wedges (GZW) in Pine Island Bay are modified from Graham et al. (2010). Thin black lines are 500 m isobath lines A. Inner Pine Island Bay B. Outer Pine Island Bay C. Outer Shelf D. Getz/Dotson region (Graham et al., 2009). E. Multibeam map displaying shelf edge gullies (from Lowe and Anderson, 2002 and Nitsche et al., 2007).**

### **3.2 Regional setting and existing data**

Pine Island Bay is located in the polar setting of the ASE. It is the third-largest drainage outlet for the West Antarctic Ice Sheet (WAIS) and the primary drainage path for eastern Marie Byrd Land and western Ellsworth Land (Figure 3-1). Pine Island Bay currently hosts two major ice streams, the Pine Island and Thwaites ice streams, and a smaller ice stream from Smith Glacier (Dotson Ice Shelf). Together they drain ~5% of ice from Antarctica (Vaughan et al., 2001), one of the three main drainage paths of the WAIS. Seismic records illustrate that interior PIB (Figure 3-1), south of ~73.4°S, has a crystalline substrate (Lowe and Anderson, 2002 and Uenzelmann-Neben et al., 2007), characterized by glacially carved features such as p-forms, drumlins, and anastomosing and linear channels (Figure 3-1 A). The erosional seascape has been interpreted as conducive to hosting an organized, convergent seaward subglacial meltwater drainage system, based on the connectivity of basins and channels (Lowe and Anderson, 2002 and Lowe and Anderson, 2003). This geomorphic province will henceforth be referred to as inner PIB as demarcated in Figure 3-1.

Onlapping the crystalline basement is a thick, landward-dipping sedimentary package of outer PIB (Lowe and Anderson, 2002). This change in basement lithology

results in different processes controlling the seascape, creating a distinct region that will be referred to as outer PIB (Figure 3-1). This region includes the Pine Island Thwaites Paleo Ice Stream Trough (PITPIS) of Graham et al. (2010). The geomorphology of outer PIB is characterized by mega-scale glacial lineations (MSGs), two large, broad, grounding zone wedges (GZW #4 and #5, nomenclature from Graham et al., 2010), corrugation ridges, corrugated furrows and iceberg plow moraines (Figure 3-1B; Figure 3-2) (Lowe and Anderson, 2002, Evans et al., 2006, Graham et al., 2010 and Jakobsson et al., 2011).

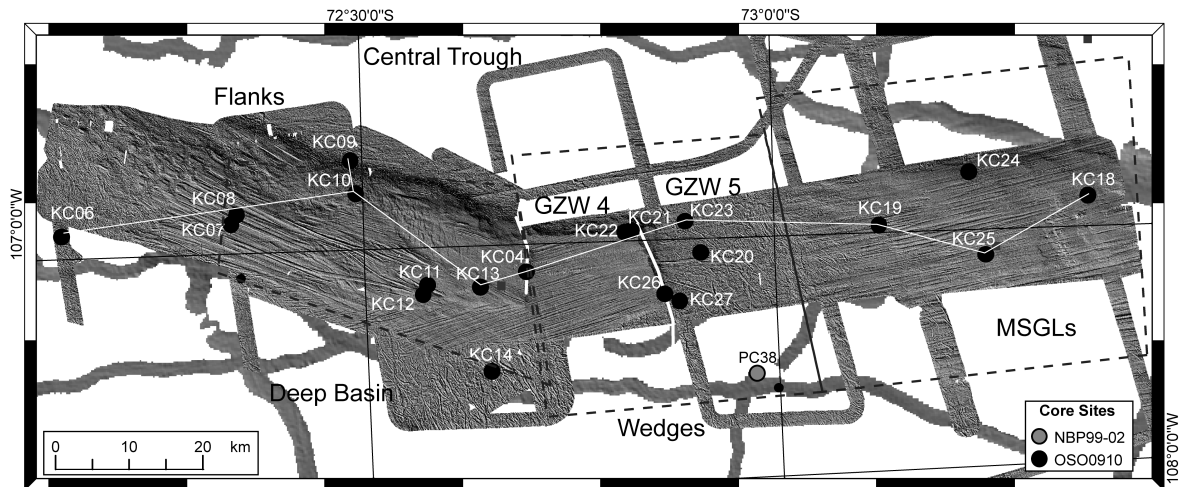


**Figure 3-2 Bathymetry of outer PIB acquired aboard I/B Oden.**

**Geomorphic regions referred to in text are delineated by dashed lines, from north to south; trough flanks, deep basin, grounding zone wedges (Wedges), and mega-scale glacial lineations (MSGs). Sediment cores from OSO0910 are black circles and NBP99-02 are gray circles. Solid white line shows locations of cores in Figure 3-6.**

Heretofore, few cores have been collected from the outermost Pine Island Bay trough region due to persistent sea ice coverage. The northernmost section of the ASE, the outer shelf, contains a relatively flat, broad shelf at 450–550 m water depth that is

covered by iceberg furrows and contains two small grounding zone wedges (GZW #1 and #2 as named by Graham et al., 2010). This geomorphic zone extends to the shelf break and is characterized by gullies that extend seaward to the upper slope (Figure 3-1C, E). The northernmost geomorphic province will henceforth be referred to as the outer shelf, which includes the Pine Island Trough East (PITE) of Graham et al. (2010).

The established deglaciation chronology for the ASE is based on one marine and one terrestrial study in PIB (Lowe and Anderson, 2002 and Johnson et al., 2008) (Figure 3-1A, B, C; Figure 3-2) and two marine studies in the western ASE, in the nearby Getz/Dotson region (Hillenbrand et al., 2010 and Smith et al., 2011) (Figure 3-1D). The Pine Island Bay marine record is limited to seven radiocarbon dates from benthic foraminifera in five cores (Table 3-1) (Lowe and Anderson, 2002). Integrating the geomorphic data and the scant chronologic constraints, Lowe and Anderson (2002) proposed a stepped glacial retreat for the ice sheet, from a grounding line position at the shelf edge during the LGM. The LGM configuration in PIB includes the convergence of the Thwaites and Pine Island ice streams into a large, confluent ice stream (Lowe and Anderson, 2002 and Graham et al., 2010). The ice sheet is interpreted to have stabilized on a bathymetric high near Burke Island (Figure 3-1) in outer PIB from ~16 14C kyr to ~12 14C kyr, based on one radiocarbon date from core NBP99-02 PC39. Following this ~4 kyr pause, the ice retreated to within ~250 km of the modern grounding line (core location NBP99-02 PC41) (Lowe and Anderson, 2002). However, the dates constraining the retreat from the continental shelf edge to the modern location have a large error due to small sample size. This leads to uncertainty in the timing of retreat from the shelf edge and associated mechanism of destabilization.

Study	Expedition <sup>a</sup>	Core ID <sup>b,c</sup>	Lab ID	Material Dated <sup>d</sup>	Water Depth (m)	Sample Depth Interval (cm)		Facies <sup>e</sup>	Geomorphic Region <sup>f</sup>	Lithologic Description <sup>g</sup>	Conventional <sup>14</sup> C age (yr BP)	±(yr)	R <sup>h</sup> (yr)	Calibrated <sup>h</sup> age (cal yr BP)	2σ <sup>i</sup>
						From	To								
This Study (Kirshner et al., submitted)	OSO0910	KC04	87467	Foraminifera	729	14	16	Subunit 1-B	Deep Trough	sandy mud with rd	6670	90	1300	6165	246
	OSO0910	KC06	LuS9030	shell fragment	612	70	80	Subunit 2-C	Flanks	sandy mud with rd	10840	65	1300	10876	259
	OSO0910	KC06	79320	Foraminifera	612	74	76	Subunit 2-C	Flanks	sandy mud with rd	10560	110	1300	10572	358
	OSO0910	KC06	LuS9031	shell fragment	612	80	85	Subunit 2-C	Flanks	sandy mud with rd	10655	75	1300	10731	306
	OSO0910	KC06	LuS9032	Foraminifera	612	90	92	Subunit 2-C	Flanks	sandy mud with rd	8645	70	1300	8199	199
	OSO0910	KC09	78789	Foraminifera	548	30	32	Subunit 2-C	Flanks	muddy sand with rd	8190	30	1300	7767	154
	OSO0910	KC10	87468	Foraminifera	687	4	6	Subunit 1-B	Deep Trough	sandy clay with rd	5400	100	1300	4701	322
	OSO0910	KC10	79316	Foraminifera	687	14	16	Subunit 1-B	Deep Trough	sandy clay with rd	6590	50	1300	6094	180
	OSO0910	KC10	78790	Foraminifera	687	30	32	Subunit 1-C	Deep Trough	sandy silt with rd	7255	35	1300	6841	203
	OSO0910	KC10	78791	shell fragment	687	37	37	Subunit 1-C	Deep Trough	sandy silt with rd	805	25	1300	modern	na
	OSO0910	KC11	LuS9033	shell	733	54	54	Subunit 2-A	Deep Trough	sandy silt with rd	1290	50	1300	modern	na
	OSO0910	KC13	LuS9034	shell fragment	742	150	160	Subunit 2-C	Deep Trough	silty sand with rd	>48000	na	na	na	na
	OSO0910	KC13	LuS9035	shell	742	170	180	Subunit 2-C	Deep Trough	sandy silt with rd	18715	160	1300	na	na
	OSO0910	KC15	78794	Foraminifera	1257	110	112	NA	Ferraro Bay	sandy clay	10000	120	1300	9855	337
	OSO0910	KC15	78793	shell fragment	1257	130	130	NA	Ferraro Bay	clayey sand	10695	35	1300	10736	219
OSO0910	KC19	92259	Foraminifera	782	77	79	Unit 3	MSGLS	sandy mud	10600	60	1300	10618	280	
OSO0910	KC19	92260	Foraminifera	782	84	86	Unit 3	MSGLS	sandy mud	10960	90	1300	10957	290	
OSO0910	KC19	LuS9037	Foraminifera	782	90	92	Unit 3	MSGLS	sandy mud	11775	100	1300	12297	328	
OSO0910	KC23	LuS9036	shell fragment	660	0	7	Subunit 1-A-B	Wedges	sandy silt with rd	na	na	na	na	na	
OSO0910	KC23	LuS9038	Foraminifera	660	20	22	Subunit 2-A Subunit 1-C	Wedges	muddy sand with rd	11170	110	1300	11411	355	
OSO0910	KC26	78792	shell fragment	689	50	59	Subunit 2-B	Wedges	sandy mud with rd	1235	25	1300	modern	na	
DF81	PC03	79317	Foraminifera	1009	31.5	34	Subunit 1-B	Shelf Break	mud	17125	55	1300	19071	298	
DF81	PC07	79319	Foraminifera	475	121	122.5	Subunit 1-B	Shelf Break	mud	14880	40	1300	16705	246	
DF81	PC07	79318	Foraminifera	475	154	156	Subunit 1-B	Shelf Break	mud	14725	40	1300	16452	426	
NBP9902	PC37	AA38695	Foraminifera	438	28	28	Subunit 1-B	Wedges	sandy diamiction	3040	66	1300	1738	229	
NBP9902	PC37	AA38696	Foraminifera	438	70	70	Subunit 1-C	Wedges	sandy diamiction	7430	160	1300	7027	376	
NBP9902	PC37	AA38697	Foraminifera	438	192	192	Subunit 1-C	Wedges	sandy diamiction	5119	81	1300	4306	311.5	
NBP9902	PC38	AA38698	Foraminifera	652	cc	cc	Unit 2 (base)	Flanks	stiff diamiction	11830	420	1300	12199	1044	
NBP9902	PC39	AA38699	Foraminifera	495	14	14	Subunit 2-A	Central Trough	stiff diamiction	15800	3900	1300	16725	9410	
NBP9902	PC40	AA38700	Foraminifera	953	10	10	na	Central Trough	silty diamiction	not enough sample	na	na	na	na	
NBP9902	PC41	AA38701	Foraminifera	957	213	213	Subunit 2-A	Flanks	silty diamiction	10150	370	1300	10100	946	
NBP9902	TC49	AA38702	Foraminifera	852	25	25	Subunit 1-A	Inner PIB	Clay	2270	800	1300	1292	1291	
NBP9902	PC54	AA38703	Foraminifera	1202	6	6	na	Inner PIB	Clay	not enough sample	na	na	na	na	

Table 3-1 Radiocarbon constraints on West Antarctic Ice Sheet retreat following the

**Last Glacial Maximum (LGM) in Pine Island Bay. Compiled uncorrected and calibrated radiocarbon ages representing minimum estimates of glacial retreat**  
<sup>a</sup> OSO0910: Oden Southern Ocean 2009-2010; NBP9902: Nathan B. Palmer 1999-02; DF81: Deep Freeze 1981 <sup>b</sup> PC: piston core; KC: kasten (gravity) core; TC trigger core <sup>c</sup> For core locations, see Figure 3-1; 3-2, Table 3-3 <sup>d</sup> Foraminifera: N. Pachyderma; Shell Fragment: unidentified shell fragment; Shell: articulated unidentified shell <sup>e</sup> Assigned Facies Unit <sup>f</sup> See Figure 3-1 <sup>g</sup> Naming scheme following Folk and Ward (1957) <sup>h</sup> Reservoir age for Antarctic marine carbonates estimated as  $1300 \pm 70$  (Berkman and Forman, 1996).  $\Delta R = 897 \pm 70$ . This reservoir correction is based on closest possible calibration point. <sup>i</sup> Calibrated using CALIB program v. 6.0 (Stuiver et al. 1998) with Marine09 curve. Ages reported in calendar years before present (cal yr BP). Prior study (Lowe and Anderson, 2002) ages have been recalibrated. <sup>j</sup> Calibrated sigma age range using CALIB v 6.0

The marine record from western ASE (Figure 3-1D) primarily utilizes acid insoluble (AOI) dating to constrain the age of deposition of the uppermost glacimarine unit, marking the onset of seasonably ice-free waters (Hillenbrand et al., 2010 and Smith et al., 2011). This deposition occurred on the western mid-shelf before 13.8 k cal yr BP and the inner shelf to within ~10–12 km of the present Getz/Dotson ice-shelf front between ~12.6 k cal yr BP and ~10.0 k cal yr BP. Terrestrial work on cosmogenic surface-exposure ages resulted in four dates in eastern ASE, recording progressive thinning of the WAIS since 14.5 kyr (Johnson et al., 2008). These combined observations in the ASE establish a general post-LGM retreat. However, both the specific timing and, therefore, mechanism(s) of retreat are not well constrained, requiring an enhanced chronologic framework.

### 3.3 Materials and methods

Data were collected aboard Icebreaker Oden during the expedition Oden Southern Ocean 0910 (OSO0910) in the austral summer of 2010, and augmented by data from cruises Deep Freeze 81(DF-81), R/V Nathaniel B. Palmer 99-02 (NBP99-02), and R/V Nathaniel B. Palmer 00-01 (NBP00-01). Icebreaker Oden acquired swath bathymetry data, chirp sub-bottom profiler data, and sediment cores from outer Pine Island Bay (Figure 3-1B; Figure 3-2). The chirp data were collected with a Kongsberg SBP120 3° sub-bottom profiler at 2.5–7 Hz. Chirp data were analyzed in real-time to identify areas for sediment coring. Bathymetric data were collected with a hull-mounted Kongsberg 12 kHz EM122 1° × 1° multibeam echo sounder. Details on the processing of multibeam data can be found in Jakobsson et al. (2012). Following processing, the bathymetric data were merged with prior cruise data (Nitsche et al., 2007). The complete bathymetric data set of Pine Island Bay was then analyzed for geomorphic context, with details described in Jakobsson et al. (2012).

Twenty-seven sediment cores were collected with a 3-m Kasten gravity corer. This length of core is sufficient to recover the entire post-LGM sequence in PIB due to low sedimentation rates (Lowe and Anderson, 2002). Once onboard, cores were photographed and visually described. The lithological descriptions include Munsell sediment color, texture, sorting, and sedimentary structures. Shear strength was measured at approximately 10 cm intervals using either a pocket penetrometer or a pocket shear vane. Following the preliminary procedures, 10 cm<sup>3</sup> sediment plug samples were extracted at 10 cm intervals for micropaleontology and grain size analysis. Each Kasten core was sub-sampled using split plastic liners for archival purposes. A shipboard multi-

sensor core logger (MSCL) was used to measure the magnetic susceptibility, gamma-ray derived density, and compressional wave (p-wave) velocity of archived sections at a 1-cm resolution following standard Geotek™ processing. Gravel and pebble concentrations were quantified by wet-sieving the remaining sediment in the Kasten core through a 2 mm and 0.5 mm mesh in 10-cm sections. Any identified shell material was extracted from each sieved sample for radiocarbon analyses. The >0.5 mm samples were weighed for an approximation of pebble abundance. Archived core halves were shipped to the Antarctic Marine Geology Research Facility in Tallahassee, Florida where X-radiographs were taken and examined for microstructures, layering, and for additional carbonate material.

Matrix grain size was measured at Rice University using a Malvern Mastersizer 2000 laser grain size analyzer following the methods of McCave et al. (1986). Bulk composition and degree of sorting was categorized following the scheme of Folk and Ward (1957) (Table 3-2).

Pine Island Bay has a dearth of carbonate material, resulting in sparse age constraints. To combat this deficiency, shipboard reconnaissance micropaleontology was performed at 10 cm intervals in every core to identify foraminiferal populations. Following this initial examination, over 52 samples were washed and picked in detail for radiocarbon material. Radiocarbon dating by Accelerated Mass Spectrometry was performed by Lund University and the University of California at Irvine Keck-CCAMS. The datable material was taken from the base of each subunit when possible, to best constrain the initial deposition of each facies. Radiocarbon dating in the Southern Ocean is known to have numerous complications including: reservoir effects, reworking, and



organism specific fractionation (e.g. Berkman and Forman, 1996; Andrews et al., 1999). To minimize such issues, we focused primarily on *Neogloboquadrina pachyderma* tests for a robust and consistent chronology. When foraminifera were absent, in-situ shell fragments were dated. Dates are reported in both uncorrected radiocarbon years ( $^{14}\text{C}$  BP) and calibrated calendar years before present (cal yr BP) using the Marine 0.9 calibration curve of the Calib 6.0 program (Reimer et al., 2009) with a reservoir age for Antarctic marine carbonates estimated as  $1300 \pm 70$  k yr (Table 3-1) ( Berkman and Forman, 1996 and Domack et al., 2001).

Pine Island Facies <sup>a</sup>	Interpretations <sup>b</sup>	Magnetic Susceptibility [10 <sup>-5</sup> SI]			Density [g/cc]			Velocity [m/s]			Sedimentology- matrix [%] <sup>c</sup>			Thickness [cm]		Silt/Clay Ratio	Color			Classification	
		mean	low	high	mean	low	high	mean	low	high	sand	silt	clay	to	from		thickness	Code <sup>d</sup>	Name	Shepard	Folk
<b>Unit 1</b>		<b>98</b>	<b>5</b>	<b>264</b>	<b>1.71</b>	<b>1.32</b>	<b>2.19</b>	<b>1543</b>	<b>1548</b>	<b>1654</b>	<b>21</b>	<b>53</b>	<b>26</b>	<b>0.0</b>	<b>49.7</b>	<b>49.7</b>	<b>2.5 Y 5/3</b>	<b>light olive brown</b>	<b>sand silt clay</b>	<b>sandy silt</b>	
1A	Distal Glaciomarine	40	12	70	1.53	1.36	1.66	1546	1528	1566	13	62	25	0.0	13.9	13.9	2.5 Y 5/3	light olive brown	clayey silt	sandy silt	
1B		89	41	153	1.69	1.41	1.96	1564	1517	1627	21	52	27	10.6	46.3	35.7	2.5 Y 5/3	light olive brown	sand silt clay	sandy mud	
1C		165	81	262	1.91	1.58	2.17	1519	1471	1602	30	44	26	27.4	57.5	30.1	2.5 Y 5/3	light olive brown	sand silt clay	sandy mud	
<b>Unit 2</b>		<b>196</b>	<b>117</b>	<b>310</b>	<b>2.10</b>	<b>1.72</b>	<b>2.33</b>	<b>1596</b>	<b>1512</b>	<b>1664</b>	<b>40</b>	<b>38</b>	<b>22</b>	<b>75.2</b>	<b>106.1</b>	<b>30.9</b>	<b>wide range</b>	<b>shades of grayish brown</b>	<b>sand silt clay</b>	<b>sandy mud</b>	
2A	Proximal Glacial	215	111	331	2.06	1.69	2.31	1588	1461	1707	44	34	22	32.8	77.7	44.9	10YR 5-4/2	dark-grayish brown	silty sand	sandy mud	
2B	Marine & Ice Shelf Break Up Facies	188	126	279	2.01	1.81	2.18	1613	1562	1649	39	38	23	57.9	78.2	20.3	2.5 Y 3-5/2	(v) (dark) grayish brown	sand silt clay	sandy mud	
2C		176	79	283	2.09	1.70	2.29	1608	1530	1670	43	36	21	71.6	100.3	28.7	2.5 Y 3-4/1-2	(very) dark gray (ish brown)	sand silt clay	sandy mud	
2D		203	152	348	2.25	1.67	2.53	1576	1494	1629	32	45	23	138.7	168.2	29.5	wide range	(v) dark (olive) gray(ish brown)	sand silt clay	sandy mud	
<b>Unit 3</b>	Sub-Ice Shelf Facies	<b>112</b>	<b>66</b>	<b>185</b>	<b>1.64</b>	<b>1.47</b>	<b>1.84</b>	<b>1632</b>	<b>1604</b>	<b>1684</b>	<b>9</b>	<b>50</b>	<b>41</b>	<b>71.8</b>	<b>86.5</b>	<b>14.8</b>	<b>5Y 5/2</b>	<b>olive gray</b>	<b>clayey silt</b>	<b>mud</b>	
<b>Unit 4</b>	Winnowed	<b>120</b>	<b>42</b>	<b>239</b>	<b>2.06</b>	<b>1.57</b>	<b>2.28</b>	<b>1719</b>	<b>1654</b>	<b>1778</b>	<b>72</b>	<b>19</b>	<b>10</b>	<b>96.5</b>	<b>129.2</b>	<b>32.7</b>	<b>2.5Y 4-5/1-3</b>	<b>light olive- dark grayish brown</b>	<b>silty sand</b>	<b>muddy sand</b>	
<b>Unit 5</b>	Till	<b>120</b>	<b>72</b>	<b>243</b>	<b>2.14</b>	<b>1.68</b>	<b>2.47</b>	<b>1233</b>	<b>1479</b>	<b>1678</b>	<b>30</b>	<b>45</b>	<b>25</b>	<b>133.5</b>	<b>210.0</b>	<b>76.5</b>	<b>5 Y 3-4/1-2-2</b>	<b>shades of dark (bluish) gray</b>	<b>sand silt clay</b>	<b>sandy mud</b>	

**Table 3-2 Attribute table of physical properties for cores collected in Pine Island Bay.**

**Each measurement is an average of all 25 cores analyzed. <sup>a</sup> Units in Pine Island Bay, see text for more information <sup>b</sup>. Facies interpretations <sup>c</sup>. Matrix composition measured on the Malvern Mastersizer 2000 at Rice University <sup>d</sup>. Average Munsell Color Code**

## **3.4 Results**

### **3.4.1 Stratigraphic succession and facies distribution**

This study focuses primarily on outer PIB (Figure 3-1B; Figure 3-2), an area identified as being crucial to understanding the retreat history (e.g. Lowe and Anderson, 2002, Lowe and Anderson, 2003, Evans et al., 2006 and Graham et al., 2010) but includes cores from both the outer shelf and inner PIB, allowing us to reconstruct a near-surface stratigraphy within the eastern ASE (Figure 3-3). Sediment facies in Pine Island Bay are described herein, from seafloor to the base of the cores. Without exception the following units occur in stratigraphic order in every core. A sample stratigraphic section for each geomorphic region, as demarcated in Figure 3-1, is provided in Figure 3-3. Additional information on each core analyzed is provided in the Appendix A.

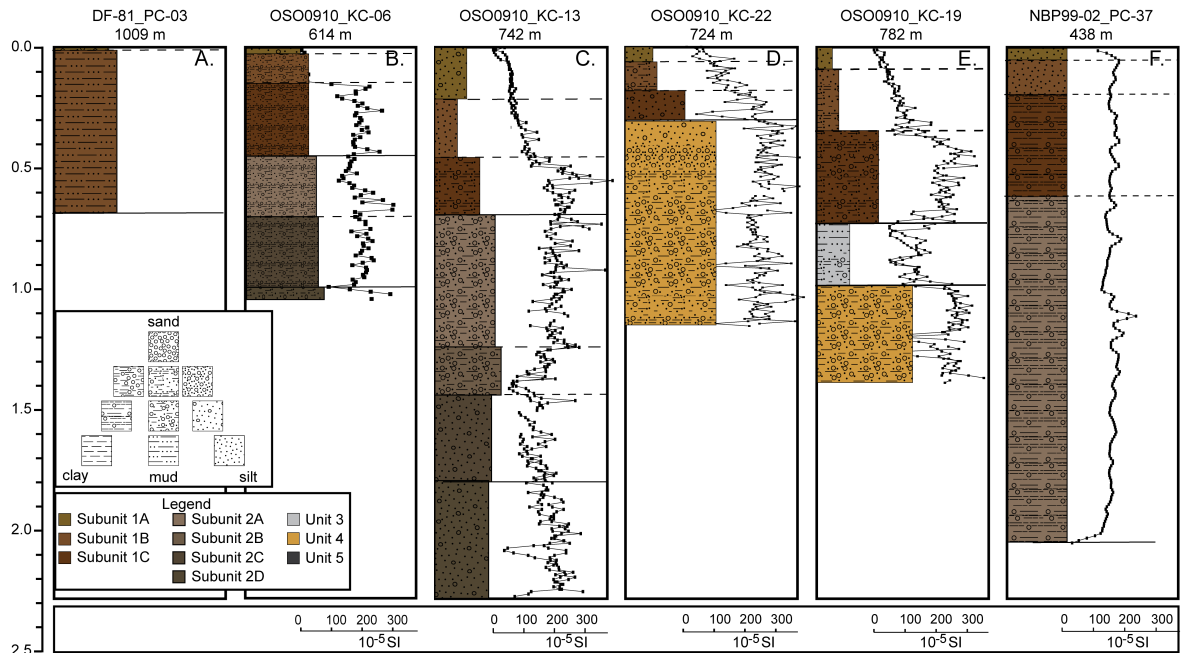


**Figure 3-3 Example core for each geomorphic region**

from north (left) to south (right) (see Figure 3-1 and Figure 3-2 for specific locations). Depth axis to left in meters. Curve to right of cores is magnetic susceptibility, with scale at the base of each curve in units of  $10^{-5}$  SI. Additional information for every core in this study can be found in Appendix A. A. Outer shelf-upper slope region. B. Outer PIB-flanks region. C. Outer PIB-deep basin region. D. Outer PIB-wedges region. E. Outer PIB-MSGL region. F. Inner PIB.

### 3.4.1.1 Unit 1

Unit 1, the youngest unit, is a massive, light olive brown (2.5 Y 5/3) sandy silt (Table 3-2). The clay component varies slightly throughout the interval (ranging between 25 and 27% on average), while the sand and silt fraction vary notably with depth (Figure 3-4A, B, C). Unit 1 coarsens down section, with the concentration of sand increasing two fold near the base of the unit and sorting decreasing down section (Figure 3-5). Pebble concentrations are low but increase slightly near the base of the unit. Pebbles are

primarily of mafic rock types. The magnetic susceptibility character mirrors the sand and pebble concentrations, with low and uniform values that increase slightly down unit to higher and more varied values at the base (Figure 3-3). Unit 1 is devoid of sedimentary structures or bioturbation and has low shear strength (~1.96–2.94 kPa). Abundant and diverse foraminifera exist in the upper part of the unit, decreasing in abundance down section, but the unit is diatom barren. In the chirp sub-bottom profiles, Unit 1 is acoustically layered and draping (Anderson et al., 2010 and Jakobsson et al., 2012). Its thickness increases towards the modern grounding line and with increasing water depth. Three subunits are defined in Unit 1, from top to bottom, subunits 1-A, 1-B and 1-C, and always occur in stratigraphic order.

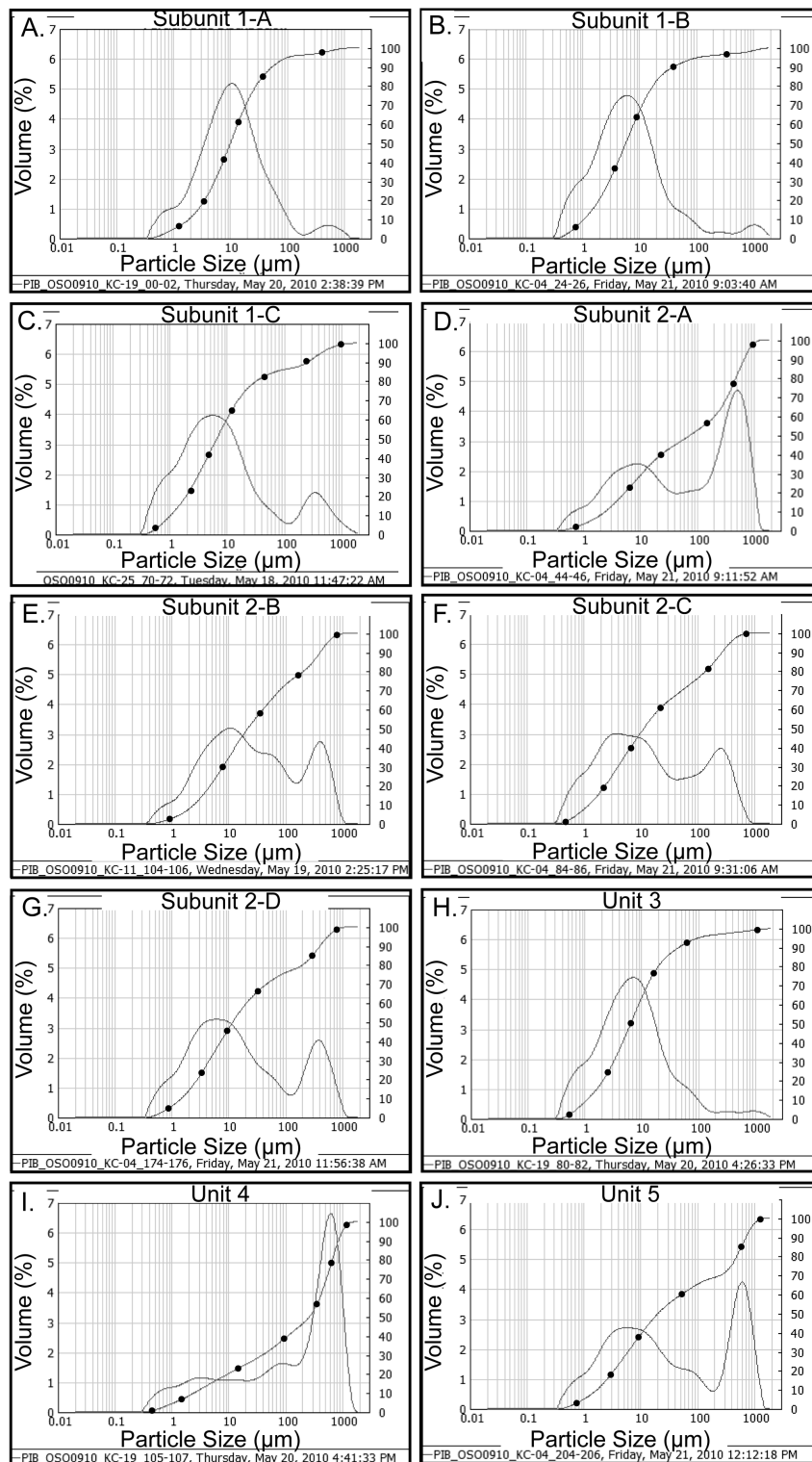
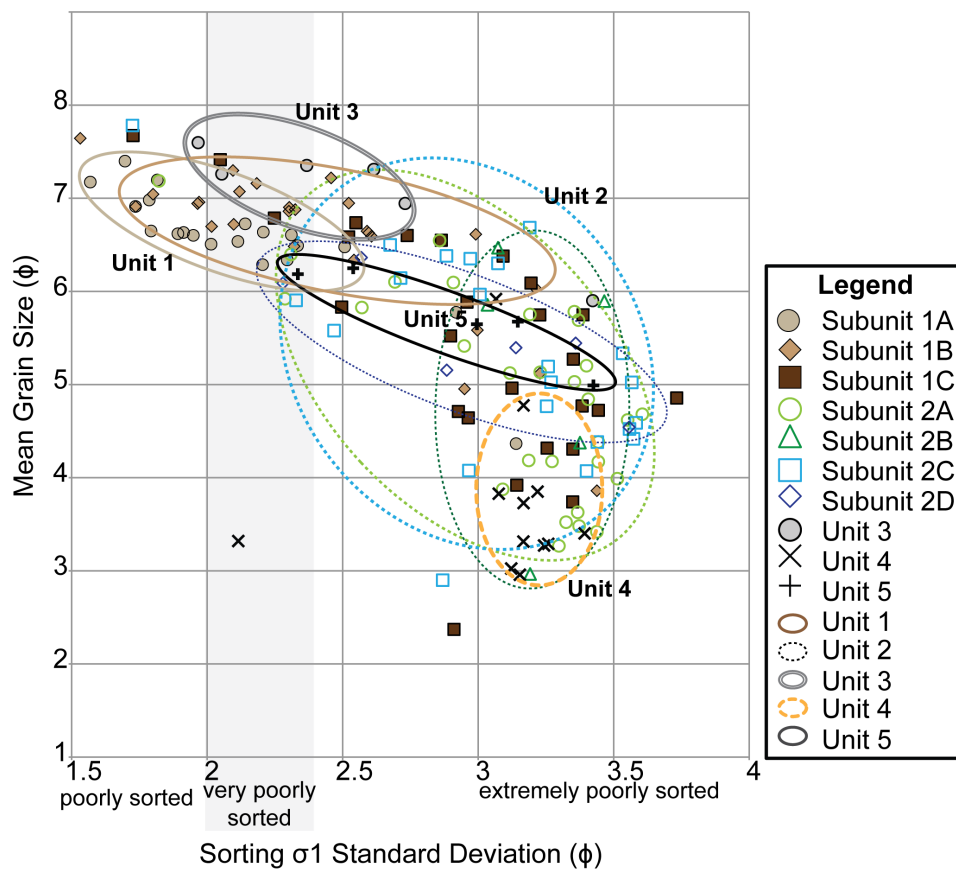


Figure 3-4 Representative grain size curves for each subunit.

The curves displayed are frequency (solid line) and cumulative (line with dots) curves. The truncation of curves at sizes larger than 2000  $\mu\text{m}$  is an artifact of the sample preparation and measurement process, as all samples were sieved at 2000  $\mu\text{m}$ . A. Subunit 1-A, sample from OSO0910 KC19 at 0–2 cm core depth. B. Subunit 1-B sample from OSO0910 KC04 at 24–26 cm core depth. C. Subunit 1-C, sample from OSO0910 KC 25 at 70–72 cm core depth. D. Subunit 2-A, sample OSO0910 KC04 at 44–46 cm core depth. E. Subunit 2-B, sample from OSO0910 KC11 at 104–106 cm core depth. F. Subunit 2-C, sample from OSO0910 KC04 at 84–86 cm core depth. G. Subunit 2-D, sample from OSO0910 KC04 at 174–176 cm core depth. H. Unit 3, sample from OSO0910 KC19 at 80–82 cm core depth. I. Unit 4, sample from OSO0910 KC19 at 105–107 core depth J. Unit 5, sample from OSO0910 KC04 at 204–206 cm core depth.

#### 3.4.1.1.1 Subunit 1-A

Subunit 1-A is the uppermost facies. It is a light olive brown (2.5 Y 5/3) sandy silt with a low sand content (mean 13%), high silt content (mean 62%), and is virtually devoid of pebbles (Table 3-1). Grain size analysis shows a single mode with normal distribution and is the most sorted unit found in PIB (Figure 3-4A; Figure 3-5). Magnetic susceptibility and bulk density signatures are constant throughout the subunit and are the lowest values recorded in Pine Island Bay sediments (Figure 3-3). Subunit 1-A has very low shear strength. Microfauna include abundant calcareous, agglutinated, and planktonic foraminifera. Unit 1-A thickens towards the modern grounding line.



**Figure 3-5 Plot of mean grain size ( $\phi$  units) and degree of sorting (sigma one standard deviation) for all samples analyzed.**

Samples are labeled by subunit. Grain size measurement for each sample is truncated at 2000  $\mu\text{m}$  in size from measurement process. Subunit fields are generalized and delineated by encompassing a maximum number of samples.

#### 3.4.1.1.2 Subunit 1-B

Subunit 1-B is a light olive brown (2.5 Y 5/3) sandy mud. Color varies slightly from olive gray (5 Y 4/2) in interior PIB to light olive gray (5Y 5/2) on the outer shelf. Subunit 1-B has greater pebble and sand content, 8% sandier on average, relative to subunit 1-A (Figure 3-4B). This corresponds to an increase in both magnetic susceptibility and bulk density values, with a low degree of variability in both and a



decrease in sorting (Figure 3-5). Rare rip-up clasts (KC12) and distorted bedding (KC18) exist in some cores. The majority of cores contain few to some agglutinated foraminifera, while cores from shallower water-depths contain some to abundant calcareous, agglutinated, and planktonic foraminifers. Subunit 1-B is always located below Subunit 1-A (when present).

#### **3.4.1.1.3 Subunit 1-C**

Subunit 1-C is a light olive brown (2.5 Y 5/3) sandy mud with a high abundance of pebbles (Figure 3-4C). It has the highest and most varied magnetic susceptibility, the highest bulk density and acoustic velocity values, and the least sorting in Unit 1 (Table 3-1; Figure 3-3; Figure 3-5). Sedimentary structures are limited to laminae observed in a single core (KC13). Few to some calcareous and agglutinated foraminifera occur in cores collected in water shallower than ~730 m water depth. Subunit 1-C is located below subunit 1-B with an average thickness of 23 cm. This subunit thins basinward and was not sampled on the outer shelf (Figure 3-3A).

#### **3.4.1.2 Unit 2**

Unit 2 is a medium-stiff, pebbly, sandy mud that varies from dark gray to very dark grayish brown (2.5 Y 3-5/2 to 10 YR 4/1) (Table 3-2). Pebble content increases down-unit and is an order of magnitude higher than Unit 1 and with more varied lithologies. Unit 2 is generally massive with occasional layering, no evidence for bioturbation, and has the highest degree of scatter in both mean grain size and sorting in PIB sediments (Figure 3-5). When present, foraminiferal assemblages are relatively diverse and the unit is always barren of diatoms. On average, it has a medium shear

strength which increases down section from ~2.0 to 18.0 kPa. Unit 2 exhibits discrete changes in character, more precisely defined in four subunits: subunits 2-A, 2-B, 2-C, and 2-D, which are always found in stratigraphic order. A sharp contact separates Unit 1 and Unit 2. Unit 2 was penetrated in a few cores (e.g. KC04, KC05), directly overlying Unit 5. It is sampled in ~60% of cores collected and is more commonly observed seaward of the prominent grounding zone wedges (GZWs 4 and 5) in outer PIB (Figure 3-3B, C).

#### **3.4.1.2.1 Subunit 2-A**

Subunit 2-A is a pebbly, sandy mud that is dark-grayish brown (10 YR 5-4/2), varying slightly in color throughout outer PIB (Figure 3-4D; Figure 3-5). Magnetic susceptibility values are high and varied. There are rare rip-up clasts (KC11) and layering (KC13, Figure 3-3C) primarily observed in cores collected from deeper water-depths. Subunit 2-A has higher shear strength relative to Unit 1. It contains pelletized clays in some locations. Microfauna are barren to sparse, but when present are composed of a diverse population. Subunit 2-A is present in 60% of cores sampled and is situated directly below Unit 1. The basal contact of subunit 2-A with subunit 2-B is gradational (when present) and sharp with subunit 2-C. This subunit is primarily located in the wedge geomorphic region of outer PIB and seaward (Figure 3-2; Figure 3-3B, C). However, a more southern core (KC24) in the outer Pine Island Bay trough sampled subunit 2-A. This is the only subunit of Unit 2 to have a correlative increase in thickness as water depth increases.

#### **3.4.1.2.2 Subunit 2-B**

Subunit 2-B is a transitional facies between subunit 2-A and subunit 2-C, displaying gradational changes in color, grain size, and magnetic susceptibility (Figure 3-4E.). It is a dark grayish brown (2.5 Y 3-5/2) pebbly, sandy mud. Magnetic susceptibility is low compared to subunit 2-A. This subunit is primarily massive and homogeneous, however, two cores, KC13 and KC23, display isolated layering. Subunit 2-B contains some benthic and planktonic foraminifera in cores collected between 957 m and 495 m water depth. It is only present in locations in the wedge geomorphic region of outer PIB and seaward, and is most prominent in the deep outer basin (Figure 3-2; Figure 3-3B, C).

#### **3.4.1.2.3 Subunit 2-C**

Subunit 2-C is a massive, very dark gray to dark grayish (2.5 Y 3-4/1-2) pebbly, sandy mud (Figure 3-4F). This subunit has low bulk density and low magnetic susceptibility and medium shear strength. There are few to barren foraminifera and pebbles are abundant. Subunit 2-C was sampled in the wedge geomorphic region of outer PIB and seaward (Figure 3-2; Figure 3-3B, C). The subunit is marked by a sharp contact below subunit 2-B (when present) or subunit 2-A, and a sharp basal contact with underlying subunit 2-D.

#### **3.4.1.2.4 Subunit 2-D**

Subunit 2-D is a dark gray to olive gray (2.5 Y 3/1 to 10 YR 4/1) pebbly, sandy mud (Figure 3-4G). This subunit has higher magnetic susceptibility and bulk density values than the overlying units. Subunit 2-D contains abundant pebbles and is massive,

but contains isolated 1 to 3 cm thick dark gray layers and sedimentary clasts. Foraminifera occur in high abundance in core KC06, which was collected at 612 m water depth. In cores that sampled this subunit below 720 m water depth, foraminifera are absent. Subunit 2-D was only sampled in the deep basin of outer PIB and more seaward (Figure 3-2; Figure 3-3B, C). Both the upper contact with subunit 2-C and the basal contact to Unit 5 are sharp.

#### **3.4.1.3 Unit 3**

Unit 3 is a massive, homogeneous, olive gray (5Y 5/2) mud (Table 3-2). This is an extremely fine-grained unit, containing an order of magnitude less sand than any other unit, devoid of pebbles, and is on average the most sorted unit (Figure 3-4H; Figure 3-5). Faunal assemblages include some to high abundance of planktonic foraminifera (*N. pachyderma*), pyritized worm tubes and rare bryozoans. The unit is diatom barren. Unit 3 was only sampled in the MSGSL region of outer PIB (Figure 3-2; Figure 3-3E). It occurs below a sharp contact from subunit 1-C and above a sharp contact with either underlying Unit 4 (e.g. KC19, Figure 2-3E) or Unit 5 (e.g. core KC25). Unit 3 was never sampled in the same core as Unit 2.

#### **3.4.1.4 Unit 4**

Unit 4 is a light olive to dark grayish brown (2.5 Y 4-5/1-3) muddy sand (Table 3-2). Mean matrix composition of Unit 4 includes 67% sand. The grain size distribution is truncated at 100–200  $\mu\text{m}$ , displaying a sorted peak in the coarse fraction, but is generally extremely poorly sorted (Figure 3-4I; Figure 3-5). In core KC18, there is a marked transition in color from light olive brown and 63% sand composition to a dark grayish

brown interval and 80% sand composition. Unit 4 is barren of microfauna. The upper contact is very sharp with either Unit 1 or Unit 3. The basal contact remains unsampled, as the unit was never penetrated to its base. Unit 4 was sampled throughout PIB and never sampled in the same core as Unit 2.

#### **3.4.1.5 Unit 5**

Unit 5 is a massive, homogeneous diamicton with a sandy mud matrix and very high shear strength (Figure 3-4J; Figure 3-5; Table 3-2). Two distinctly different colored diamictons were sampled within Pine Island Bay, one being very dark olive gray (5 Y 3-4/1-2) and the other a dark blueish gray (2 Gley 4/10B) color. The unit contains large cobbles, up to the width of the core barrel in size, that range in lithology from mafic to felsic. Unit 5 is barren of fauna and lacks any discernable layering or evidence of bioturbation. It has the highest average bulk density (2.53 g/cc) measured in PIB and high shear strength (~7.0–40.0 kPa). Only three of the cores collected during expedition OSO0910 penetrated into Unit 5, and no cores penetrated it completely. The unit was sampled in outer PIB, in both the deep trough and the MSGL region (Figure 3-2). It is likely present in other locations, but its recovery was limited by the coring method (gravity cores). Piston coring in prior cruises sampled Unit 5 in additional cores (e.g. NBP99-02 PC39 in MSGL region). This is the basal unit below a sharp contact of overlying units, Unit 2 and Unit 3.

#### **3.4.2 Radiocarbon analysis**

Twenty-four new radiocarbon dates are presented from outer Pine Island Bay, adding to the nine ages reported by Lowe and Anderson (2002). Two of the radiocarbon

dates from the OSO0910 cores were included in Jakobsson et al. (2011). Table 3-1 lists radiocarbon results for each sample in both  $^{14}\text{C}$  years and calibrated years and the assigned sedimentary unit. All dates are from carbonate material, primarily tests of planktonic foraminifera. Locations of cores are shown in Figure 3-1 with additional information given in Table 3-3.

Radiocarbon ages in outer Pine Island Bay occur in chronologic order down core in all locations with one exception (KC06). This consistency is additional verification of the integrity in the dating methods and results and this implies limited bioturbation or reworking. Core KC06 was collected in relatively shallow water (612 m) on the flank of the outer Pine Island Bay trough (Figure 3-1B; Figure 3-2), an area that is highly iceberg turbated. Core KC06 yielded three ages of 10.7 kyr from foraminifera tests and shell material within subunit 2-C, while down core in the same subunit an age of 8.2 kyr was derived from foraminifera tests, thus constraining the age of deposition of KC06 post-glacial sediments as older than ~8.2 kyr. All other ages are in stratigraphic order.

Radiocarbon ages in Unit 1 span ~7 kyr to present in outer and inner PIB. Subunit 1-A is dated in one core (TC49) as 1.3 k cal yr BP in inner PIB. Subunit 1-B ages vary by location; outer shelf age constraints include 19.0 k cal yr BP from the upper slope (PC03) and 16.7 k cal yr BP from the shelf edge (PC07), while subunit 1-B ages in outer PIB range from 6.2 (KC04) to 1.7 k cal yr BP (PC37). Subunit 1-C yields calibrated ages including 6.8 k cal yr BP (KC10) in outer PIB and 7.0 k cal yr BP to 4.3 k cal yr BP in inner PIB (PC37).

Unit 2 ages range from 12.2 to 7.8 k cal yr BP in outer PIB. Subunit 2-A yielded ages ranging from 10.1 (PC41) to 11.4 k cal yr BP (KC23) in outer PIB. Subunit 2-C yielded ages from 10.9 (KC06) to 7.8 k cal yr BP (KC09). Two shell samples from subunit 2-C, both in core KC13, were dated as radiocarbon dead, implying an age prior to the LGM and reflecting reworking. Subunits 2-B and 2-D were not dated due to a lack of carbonate material.

Unit 3 yielded ages which span 10.6 to 12.3 k cal yr BP (KC19). Samples from Ferrero Bay (Figure 3-1), outer PIB, range in age from 10.7 to 9.8 k cal yr BP (KC15). Units 4 and 5 were not dated due to a dearth of carbonate material.

Cruise <sup>a</sup>	Core <sup>b</sup>	Longitude [°W]	Latitude [°S]	Water Depth [m]	Core Length [cm]
OSO0910	KC04	-107.1105	-72.6971	729	208.8
OSO0910	KC05	-107.1105	-72.6971	729	245
OSO0910	KC06	-106.9100	-72.1325	612	102.8
OSO0910	KC07	-106.8823	-72.3394	707	50
OSO0910	KC08	-106.8439	-72.3469	711	40
OSO0910	KC09	-106.6390	-72.4867	548	45
OSO0910	KC10	-106.7736	-72.4923	687	88
OSO0910	KC11	-107.1518	-72.5762	733	150
OSO0910	KC12	-107.1908	-72.5705	735	104.5
OSO0910	KC13	-107.1687	-72.6407	742	226
OSO0910	KC14	-107.5130	-72.6503	639	72
OSO0910	KC15	-101.8362	-73.3603	1257	130
OSO0910	KC16	-102.0792	-73.4540	706	38
OSO0910	KC17	-102.8267	-73.4197	855	147
OSO0910	KC18	-106.8710	-73.3835	894	148.5
OSO0910	KC19	-106.9688	-73.1285	782	139
OSO0910	KC20	-107.0567	-72.9102	671	-1
OSO0910	KC21	-106.9563	-72.8268	728	60
OSO0910	KC22	-106.9633	-72.8187	724	115
OSO0910	KC23	-106.9243	-72.8923	660	36
OSO0910	KC24	-106.7568	-73.2398	807	160
OSO0910	KC25	-107.1057	-73.2570	838	77
OSO0910	KC26	-107.2223	-72.8645	689	106
OSO0910	KC27	-107.2548	-72.8828	666	52
DF81	PC03	-110.3500	-71.2167	1009	68
DF81	PC07	-109.0000	-71.2500	475	260
NBP9902	PC37	-109.8830	-72.8970	438	203
NBP9902	PC38	-107.5680	-72.9730	652	nr
NBP9902	PC39	-105.6710	-73.1870	495	59
NBP9902	PC40	-106.0500	-73.7900	953	58
NBP9902	PC41	-106.6480	-73.9170	957	215
NBP9902	TC49	-104.7500	-74.7590	852	48.5
NBP9902	PC54	-105.1370	-74.3060	1202	224

**Table 3-3 Information for sediment core sites for eastern Amundsen Sea Embayment**

<sup>a</sup>. OSO0910: Oden Southern Ocean 2009-2010; NBP9902: Nathan B. Palmer 1999-02; DF81: Deep Freeze 1981. <sup>b</sup>. PC: piston core; KC: kasten (gravity) core; TC: trigger core



### 3.5 Discussion

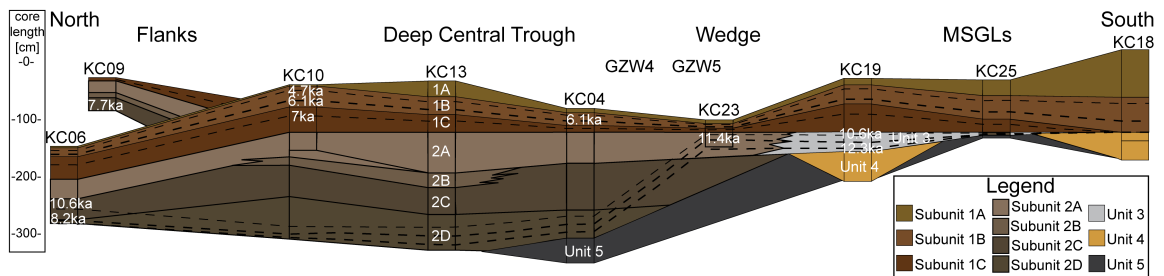


**Figure 3-6 Stratigraphic cross section of depositional facies in Pine Island Bay constructed along axis of trough.**

**Transect core locations delineated in Figure 3-2 (solid white line) and detailed core information found in Appendix A. Datum is the base of Unit 1, which is interpreted as a modern depositional unit (see text). Black dashed lines are isochrons for ages of deposition. Sedimentary units are designated on cores KC13, KC04 and KC19.**

#### 3.5.1 Depositional environment/sedimentary facies model

A detailed microstratigraphic approach was taken in examining cores from Pine Island Bay (Figure 3-6). Interpretations for each sedimentary unit are as follows, from basal Unit 5 through surficial Unit 1. The basal diamicton, Unit 5, is interpreted as till. It is characterized by high stiffness and lack of sorting, sedimentary structures or fauna, and a wide range of pebble lithologies (Anderson, 1999). The matrix grain-size distribution of the tills is similar in all locations despite color variations.

Muddy-sand Unit 4 is interpreted as a proximal glacimarine deposit. Its sorted coarse fraction and truncated fine fraction indicate winnowing (e.g. residual glacial marine sediment of Anderson et al., 1980) (Figure 3-4I). Based on the deep water occurrence (700–900 m), it is hypothesized that currents active near the grounding line,

potentially from water emanating from the ice-sheet front, were responsible for winnowing. This unit displays evidence for a reduction in current strength with time and theoretically increased distance from the grounding line, as seen in core KC18 by a decrease in sand content and corresponding increase in silt and clay content up-section.

Unit 3 is considered a sub-ice shelf facies based on an extremely low abundance of pebbles or sand (ice-rafted material) (Figure 3-4; Figure 3-5) (Kennedy and Anderson, 1989, Domack et al., 1999, Evans and Pudsey, 2002 and Kilfeather et al., 2011). There is, however, a high abundance of planktonic foraminifers (*N. pachyderma*), which also characterize sub-ice shelf sediments deposited beneath the Larsen B Ice Shelf and Amery Ice Shelf ( Domack et al., 2005 and Hemer et al., 2007). Unit 3 in outer PIB has sedimentological similarities to Facies 5 of Smith et al. (2011) in the western ASE (Figure 3-1D). Facies 5 is a homogenous, terrigenous silty clay, which contains a more diverse assemblage of foraminifera than Unit 3.

Unit 2 is an extremely poorly-sorted pebbly sandy mud that is interpreted as a proximal glacimarine facies, deposited near the grounding line of an ice sheet (Anderson et al., 1980 and Anderson et al., 1991). The high degree of scatter in mean grain size and sorting is a reflection of the low degree of influence by marine processes (Figure 3-5). The IRD composition is roughly the same as till (Unit 5), a characteristic of proximal glacimarine sediments. It has a discrete microstratigraphy of four subunits which record a change in depositional setting, from a “lift-off” facies near the grounding line to sub-ice shelf setting (Anderson, 1999 and Lowe and Anderson, 2002). The slight decrease in IRD upwards in the section is interpreted as either due to a decrease in current winnowing and/or ice rafting with increasing distance from the grounding line. Subunit 2-A is

interpreted as associated with an ice-shelf break-up event based on the presence of pelletized clays in some locations (granulated facies of Domack et al., 1999), abundance of IRD, and a small but diverse microfauna population, perhaps reflecting changing water mass conditions (Kilfeather et al., 2011).

The uppermost facies in all cores, Unit 1, is considered to be a distal meltwater-derived glacimarine deposit (possibly a 'plumite' as defined by Hesse et al., 1997). This interpretation is based on the fine grain-size, low microfossil content, low abundance of IRD and the draping character as observed in the chirp sub-bottom profiler data (Anderson et al., 2010). Subunits of Unit 1 do not display layering; rather they are very homogenous. Typically, turbid meltwater plumes are laminated in ice-proximal settings and become more massive with increased distance from the grounding line (O'Cofaigh and Dowdeswell, 2001), therefore we consider Unit 1 to be an ice distal deposit. The pebble content is limited in lithology to primarily mafic rock types, in contrast to the wide compositional range of pebbles in Units 2 and 5. The pebbles are likely derived from icebergs that are sourced from a limited surrounding region, as opposed to an ice stream that samples a vast area. Lowe and Anderson (2002) recognized this meltwater-derived silt in interior PIB where its thickness increases towards the modern grounding line. A similar facies in Marguerite Bay, Bellingshausen Sea is also suggested as derived from subglacial meltwater (Kennedy and Anderson, 1989, Anderson et al., 1991 and Kilfeather et al., 2011).

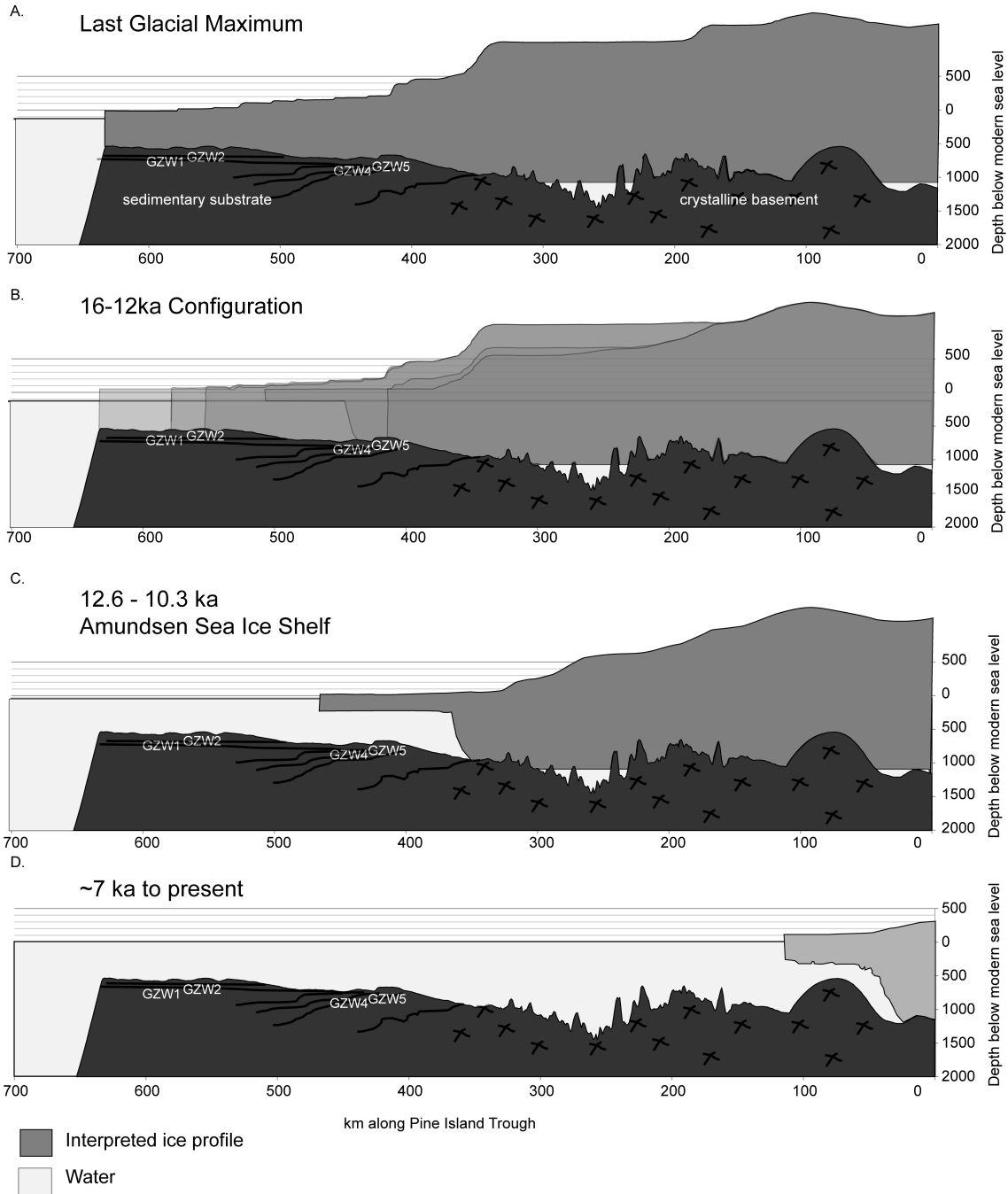


**Figure 3-7 Reconstructed cross section from continental shelf edge to the modern grounding location through the Pine Island Trough at significant intervals of the Pine Island Glacier retreat history.**

**Grounding zone wedges (GZWs) following nomenclature of Graham et al. (2010). Basement type interpreted from seismic data. A. Last Glacial Maximum**

**configuration. B. Deglaciation between ~16.4-12.3 k cal yr BP characterized by multiple stages of back stepping and a changing ice profile. C. Period of stability from ~12.3–10.6 k cal yr BP during which a large Amundsen Sea Ice Shelf was present. D. Location of the modern ice sheet.**

### 3.5.2 Deglacial history

To establish a deglacial history within Pine Island Bay, we first developed a careful foundation of depositional facies and stratal relationships. We then placed the radiocarbon results into our constructed stratigraphic framework, thus reducing ambiguity within the data and providing a more accurate deglacial chronology. The radiocarbon ages, whilst accurate and reliable, only provide a minimum age for deposition.

During its maximum extent the PIB ice sheet is suggested to have included one large ice stream and to have extended to the shelf edge (Figure 3-7A; Figure 3-8A). The shelf edge position is, however, tenuous and is based on a glacial unconformity imaged in seismic records and on the occurrence of gullies on the upper slope that are believed to have been conduits for sediment-laden water debouching from the ice sheet grounding line (Lowe and Anderson, 2002, Dowdeswell et al., 2006, Evans et al., 2006 and Graham et al., 2010). However, similar gullies occur on non-glaciated continental margins and may simply reflect upper slope mass movement (Walsh and Nittrouer, 1999, Pratson et al., 2007 and Fedele and Garcia, 2009). The unconformity is situated just a few tens of meters below the seafloor, but the surface is yet to be dated. Therefore, GZW1 is the most seaward limit for which there is conclusive evidence of grounding during the LGM and it is located ~450 km from the modern Pine Island Glacier terminus, or ~65 km from the shelf break (Graham et al., 2010).

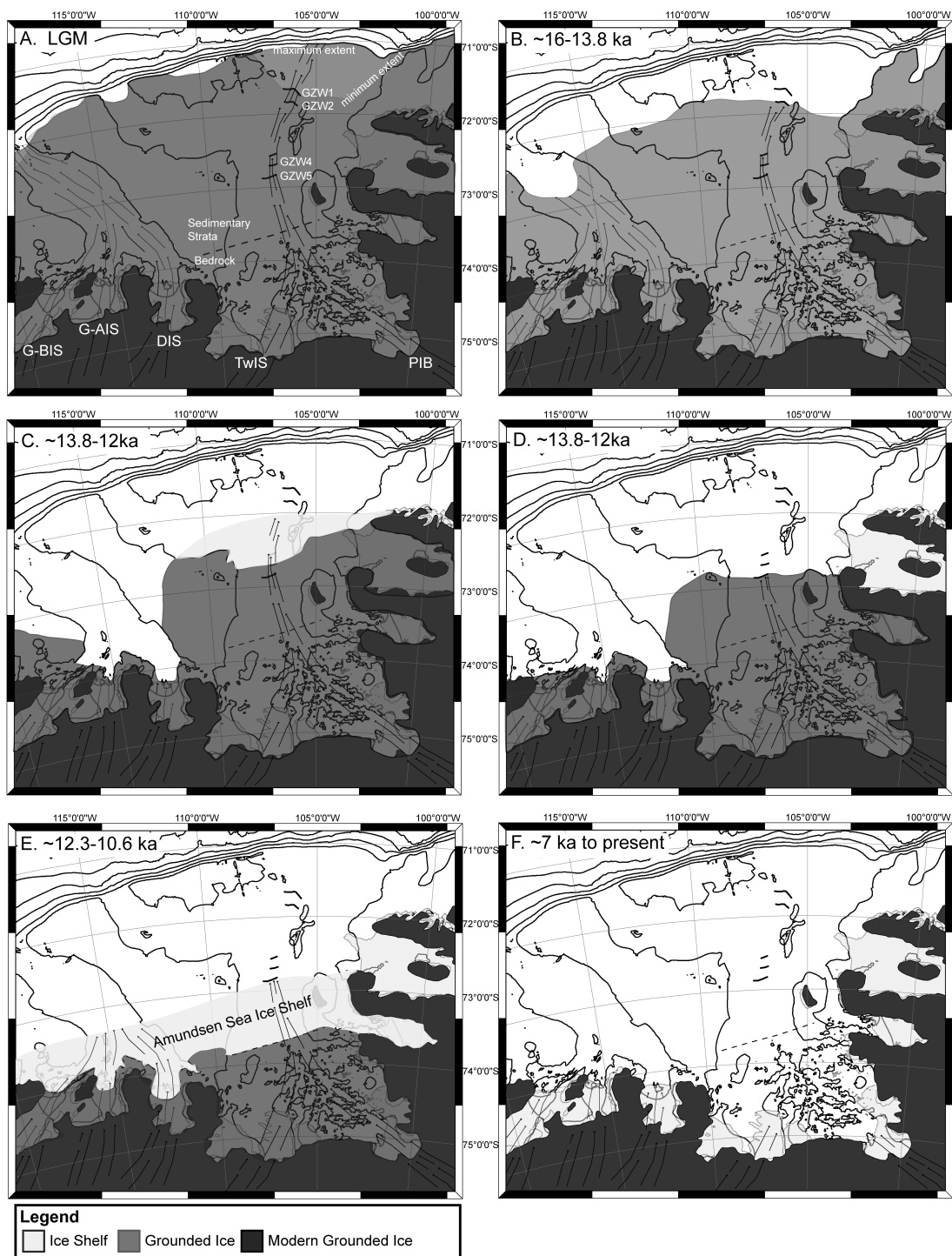


**Figure 3-8 LGM to Present Ice Sheet reconstruction for the Amundsen Sea Embayment.**

**Grounded ice in dark gray, Ice shelves in light gray. Black lines are 500 m isobaths. Interpreted flow lines are delineated by arrows pointing in the direction of flow. A. Last Glacial Maximum, B. ~16–13.8 k cal yr BP, C. ~16–12 k cal yr BP, D. ~16–12 k cal yr BP, E. ~12.3–10.6 k cal yr BP F. ~7 k cal yr BP to present configuration.**

In western ASE, ice sheet retreat from the outer shelf has been interpreted as having been underway as early as ~22.4 k cal yr BP (VC436 in 466 m water depth) (Smith et al., 2011). However, the outer shelf is riddled with iceberg furrows making it virtually impossible to acquire an undisturbed stratigraphic record of ice sheet retreat. What can be said is that glacial marine sediments began accumulating on the eastern ASE outer shelf before 16.4 k cal yr BP (DF-81 PC7), providing a minimum age for initial retreat of the ice.

Our results show that the ice sheet stepped landward from the position of GZW 1 to the middle shelf area (constrained by PC38 Figure 3-1B) between ~16.4 and 12.2 k cal yr BP (Figure 3-7B; Figure 3-8B, C, D). Retreat of the grounding line from the outer shelf in western ASE occurred over a similar time interval, reaching the mid-shelf before 13.8 k cal yr BP (Smith et al., 2011). The episodic nature of grounding line retreat on the mid shelf in eastern ASE is manifested as sharp contacts that separate discrete subunits of ice-proximal Unit 2, by mega-scale glacial lineations overprinted by grounding zone wedges, and by the formation of at least three additional grounding zone wedges (GZWs 2, 4, and 5) south of GZW 1 (Evans et al., 2006; Graham et al., 2010; Jakobsson et al., 2011, 2012). These grounding zone wedges, described in morphological detail in Jakobsson et al. (2012), record sediment accumulation at the grounding line during pauses in retreat. The lower-most subunit of Unit 2 (2-D) is restricted in distribution to

north of GZW 4 in outer PIB. This indicates that grounding-line proximal subunit 2-D formed while the grounding line was located at GZW 4. This is proposed by Jakobsson et al. (2011) as the most likely grounding line location associated with a major break-up of an ice shelf, and likely rapid retreat of the PIB ice stream. We interpret the sharp contact separating subunit 2-D and overlying 2-C as marking this rapid back-stepping of the grounding line and sediment source. Subunit 2-C was sampled on and seaward of GZW 5, necessitating a location of ice-sheet grounding south and proximal to this wedge. Overlying subunit 2-B is a transitional facies between subunits 2-C and 2-A that records more gradual retreat of the grounding line.

Sub-ice shelf deposits of Unit 3 record a period of grounding line stability that occurred between ~12.3 to ~10.6 k cal yr BP. Facies 5 in eastern ASE is remarkably similar and possibly records similar conditions at ~11.4 k cal yr BP (Smith et al., 2011). This interpretation calls for a large, continuous Amundsen Sea Ice-Shelf (ASIS) that would have extended across the mid shelf of the entire Amundsen Sea Embayment (Figure 3-7C; Figure 3-8E). A pan-ASE ice shelf was inferred by Hughes (1981) based on coastline physiography that encourages both the buttressing of the Pine Island and Thwaites Ice Streams and pinning against small islands. The most dynamically favorable grounding zone position at this time would be the transition between sedimentary and crystalline substrate (Figure 3-7C; Figure 3-8E) (Lowe and Anderson, 2002). The Pan-ASE ice shelf configuration remains speculative and requires further investigation to test this hypothesis.



An episode of rapid grounding line retreat and associated collapse of the ASIS ended the ~2.3 k yr period of ice shelf stability between ~12.3 and 10.6 k cal yr BP. This break-up is recorded both sedimentologically and geomorphically (Jakobsson et al., 2012). Geomorphic evidence includes regularly spaced corrugated furrows within the MSGLs that are attributed to a large coherent ice mass calving at the grounding line. This is both south of, and more recent than, the event observed by Jakobsson et al. (2011), where similar corrugation-furrows between GZW 2 and GZW 4 were interpreted as marking the collapse of an ice-shelf. We interpret subunit 2-A as having been deposited during this latter break-up event. We also note an abundance of ~10.7 k cal yr BP ages from reworked sediments within subunit 2-C (core KC06). A re-advance of the ice has been observed in the mapped landforms (Jakobsson et al., 2012). However, this did not leave an imprint in the stratigraphy captured in our sediment cores. This may be due to that the re-advance is both short time duration and spatially limited.

There is no geomorphic record of the ice sheet's retreat across the rugged inner bay where crystalline basement is exposed at the seafloor (Lowe and Anderson, 2002, Uenzelmann-Neben et al., 2007 and Graham et al., 2009). However, there is a mere ~0.8 k yr age difference between proximal glacimarine sediments of Unit 2 and distal glacimarine sediments of Unit 1, suggesting rapid grounding line retreat across the inner trough. We speculate that it is at this point in time when the confluent, large paleo-ice stream that occupied the outer Pine Island Bay trough split into two independent ice streams, the Pine Island and Thwaites, which occupied separate troughs (Figure 3-7D; Figure 3-8F).

The draping deposits of Unit 1 record the most recent conditions in PIB, dominated by widespread dispersal of fine-grained sediments. There is a virtual absence of diatoms and other biogenic material. Unit 1 contains three discrete subfacies with sharp contacts, recording punctuated deposition in PIB. Accumulation of Unit 1 began ~7.0 k cal yr BP. Subunit 1-B yielded radiocarbon ages of 6.1 k cal yr BP in two separate cores (KC04 and KC10) and an age of 4.7 k cal yr BP in one of the cores (KC10), documenting a minimum age span of deposition. Uppermost subunit 1-A began accumulating by ~1.3 k cal yr BP in inner PIB (TC49).

### **3.5.3 Mechanisms of glacial retreat**

An understanding of the mechanisms responsible for retreat in PIB, in conjunction with results from the western ASE (Smith et al., 2011), provide important constraints for glacial models, a longer-term context in which to evaluate modern changes, and insight into the processes which allow for ice sheets to self-destruct. The geologic record supports varied mechanisms influencing marine ice sheet retreat, including sea-level rise, oceanographic circulation, subglacial geology, trough morphology, and possibly subglacial meltwater storage and release.

Deglaciation commenced in eastern ASE after the LGM and before ~16.4 k cal yr BP. An elevated rate of eustatic rise of 5–7 mm/yr characterizes this period (Bard et al., 1996, Lambeck and Chappell, 2001 and Clark et al., 2009). This rate of sea-level rise undoubtedly contributed to instability of ice grounded on the relatively flat outer ASE continental shelf, especially if the ice sheet had a low profile as expected for a large paleo-ice stream. Sea-level rise has been suggested as the driving force in marine ice

sheet retreat from the Antarctic Peninsula continental shelf during about this same time interval (Heroy and Anderson, 2007). We hypothesize that the initial retreat was contemporaneous in both the eastern and western ASE given their similar outer-shelf physiographies.

Rapid, stepped retreat of the grounding line occurred in outer PIB between ~16.4–12.2 k cal yr BP. Pauses in retreat are recorded by at least three prominent grounding zone wedges and multiple subfacies of ice-proximal deposits. Over 40 m of sea-level rise occurred during this time interval, with a time-averaged rate of ~12 mm/yr (Clark et al., 2009). This was also a time of punctuated sea-level rise, including meltwater pulse 1-a (MWP 1-a), where sea-level rose by ~10–20 m in the short period between ~14.65–13.7 k cal yr BP (Fairbanks, 1989 and Clark et al., 2009). This particular event has been suggested as the mechanism for destabilizing portions of the ice sheet in the western ASE (Smith et al., 2011) and on the Antarctic Peninsula continental shelf (Heroy and Anderson, 2007). Given our chronologic constraints in PIB, we are unable to resolve the back-stepping as occurring in association with MWP 1-a. However, at this rate of sea-level rise the gentle relief of the eastern ASE provided ample opportunity for stepped grounding line retreat. The grounding zone wedges are located in narrow portions of the trough, implying a bottlenecking phenomenon in which the ice stream flow and retreat was also controlled by trough geometry (Jakobsson et al., 2012). In contrast, the western ASE appears to have deglaciated quickly and continuously, possibly a run-away retreat over the deep, landward-sloping Getz/Dotson trough (Smith et al., 2011). Modeled deglaciation in similar settings demonstrates that isolated eustatic events are not required for stepped retreat, rather more continuous sea-level rise coupled with variable trough

morphology can regulate grounding line retreat (Jamieson et al., 2011). The degree in which sea-level rise was compensated by isostatic uplift in the ASE is not constrained for this time period. It is assumed to be a negligible contribution based on the geomorphic features in outer PIB, particularly MSGs that imply the ice was streaming and had a low profile, thus exerting minimal force from loading and having almost neutral buoyancy. This is a configuration similar to the modern Ross Ice Sheet (Hughes, 1981).

The overall retreat of the marine ice sheet from PIB included at least two episodes of ice shelf disintegration (Jakobsson et al., 2011). CLIMAP solutions allow for an ice shelf to deteriorate in less than 100 years (e.g. Hughes, 1981). This model was recently verified by the collapse of the Larsen B ice-shelf in response to rapid atmospheric warming (Domack et al., 2005). However, given the polar location of the ASE, it is unlikely that isolated atmospheric change was the mechanism responsible for the disintegration of these ice shelves. The presence of planktonic foraminifers in the sub-ice shelf facies associated with the disintegration event from ~12.3–10.6 k cal yr BP seems to provide evidence for oceanic waters flowing onto the continental shelf during this time. The exact temperature and nature of the water mass is unconstrained, however, it was likely 3–4 °C warmer than the sub-ice shelf waters based on modern measurements (Jacobs et al., 1996 and Jacobs et al., 2011). Similarly, a presence of abundant, well-preserved planktonic foraminifera in sub-ice shelf sediments have been associated with landward currents beneath the Amery Ice Shelf (Hemer et al., 2007). Both the eastern and western ASE sediments record coincident onset of ice-shelf retreat, despite separate troughs incising into the outer shelf to different depths (400–500 m water depth in the west and 550–640 m water depth in the east) and an expansive topographic high between

them. The western ASE trough is much broader than the eastern trough, and appears to flatten with increased distance towards the shelf break. Contemporaneous ice shelf disintegration across the entire region suggests that the mechanism for delivering warmer water onto the inner shelf and in contact with the ice affected the entire ASIS. This is in contrast to circumpolar warm deep water presently impinging via the deeply incised Pine Island Trough (Jacobs et al., 1996 and Jacobs et al., 2011). Therefore, we propose that the collapse of the ASIS after 10.3 kyr was the result of a warmer water mass encroaching onto the broad continental shelf and thermally eroding the base of the ice shelf. Regional grounding line retreat was then promoted by the removal of an ice shelf.

The rather sudden shift in style of deposition in PIB, from grounding-line proximal and sub-ice shelf facies to a draping silt unit, occurred within a relatively short (0.8 k yr) time interval. This change in sedimentation was associated with grounding-line retreat from the flat outer portion of PIB onto the rugged seafloor of inner PIB.

Highly varied bedrock topography, in conjunction with a relatively slow rate of sea-level rise after  $\sim 7.5$  k yr, would have significantly limited the role of sea-level rise in grounding line instability. What then was the mechanism responsible for continued, and relatively rapid, grounding line retreat during the late Holocene? We suggest that underpinning of the grounding line by subglacial water may have caused this final phase of deglaciation. This hypothesis is based on the interpretation that the youngest silt facies was derived from water released from subglacial basins on the inner shelf due to a change in hydraulic potential associated with thinning of the ice sheet. The movement of subglacial water has been demonstrated in smaller systems to increase glacial speed and promote instability (e.g. Wingham et al., 2006, Fricker et al., 2007 and Stearns et al.,

2008). The three subunits of the upper Unit 1 facies may even record separate episodes of water release. Ongoing research is aimed at testing this hypothesis.

### 3.6 Conclusions

We propose that Pine Island Bay is a type-location for understanding the dynamics of marine-based ice sheets, where multiple mechanisms have affected the ice sheet throughout its deglacial history. The style of deglaciation in Pine Island Bay has varied since the Last Glacial Maximum, with accelerated retreat alternating with relative stability. The summarized post-LGM deglacial history in Pine Island Bay is as follows:

- Deglaciation from the LGM configuration commenced in eastern ASE between the LGM and ~16.4 k cal yr BP from buoying due to rising sea level.
- Grounding line retreat continued from 16.4 to 12.3 k cal yr BP during an interval of rapid global sea-level rise. Shelf morphology controlled the tempo of retreat. Eastern ASE had a gradual, stepped retreat and formed grounding zone wedges during brief intervals of stability. The western ASE deglaciated in one large event due to sea-level rise and the over-deepened, rugged seafloor morphology.
- The initial phase of deglaciation, from LGM through 12.3 k cal yr BP, in the ASE demonstrates the sensitivity of marine-based ice sheets to eustatic sea-level rise on the relatively flat outer-continental shelf, as the ~55 m rise in sea-level resulted in up to 225 km of grounding line retreat of the paleo-PIB ice sheet.
- Sediments and geomorphology record the presence and collapse of at least two ice shelves. From ~12.3–~10.6 k cal yr BP the Amundsen Ice Shelf spanned the

entire ASE. Collapse of this ice shelf and associated grounding line retreat after ~10.6 k cal yr BP is marked by an occurrence of *N. pachyderma* that indicate warmer water flowing onto the entire shelf. This event occurred after ~10.6 k cal yr BP.

- Underpinning by subglacial water may have caused the final phase of grounding line retreat across rugged inner PIB as evidenced by the geomorphic features of the inner trough (Lowe and Anderson, 2003) and by the widespread sedimentation of a draping silt unit that is interpreted as having been derived from waters flowing from beneath the ice sheet. This retreat began ~7.8–7.0 k cal yr BP.

Pine Island Bay demonstrates the complexity in what has been interpreted as “perhaps the most important challenge in glaciology; understanding how ice sheets self destruct.” (Hughes, 2011). One cause of deglaciation does not characterize the post-LGM history in this bay, rather it is a saga comprised of multiple mechanisms over a range of time scales.

# **Meltwater Intensive Glacial Retreat in Polar Environments and Investigation of Associated Sediments: example from Pine Island Bay, West Antarctica**

Modern Pine Island and Thwaites Glaciers, which both drain into Pine Island Bay, are some of the fastest changing portions of the cryosphere and is among the least stable ice streams in Antarctica. Here we show that the uppermost sediments in Pine Island Bay were deposited from a meltwater plume, a plumite, which occurred during the late stages of ice sheet retreat ~7-8.6 k cal yr BP. It is a hydraulically sorted, glacially sourced unit that we separate into three subunits. This is a draping deposit that overlies proximal glacial marine sediments and thickens towards the modern grounding line.

The inner part of Pine Island Bay contains several basins that are linked by channels with a storage capacity on the order of 70 km<sup>3</sup> of water and sediment. The



plumite is a product of non-steady-state processes in which low background sedimentation alternates with sediment sequestration in the large bedrock-carved basins and episodic purging. This is caused by changes in hydraulic potential and glacial reorganization. The most recent release of sediment coincides with rapid retreat of the grounding line, and has an order of magnitude greater flux relative to the entire unit, indicating episodic sedimentation.

Our identification of a meltwater-derived deposit has profound implications for understanding glacial instability and numerical modeling studies of ice sheet dynamics for more improved prediction of future sea level. This study demonstrates that punctuated meltwater-intensive glacial retreat occurred at least three times in the Holocene in this region. We further suggest that the modern Thwaites Glacier is poised for an analogous meltwater-intensive similar retreat.

## **4.1 Introduction**

The last few decades of Antarctic research has yielded several examples for diachronous and stepped retreat of ice sheet grounding lines around the Antarctic margin following the Last Glacial Maximum (LGM). The mechanisms that have been put forward for forcing grounding-line retreat, and thus the promotion of instability, include: buoying by sea-level rise, thinning from accelerated glacial flow, basal melting from impinging warmer waters and under-pinning by subglacial meltwater. These mechanisms were apparently active at different times and locations throughout the post-LGM retreat, due in part to bathymetric controls (e.g Heroy and Anderson, 2007; Mosola and

Anderson, 2006; Ó Cofaigh et al., 2008; Kirshner et al., 2012; Livingstone et al., 2012; Anderson et al., in press).

Subglacial water is hypothesized to play a critical role in glacial stability by altering basal the conditions that control glacial sliding and stability (Kamb et al., 1985; Kamb, 1987; Fowler, 1987; Sharpe, 1988, Alley, 1989; Walder and Fowler, 1994; Anandakrishnan and Alley, 1997). Modern remote sensing measurements have yielded evidence for the movement of considerable volumes of water beneath the Antarctic Ice Sheets (Gray et al., 2005, Wingham et al., 2006, Fricker et al., 2007; Carter et al., 2009; Schroeder et al., in review). Direct observation on Byrd Glacier documented the movement of water, corresponding to an increase in glacial flow speed (Stearns, 2008) and highlights the potential of subglacial hydrology to influence ice sheet dynamics.

Evidence for subglacial water having contributed to past instability of the ice sheet is derived from bathymetric maps of the catchment areas of former ice streams. Extensive, organized subglacial drainage networks consisting of basins linked by channels have been identified using multibeam swath bathymetry in Marguerite Bay (Anderson and Fretwell, 2008) and in Pine Island Bay (Lowe and Anderson, 2003; Smith et al., 2009; Nitché et al., 2012). Geomorphic evidence for organized meltwater drainage also exists in the Transantarctic Mountains (Sugden et al., 1991, Denton and Sugden, 2005; Lewis et al., 2006), but these drainage networks appear to be much older and more confined than those in Marguerite and Pine Island bays. The question remains, when were these drainage networks active and did they contribute to instability of the ice sheet?

Here we describe unique sedimentary deposits that, to our knowledge, have been discovered only in Marguerite Bay and Pine Island Bay and are inferred to have a meltwater origin followed by dispersal by marine currents (plumites by the nomenclature of Hesse et al., 1997). The meltwater origin of these sediments is based primarily on observed draping seismic character, sorted grain-sizes of terrigenous silt and very fine sand and a low abundance of microfossils and ice-rafted debris (e.g. Kennedy and Anderson, 1989; Lowe and Anderson, 2003; Smith et al., 2009; Kirshner et al, 2012). We extend this work with an investigation of the Pine Island Bay. This research includes: quantitative geomorphology, sedimentology, and radiometric constraints on the age of deposition. This extensive suite of data enables us to calculate the rate of deposition for meltwater deposits as well as sediment flux. We use this information to discuss a comprehensive reconstructed glacial history, assess the feedback between changes in meltwater storage, ice thickness, subglacial hydrological processes and ice stream activity, and gauge the potential magnitude of meltwater discharge and its influence on ice sheet instability.

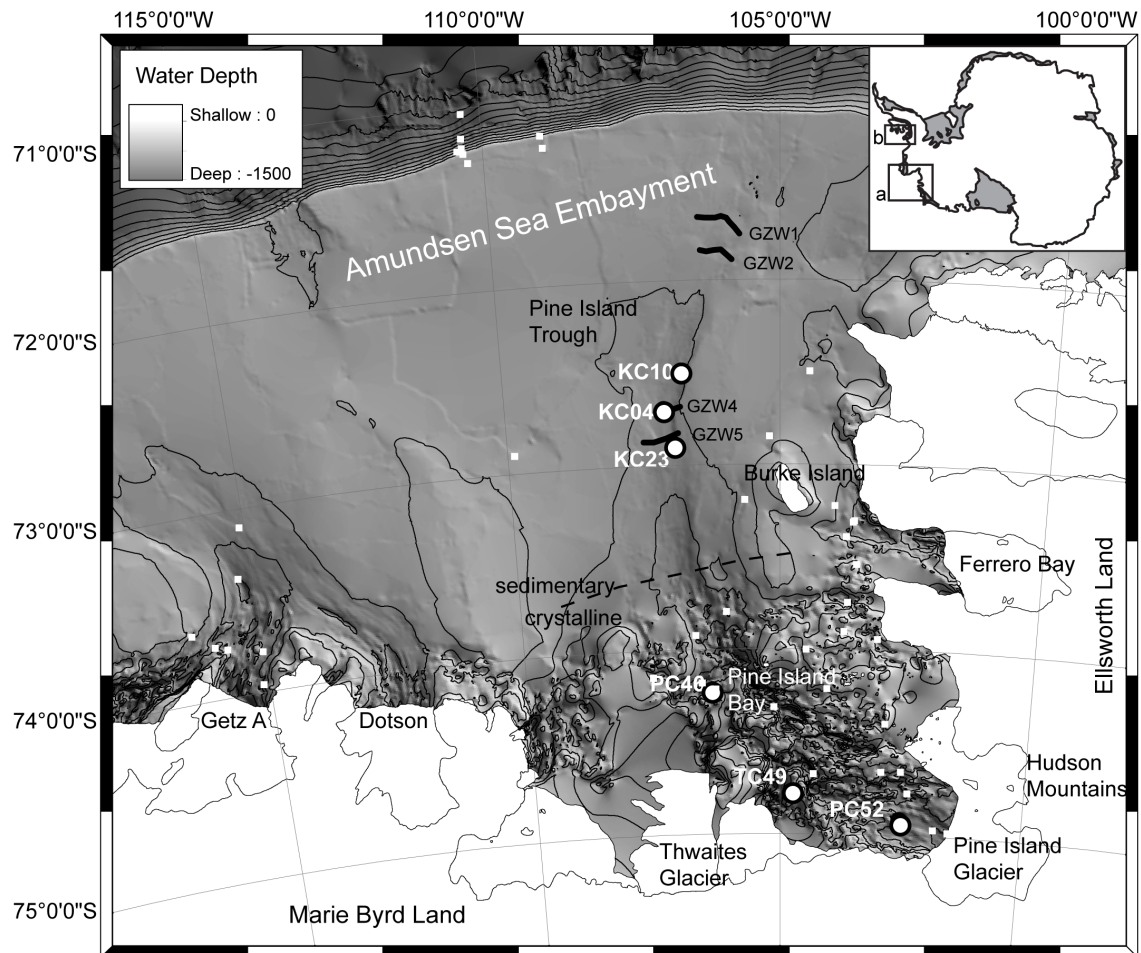


**Figure 4-1 Bathymetry map of the Amundsen Sea with inset maps showing locations of Pine Island Bay**

**(a) and Marguerite Bay (b). Bathymetric data is a compilation from all cruises to the region (Nitsche, 2007; Nitsche et al., 2012). Contour interval is at 200 m. The boundary between sedimentary and crystalline bedrock is denoted in dashed line at ~73.5°S. Cores used in this study are designated with white squares. Other cores used to map the distribution of Unit 1 are shown with white circles. KC- Kasten Core, PC- Piston Core, TC- Trigger Core. Cores were collected on expeditions NBP99-02 and OSO0910. Grounding zone wedge (GZW) nomenclature from Graham et al (2010).**

#### 4.1.1 Geologic Setting

Pine Island Bay is located in the Amundsen Sea Embayment (ASE), West Antarctica, a truly polar regime (Figure 4-1). The modern ice sheet is ~1 km thick at its grounding line, generally is 2-3 km thick, and levels off to ~3.5 km thick in the catchment region (Vaughan et al., 2006 and Holt et al., 2006). PIB is bounded to the east by the Hudson Mountains and Ellsworth Land and to the south by Marie Byrd Land. Within the bay, Burke Island lies in the northeast and the large Pine Island Trough extends across the continental shelf. Glaciers that drain into the Amundsen Sea Embayment include Pine Island Glacier to the south and Thwaites Glacier to the southwest. Further inland and to the south of Pine Island Glacier is the Bentley Subglacial Trough, and south of the Thwaites Glacier is the Byrd Subglacial Basin. The Amundsen Sea Glaciers drain approximately 25% of outflow from the entire West Antarctic Ice Sheet into Pine Island Bay (Vaughan et al., 2008). The drainage basin for the Pine Island Glacier is 184,000 km<sup>2</sup> and the Thwaites Glacier is nearly equal in area at 189,000 km<sup>2</sup> (Joughin et al., 2009). The modern glaciers draining into the ASE are thinning and accelerating at unsustainable rates, and it has been suggested that Pine Island Glacier is currently in a state of retreat (Rignot, 2008; Jenkins et al., 2010; Jacobs et al., 2011, Pritchard et al., 2012). Pine Island Glacier was grounded on a large transverse bedrock ridge as recently as the 1970's, but has recently uncoupled from this ridge (Bindschadler et al., 2002; Jenkins et al., 2010).

#### **4.1.1.1 Geomorphology**

Pine Island Bay south of  $\sim 73.5^{\circ}\text{S}$  is characterized by rugged crystalline bedrock, with bathymetric relief of over 400 m (Lowe and Anderson, 2002; Nitsche et al., 2012) (Figure 4-1). This region will henceforth be referred to as inner Pine Island Bay, following the nomenclature of Kirshner et al., (2012). The geomorphology of inner PIB has been noted as being indicative of a subglacial drainage system (Lowe and Anderson, 2003; Nitsche et al., 2012), displaying a well-organized, seaward-convergent, channel network sculpted into bedrock. The age of this seascape has yet to be determined, but is thought to have formed over numerous glacial/interglacial cycles (Lowe and Anderson, 2003). Deep channels connect otherwise isolated basins which may have the potential to store considerable volumes of water (Nitsche et al., 2012).

North of  $\sim 73.5^{\circ}\text{S}$ , Pine Island Bay has a sedimentary substrate. This region will be referred to as Outer Pine Island Bay/Outer Shelf, following the nomenclature from Kirshner et al., (2012). Geomorphic features in Outer PIB/Outer Shelf are indicative of grounded, streaming ice and include grounding zone wedges and mega-scale glacial lineations. Other geomorphic features include plough moraines, corrugation ridges and corrugation moraines (Lowe and Anderson 2002; Graham et al., 2010; Jakobsson et al., 2011; 2012).

#### **4.1.1.2 Regional Oceanography**

The Amundsen Sea Embayment contains three primary water masses. An upper  $\sim 50\text{-}100$  m surface layer that is influenced by melting sea ice and icebergs, wind, and

solar radiation, a middle layer of Ice Shelf Water (ISW), that is a mix of Circumpolar Deep Water (CDW) and ice shelf melt-water, and a lower (below ~500 m) water mass composed entirely of CDW. This CDW is warm ( $\sim 1^{\circ}\text{C}$ ), saltier and more dense than ISW. The ISW layer is seasonally modified and extends from ~100-450 m in the water column (Jacobs et al., 2011; Mankoff et al., 2012). In addition to these water masses, oceanographic measurements have revealed almost undiluted Circumpolar Deep Water below the pycnocline impinging onto the continental shelf through deep submarine troughs (Jacobs et al., 1996; Shepherd et al., 2004; Jenkins et al., 1997; Hellmer et al., 1998).

Positive temperature, salinity and current anomalies have been observed near the modern floating terminus of Pine Island Glacier, revealing a buoyant plume of melt-laden, deep outflow. This outflow becomes entrained and follows the general cyclonic circulation within PIB (Mankoff et al., 2012). Additionally, some of the outflow into PIB introduces a less buoyant plume that is well below the sea surface and unseen by satellites (Hellmer et al., 1998; Jenkins et al., 2010; Mankoff et al., 2012). Semidiurnal tides are observed in both ISW and CDW, with the strength and direction of tidal forces varying between the two layers. ISW exhibits stronger tidal influence, which are directed in and out of the ice shelf cavity, while the CDW has lower tidal energy and is directed primarily parallel to the ice-shelf cavity front. Contrast between the tidal forces contributes to mixing and circulation within the sub ice-shelf cavity (Robertson, 2010). Plume dynamics and the spatial distribution of ice melt have been modeled as influenced by both Coriolis effect and sub-shelf topography (Payne et al., 2007). Temporal variability in the presence of CDW is forced by the Amundsen Sea Low Pressure System

and, in turn, by regional winds, with periods of stronger westerly winds resulting in the on-shelf flow of CDW through the deep troughs of the continental shelf (Thoma et al., 2008). Basal melt rates of the Pine Island floating terminus are as high as one order of magnitude larger than those recorded on other Antarctic ice shelves and ice tongues, measured between 6-12.5 m/yr (Hellmer et al., 1998). The modern rapid recession of the Pine Island Glacier has been proposed to be due to thermal erosion by the impinging CDW at the grounding line and melting at the base of the ice shelf (e.g. Jacobs et al., 1996; 2011; Thoma et al., 2008).

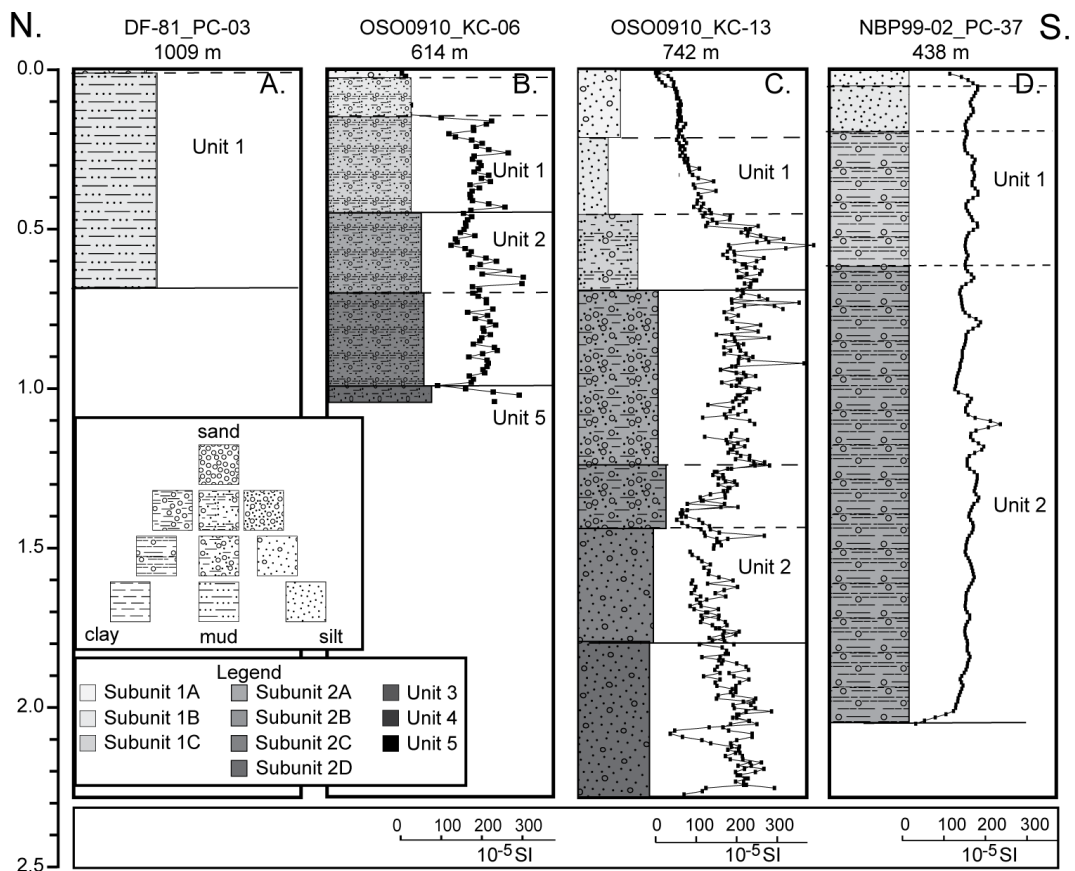




**Figure 4-2 Idealized retreat stratigraphy in Pine Island Bay using representative cores along north-south transect (modified from Kirshner et al., 2012). See Figure 4-1) for more detailed locations. Magnetic susceptibility curve in black. A. Outer shelf-upper slope region. B. Outer PIB-flanks region. C. Outer PIB-deep basin region. D. Inner PIB**

#### 4.1.1.3 Sedimentology

Sediments in Pine Island Bay have been interpreted as recording a retreat stratigraphy (Lowe and Anderson, 2002; Kirshner et al., 2012; Hillenbrand et al., 2013). A generalized facies model is consistent throughout, which is a glacimarine sandy mud, overlying ice proximal pebbly sandy mud, overlying till (Figure 4-2) (Kirshner et al., 2012). The upper glacimarine sandy mud will henceforth be called Unit 1 following the nomenclature of Kirshner et al., (2012) (lithofacies MSi, S, and MSa of Hillenbrand et al., 2013). It consists of three sandy mud subunits that always occur in stratigraphic order. Unit 1 is an interpreted meltwater-derived facies (Kirshner et al., 2012). In chirp sub-bottom profiles, Unit 1 is acoustically layered and draping (Anderson et al., 2010). Its thickness increases towards the modern grounding line and with increased water depth (Lowe and Anderson, 2002).

Unit 1 is massive, devoid of any bioturbation or sedimentary structures and has a low shear strength (~1.96 to 2.94 kPa) (Lowe and Anderson, 2002; Kirshner et al., 2012). All three subunits (1A, 1B, 1C) have been described as light olive brown (2.5 Y 5/3 Munsell color) to olive brown (2.5 Y 4/3-4). The sand and silt content vary, coarsening down unit with an almost doubling of sand and with relatively constant clay throughout the unit (~25-27%). Pebbles are primarily of mafic rock types with a low abundance, but

increase in abundance near the base of the unit. Magnetic susceptibility matches the sand and pebble concentrations, remaining low and uniform near the top with a more varied response at the base (Figure 4-2). Unit 1 contains abundant and diverse foraminifera in the upper portions of the unit, with decreasing abundance down section. It is generally diatom barren.

#### **4.1.1.4 Marine Record of Deglaciation**

The ice sheet maximum and LGM glacial configuration within inner PIB is reconstructed in relative detail on the inner shelf but more poorly constrained on the outer continental shelf (Figure 4-1) (Lowe and Anderson, 2002; Evans et al., 2006; Graham et al., 2010; Kirshner et al., 2012). During the LGM, the paleodrainage was characterized by confluence of the Pine Island Ice Stream and Thwaites Ice Stream, as well as other smaller systems, within the bay. This extended system is referred to as the Pine Island Paleo-ice stream based on the geographic location within Pine Island Bay. Initial retreat from the outer continental shelf began shortly after the LGM and before 16.4 ka, likely as a response to rising sea level. Between ~16.4 ka and ~12.3 ka the ice retreated episodically across the continental shelf, pausing for long enough to deposit at least three grounding-zone wedges (Lowe and Anderson, 2002; 2003; Evans et al., 2006; Smith et al., 2011; Jakobsson et al., 2012; Kirshner et al., 2012). Following the episodic retreat into central Pine Island Bay, the grounding line stabilized from ~12.3 to ~10.6 ka, allowing an ice shelf to form, which is hypothesized to have extended from eastern Pine Island Bay to the Getz/Dotson Region (Kirshner et al., 2012). The ice shelf collapsed sometime between ~10.6- 7.7 ka, following the period of stability in Pine Island Bay,

likely from thermal erosion by impinging warm water masses (Jakobsson et al., 2011; Kirshner et al., 2012). The facies of interest for this study, the interpreted subglacial meltwater Unit 1, began to accumulate after  $\sim 7.7$  ka, as ice retreated across the rugged inner shelf (Lowe and Anderson, 2002; Kirshner et al., 2012). During this time period, the Pine Island and Thwaites Ice Streams separated. This may have occurred as early as  $\sim 10.3$  ka, suggesting that the grounding line position in inner PIB was mostly stable throughout the Holocene, and that any episodes of fast retreat would have been short-lived (Hillenbrand et al., 2013).

## **4.2 Materials and Methods**

The facies of interest, Unit 1, was previously examined at roughly ten centimeter resolution; the unit ranges from  $\sim 5$ -450 cm thick (e.g. Lowe and Anderson, 2002; Kirshner et al., 2012). For this study we characterized this facies in more detail to test the hypothesis that it was transported by subglacial meltwater. The sediment cores and geophysical data used in this study were acquired during multiple cruises to Pine Island Bay, primarily Deep Freeze 1985, *Nathaniel B. Palmer* 1999-02, *Nathaniel B. Palmer* 2000-01, and a cruise of the Icebreaker *Oden* in 2010 (OSO0910). Additional information can be found in Appendix B.

### **4.2.1 Sediment Characterization**

Sediment cores used for in-depth investigation in this study are from expedition NBP99-02 (cores of focus include piston core PC52, both trigger and piston core TC/PC46, and trigger core TC49) and expedition OSO0910 (cores of focus include

kasten cores KC23, KC04, and KC10). Locations of these cores are shown in Figure (4-1). Details of the onboard core processing for samples collected on expedition OSO0910, including the acquisition of multi-sensor core log data, can be found in Anderson et al. (2010), and the onboard core processing for NBP99-02 in Curren (1999). Multi-sensor core log data for cores from NBP99-02 were acquired at the Antarctic Marine Research Facility at Florida State University (ARF). The multi-sensor core loggers acquired physical property data of bulk density, p-wave velocity and magnetic susceptibility. X-radiographs of cores were acquired at the ARF. The x-radiographs were analyzed for sedimentary structures and for pebble abundances. For all cores, sediment visual core description includes: Munsell sediment color, texture, sorting and sedimentary structure. From this data, Unit 1 was identified in all cores throughout PIB. Kirshner et al., (2012) described all post-LGM facies in significant detail, including the facies of interest, Unit 1. Hillenbrand et al., (2013) described Unit 1 in innermost PIB in three cores from R/V *Polarstern* expedition ANT-XXVI/3 in 2010.

Matrix grain size was quantified at Rice University following the methods of McCave et al., (1986) with a Malvern Mastersizer 2000 laser grain-size analyzer. Sample spacing was at one centimeter increments throughout Unit 1. In core TC/PC46, clasts are too coarse for laser grain size analysis. In this core, grain size was calculated by measuring two grain lengths in perpendicular directions using calibrated pixels with the Photoshop™ software. Bulk size was categorized following the naming scheme of Folk and Ward (1957).

Quartz grains were isolated for grain surface texture and shape measurements. Extreme care was taken throughout the sample preparation processes to avoid mechanical abrasion and to preserve surface textures and grain shape integrity. Approximately 1 gram of sediment from each sample interval was collected for shape and micromorphology analysis. For grain shape analysis, between 50-400 individual grains per sample were examined to calculate Fourier coefficients. The grains were grouped as very fine-to fine sand and fine-to medium sand (methods modified from Dowdeswell (1985)). The largest sand grain analyzed for shape was 1 mm, the smallest silt grain was 7  $\mu\text{m}$ . The second harmonic is a proxy for vertical elongation of grains and is correlated to Rittenhouse sphericity values (Mazzullo and Ritter, 1991). Higher harmonics are correlated with the angularity of the grains and the roughness of the surface (Krumbein and Pettijohn 1938, Lees 1964). The roughness coefficient is given by the following equation:

$$R_{ca-b} = \sqrt{0.5 \sum C_n^2} \quad (\text{Eq. 4-1})$$

The roughness coefficient,  $R_{c_{16-20}}$ , is indicative of roughness of grains. The roughness coefficient for each grain is calculated from the sum of the harmonic coefficients,  $C_n$ , from the 16th to the 20th harmonic (Dowdeswell, 1985).

A random subset of the grains that underwent Fourier grain shape analysis were used for the study of microfeatures. Over 100 grains of either sand sized or silt sized particles per sample were analyzed for surface micromorphology using a FEI Quanta 400 high-resolution field emission scanning electron microscope in high vacuum mode. The composition of each grain was verified as pure  $\text{SiO}_2$  with Energy Dispersive X-ray

Spectroscopy. Morphologic textures were identified based on the criterion and examples from Mahaney (2002). Fifteen microtextures were recorded as present or not-present in groups based on the process of microtexture formation (Sweet and Soreghan, 2010; Kirshner and Anderson, 2011). The groups include; polygenetic features comprised of fracture faces, sub-parallel linear fractures, conchoidal fractures, arc-shaped steps, linear steps, sharp angular features; sustained high stress features consisting of crescentic gouges, straight grooves, curved grooves, deep troughs, and mechanically upturned plates; percussion features of v-shaped percussion cracks and edge rounding; chemical dissolution/diagenesis features such as dissolution etching; and diagenetic physical weathering resulting in a weathered surface.

The clay size fractions (<4  $\mu\text{m}$ ) of nine samples in one down-core profile of NBP99-02 TC46 were analyzed for X-ray diffraction analysis (XRD). Powdered samples were analyzed at K/T GeoServices, Inc. using a Siemens D500 automated powder diffractometer equipped with a CuK $\alpha$  radiation source (40 Kv, 35 mA) and a solid state scintillation detector. This uses a semi-quantitative determination of the weight percentage mineralogy, weight percentage <4  $\mu\text{m}$  material and the determination of the mixed-layer clay types by weight percentage. Additional XRD data can be found in Lowe and Anderson (2002) for ten total samples in four cores and Ehrmann et al. (2011) for 64 core surface samples and 6 down-core profiles throughout the Amundsen Sea Embayment to provide geochemical context for the analysis.

#### 4.2.2 Multibeam Swath Bathymetry Mapping and Analysis

Our geomorphic investigation includes all of PIB and the outer shelf, but concentrates on inner PIB to assess the storage potential and transport paths of the proposed subglacial drainage networks. The complete bathymetric data-set used for this study was acquired over multiple cruises to Pine Island Bay including NBP99-02, NBP00-01, and OSO0910, with the regional bathymetry map based on Nitsche (2007; 2012) gridded to a spatial resolution of 200 meters. Seafloor morphology was interpreted and analyzed with the ESRI ArcGIS™ software package.

Using an interpreted ice sheet history based on Kirshner et al., (2012), subglacial basins were delineated following the contour depth at which ice is hypothesized as being grounded. The depth of grounded ice is related to ice sheet thickness based on the required buoyancy of a grounded ice shelf from the density differences of liquid water to ice (Eq. 4-2).

$$h = \left( \frac{\rho_i}{\rho_w} \right) [d + \Delta d_{LGM}] \quad \text{Eq (4-2)}$$

Here  $h$  is calculated ice thickness,  $\rho_i$  is the approximate density of ice,  $\rho_w$  is the approximate density of sea water,  $d$  is water depth from bathymetric data, and  $\Delta d_{LGM}$  is the sea level difference at the LGM, which is approximated as 120 m. The grounding positions considered are the sedimentary-crystalline boundary and a topographic high on the inner shelf (dashed line in Figure 4-1). Since the grounding zone marks the transition from grounded ice to floating ice, the depth of the modern seafloor at these two grounding positions dictates ice sheet thicknesses of 1500 m and 1300 m, respectively.

Based on these two grounding zone locations and associated ice thicknesses, two sets of subglacial basins were mapped. The length of each of these basin was measured down the longest axis of the basin that is in the interpreted direction of flow. The width of each basin was measured at the widest portion of the basin that is perpendicular to the axis along which the length was determined. Distance from the modern grounding-line was measured for each basin in a straight line from the center of the mapped basin to the grounding line in the direction of flow. The volume of each of the basins is a first order approximation using a flat surface at the elevation enclosing the site-specific perimeter. The primary paths of water flow feeding and draining the basins of inner PIB were also mapped. Longitudinal profile plots the modern seafloor depth along the axis of these mapped channels.

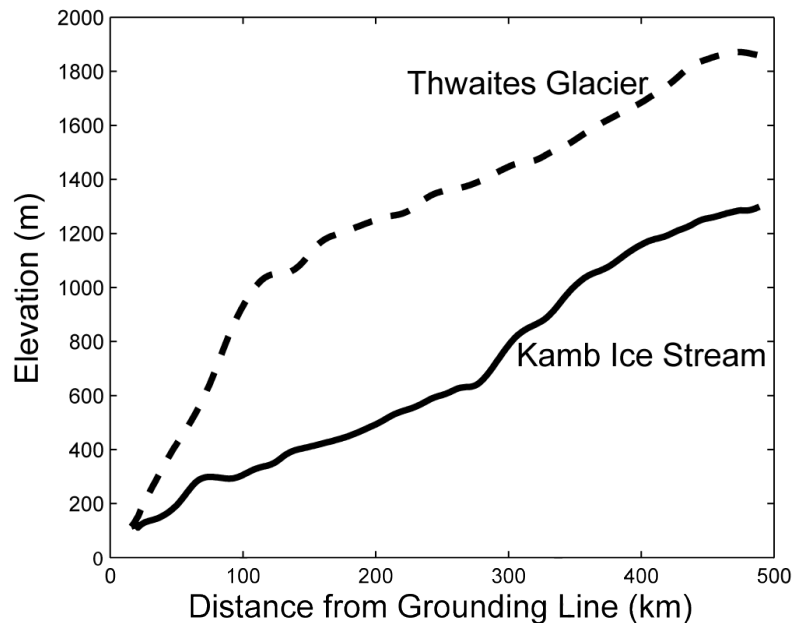


**Figure 4-3 Ice stream profiles from Kamb Ice Stream (formerly Ice Stream C) (black line) and Thwaites Glacier (dashed line) (see Figure 4-10 for location).**



### 4.2.3 Hydraulic Analysis

An analysis of potential for meltwater storage was conducted based on several ice sheet grounding scenarios determined from Kirshner et al. (2012). Two end member ice sheet profiles were considered, using the shallowly sloped Kamb Ice Stream (formerly Ice Stream C) and the steeply sloped Thwaites Ice Stream (Figure 4-3). Slopes were acquired from BEDMAP elevation (Lythe et al., 2000), and then smoothed over a 15 km window using a normally weighted average of adjacent pixels to ensure that the effects of surface roughness associated with these locales on our hydraulic interpretation were minimized. Ice sheet thicknesses were computed with neutral buoyancy at the grounding line and assumed initially to fill all the cavities in the bathymetry. The hydraulic head (ice overburden pressure) was then computed, where local head minima are the points about which subglacial water may have accumulated. This subglacial lake identification algorithm was modeled after Carter et al., (2007). Lakes are traced around hydraulically flat regions larger than 1 km equivalent diameter, where flatness is defined as a change in hydraulic head of less than 0.1% over the lake area. Lake volumes fill the bathymetry to a flat ice base at the maximum elevation of the lake shoreline. Lakes found on relative bedrock highs are excluded. This numerical simulation considers plausible configurations, but does not determine the extent to which subglacial basins were filled with meltwater.

### 4.2.4 Dating Methods

Samples from Unit 1 were examined in intervals denoted in each cruise report as containing foraminifera or other forms of carbonate material. No new radiocarbon dates

were collected for this study, but the previously collected data provide a valuable chronologic framework. Sediment accumulation rates for the last century were assessed through  $^{210}\text{Pb}$  and  $^{137}\text{Cs}$  analysis. Gamma spectroscopy using a Canberra GX2520 high-purity coaxial germanium detector determined the activities of both isotopes.  $^{210}\text{Pb}$  profiles were generated for five cores (core locations denoted in Fig 4-1). The cores of interest are located along a transect from inner PIB to the outer shelf region to evaluate sedimentation rate with increased distance from the modern glacial front. Sediment accumulation rates were calculated from the decrease of excess  $^{210}\text{Pb}$  activities with sediment depth following Harden et al. (1992). Excess  $^{210}\text{Pb}$  activities were determined by subtracting the average supported activity taken from the sample below the region of radioactive decay from the total activity. The activity of  $^{137}\text{Cs}$  was measured as below detection levels in all cores and was not used for further analysis.

#### **4.2.5 Sediment Flux Calculation**

Following the establishment of sediment accumulation rates throughout PIB, we calculate a first order sediment flux for Subunit 1A and entire Unit 1. These two intervals were selected due to robustness of age and sedimentation rate. Based on seismic data, which is discussed below, it is assumed that Unit 1 and Subunit 1A blanket Pine Island Bay between the bathymetric high of 300- 500 m water depth at  $113^\circ\text{W}$  to  $103^\circ\text{W}$  and extend to the shelf edge, an accumulation area of approximately  $120,000 \text{ km}^2$ . There were 59 cores for which we determined the thickness of Unit 1 and 36 cores for which we have determined the thickness of subunit 1A. Unit thicknesses were interpolated using an inverse distance weighted method across this region. The volume of sediment contained

within these units was calculated on a cell-by-cell basis. Age constraints and sediment accumulation rates were used to calculate an average sediment flux for subunit 1A and Unit 1.

### **4.3 Results**

#### **4.3.1 Sedimentology of Unit 1**

Unit 1 is identified based on physical property measurements and visual core descriptions (Lowe and Anderson, 2002; Kirshner et al., 2012; Hillenbrand et al., 2013), and can be divided into three subunits (Kirshner et al., 2012). In all locations, subunit 1A is separated from subunit 1B by a clear but transitional contact with subunit 1B, exhibiting slightly increased sand content and stiffness. Subunit 1B overlies subunit 1C with a clear but transitional contact, and subunit 1C exhibits increased sand abundances and stiffness.

The contact between Unit 1 and underlying Unit 2 is marked by an increase in stiffness, decrease in sorting and greater ice-rafted component. In no instance is this depositional sequence found out of order in Pine Island Bay, nor does Unit 1 inter-finger with any other facies.

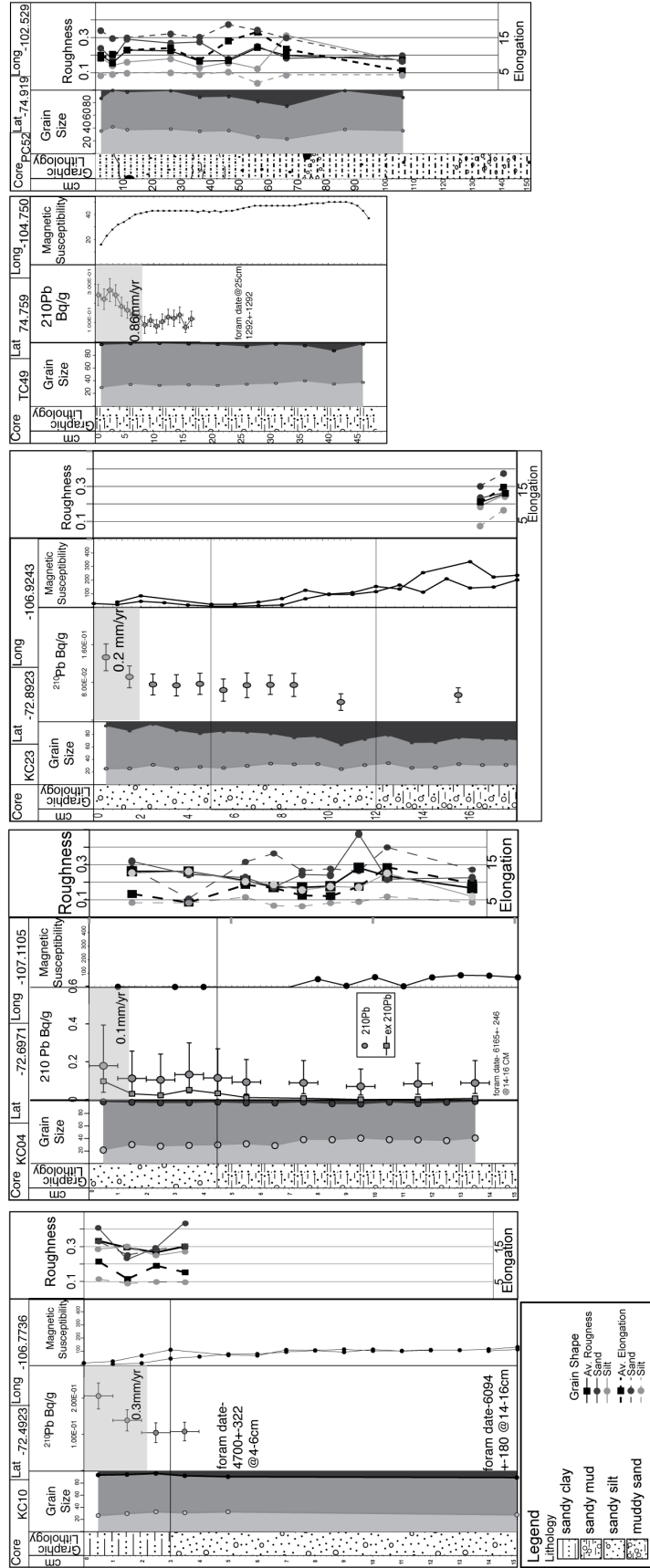


#### **Figure 4-4 Stratigraphy of Unit 1 in focus cores**

**(for location see Figure 4-1). Data includes (from left to right); depth in core in cm, graphic lithology, grain size, 210Pb activity and 14C data, magnetic susceptibility, grain roughness and grain elongation. Cores are shown from proximal to the modern Pine Island Glacier front (right) basinward (left).**

##### **4.3.1.1 Core Lithology and Physical Characteristics**

Core NBP99-02 PC52 was taken in 866 meters water depth in inner Pine Island Bay. It was collected within a basin where a thin sediment layer overlies crystalline bedrock, directly north of the modern Pine Island Glacier front (Figure 4-1). Sediments recovered in Core PC52 are massive and generally structureless with thin, convolute layering near the base of the core. Unit 1 is overall dark gray (Munsell color 2.5 Y 4/1) clay with some intervals of higher silt content (Figure 4-4). Magnetic susceptibility (MS) is low and uniform throughout. This core recovered only Unit 1, showing no contact with underlying units. The contacts between subunits is based on color change and slight increase in stiffness. Subunit 1A is grayish brown (2.5 Y 5/2), silt-rich mud with no pebbles. Subunit 1B is slightly darker, dark gray (2.5 Y 4/1) silt-rich mud with more pebbles relative to Subunit 1A. Subunit 1C is also dark gray (2.5 Y 4/1) but is more firm than above subunits.

Core NBP99-02 TC49 was acquired in 852 m water depth where a thin sediment layer covers crystalline bedrock (Figure 4-1). This core was collected in front of the Thwaites Glacier and proximal to a bedrock carved channel. Sediments within Core TC49 are massive and structureless based on both visual inspection and in X-radiographs (Figure 4-4). Unit 1 is grayish brown (Munsell color 2.5 YR 5/2), silt-rich mud with rare

subangular to subrounded, very fine to fine sand. Magnetic susceptibility is uniform, which mirrors the massive, homogenous nature of the unit. This core recovered only Unit 1, showing no contact with underlying units.

Core OSO090 KC23 was collected on top of a prominent grounding zone wedge at 660 m water depth in outer PIB (Figure 4-1 ). Core KC23 sampled sediments that are generally massive and structureless, with a few intervals exhibiting minor bioturbation. Unit 1 is light olive brown (Munsell color 2.5 Y 5/3) (Figure 4-4). MS data are low and uniform down-core through subunits 1A and 1B. Subunit 1C MS data are slightly more elevated and variable. The contacts between subunits 1A and 1B are gradational but evident, with sand being more concentrated in subunit 1B. The contact between subunit 1B to subunit 1C is marked by change in color and an increase in stiffness. The contact from Unit 1 to underlying Unit 2 is also distinct, defined by an increase in sand and increase in the bulk density.

Core OSO0910 KC04 was taken directly in front of a prominent grounding zone wedge at 729 m water depth (Figure 4-1). The sediments within this core are generally massive in X-ray with very slight bioturbation. They are light olive brown (Munsell color 2.5 Y 5/3) (Figure 4-4). Pebbles are rare but increase in number slightly with depth in the unit. MS is low but increases slightly down unit. Clear but transitional contacts separate the three subunits and are characterized by increasing pebble and sand abundance and in stiffness down core. The contact between Unit 1 and underlying Unit 2 is distinct and characterized by greater stiffness, darkening of color and increase in pebble count within

Unit 2 relative to Unit 1. There is also an increased and more varied MS response, as well as increase bulk density and p-wave velocity in Unit 2.

Core OSO0910 KC10 was collected in 687 m water depth, on the flank of Pine Island Trough in Outer PIB (Figure 4-1). Sediments sampled by this core are generally massive and structureless, with a few intervals exhibiting minor bioturbation. There is a very low amount of sand, which increases slightly down section, and the sediment is light olive brown (Munsell color 2.5 Y 5/3). The MS profile is very uniform, increasing slightly down section. The contact between subunit 1A and subunit 1B is distinct, exhibiting an increase in coarse sand and more abundant pebbles downward in the section. The contact between subunit 1B to subunit 1C is gradational, based on slight color change, increase in MS, pebbles, sand, and density. The contact from Unit 1 to Unit 2 is clearly marked by an increase in sand, a change in the character of all MSCL data, and increase in stiffness.

The additional core of focus for this study, NBP99-02 TC/PC 46, was collected at 855 m water depth within a channel in Inner PIB (Figure 4-1 ) (Lowe and Anderson, 2002; 2003). Sediments within this core consist of disorganized gravel at the base that grades upwards into graded gravel, sand, silt and clay at the top of the core. Clay rip-up clasts are present throughout the graded sequence. The trigger core (TC46) in this location sampled Unit 1 resting sharply above the graded sequence in the piston core. Unit 1 in this core is dark grayish brown (Munsell color 10 YR 4/2), with heavy mineral-rich mud and minor sand.

### 4.3.1.2 Detailed Quantitative Grain Size Distributions

Unit 1 mean grain size ranges from fine to medium silt. Interior cores have a mean grain size of 7.7  $\mu\text{m}$  in core PC52 and 5.9  $\mu\text{m}$  in core TC49 (Figure 4-4). More basinward cores have mean grain sizes of 14.3  $\mu\text{m}$  in KC23, 6.6  $\mu\text{m}$  in KC04 and 10.3  $\mu\text{m}$  in KC10. Thus, there is offshore coarsening with the exception of core KC04. There is a slight increase in mean grain size down-core and between subunits. Cores collected at shallower water depths have a higher average sand content (KC23 24% sand and KC10 13% sand) relative to cores collected at deeper water depths (PC52 10% sand, TC49 4% sand, and KC04 4% sand) regardless of location in the basin.

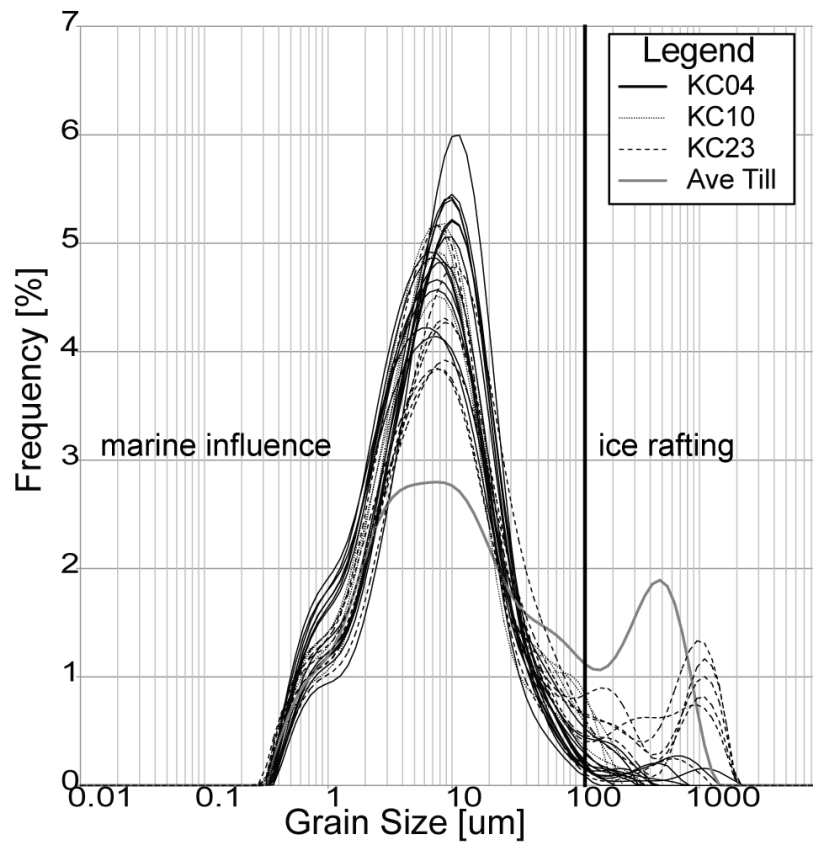


Figure 4-5 Grain size frequency curves for samples of Unit 1.



**Samples were analysed at a 1 cm interval as follows; Core KC04 from 0-14 cm core depth, core KC10 from 0-4 cm core depth, core KC23 from 0-7 cm. An average till grain size curve from four different till samples within core KC04 is also shown. Black vertical line at 125  $\mu\text{m}$  indicates an approximate boundary of marine influences <125  $\mu\text{m}$  and material derived from ice rafting >125  $\mu\text{m}$ .**

The grain size frequency data for Unit 1 in Pine Island Bay is generally a normal, symmetric distribution reflecting variable degrees of sorting (Figure 4-5). Included in the sediment is a sorted very fine sand fraction and an unsorted sand fraction. The latter is derived from ice rafting. Relative to till, the very fine sand is more concentrated and is assumed to include material that was transported in suspension by marine currents. The change in the ratio of very fine sand/total sand is a measure of the relative influence of marine currents versus ice rafting (Anderson, 1999). Grain size data for all cores in PIB have <3% very fine sand and coarser material (material >125  $\mu\text{m}$ ), so this particular proxy is based on a small component of each sample. The assumption here is that there is minimal input of very fine sand via eolian transport because there are no known sources for this material.

Core PC52 is almost 2.5 m long, consisting completely of Unit 1. PC52 is generally constant throughout, and has an average of 34% clay, 56% silt, and 10% sand (Figure 4-4). This varies slightly between subunits. The silt/sand ratio in core PC52 is generally low and constant, with a few outlier values of increase silt/sand. The very fine sand/total sand ratio is the highest in Subunits 1A and 1B, with an average of 0.79, demonstrating no systematic removal of the very fine sand component in this interval. Subunit 1C shows a marked decrease in very fine sand/ total sand, which remains

relatively constant throughout the rest of the core at 0.33 on average, a decrease in the abundance of very fine sand compared with total sand.

Core NBP99-02 TC49 has an average of 36% clay, 61% silt and 4% sand, remaining constant throughout the core (Figure 4-4). There is generally low sand abundances with a small increase near the base of the core. The grain size data for this sample show a very well-sorted medium silt that is finely skewed. The silt/sand ratio generally increases up section. The very fine sand abundance mirrors the total sand abundance throughout the core, with the highest abundances occurring near the base of the core. The ratio of very fine sand/total sand generally increases towards the top of the core, with an average of 0.63 for the entire core.

Core KC04 contains an average of 33% clay, 62% silt, and 4% sand (Figure 4-4). The unit is generally symmetrical in skewness, with two finely skewed intervals. KC-04 slightly coarsens up section, decreasing the abundance of clay-sized material up unit, with the sand content remaining relatively constant throughout. The very fine sand/total sand ratio in core KC04 varies widely.

Core KC10 has an average of 27% clay, 58% silt, and 13% sand, and shows a slight fining up-core (Figure 4-4). The clay and sand abundance remain relatively constant, and the sand content decreases up-core. The very fine sand/ total sand ratio increases up core, but within each subunit the ratio remains constant.

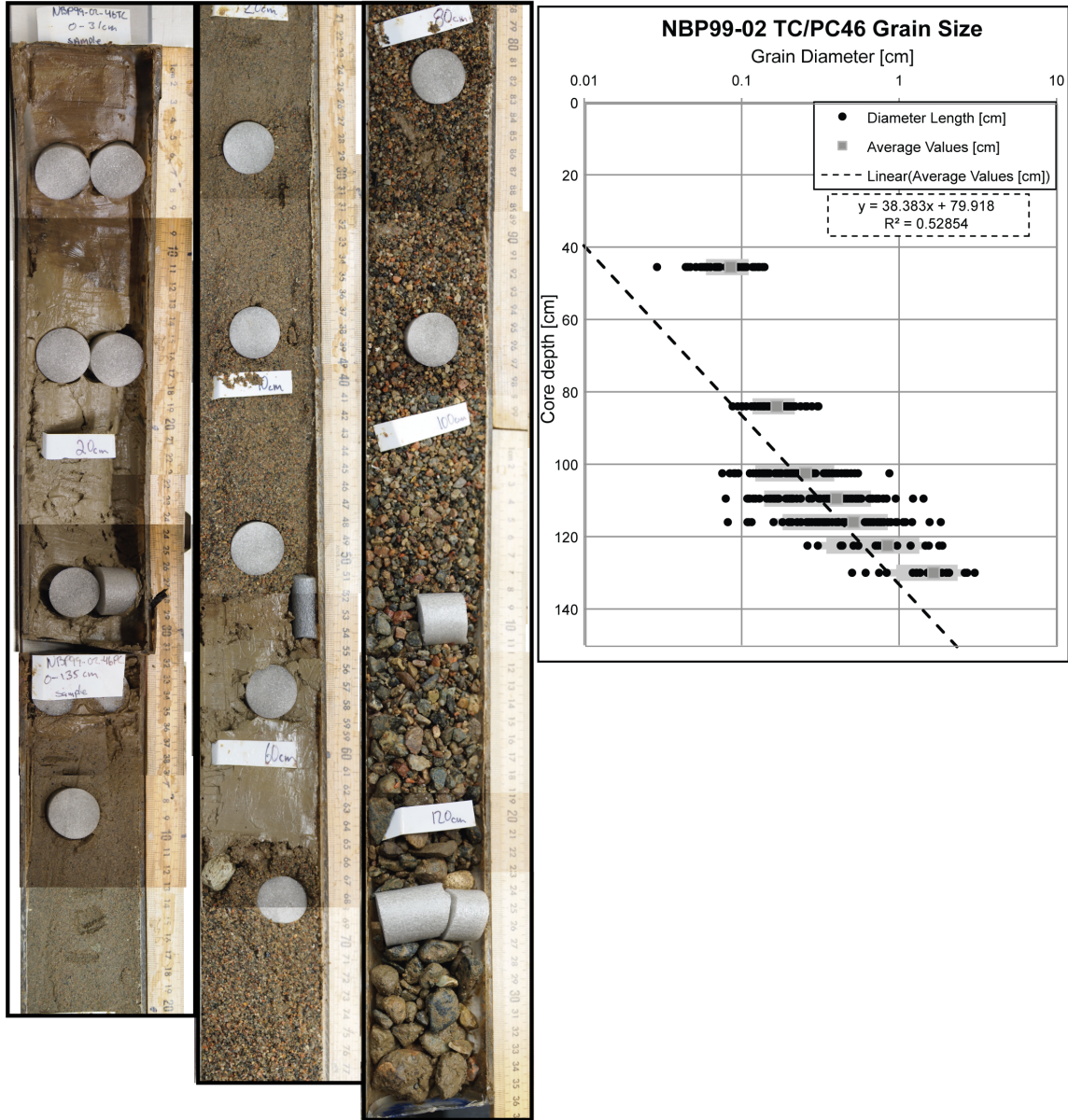


**Figure 4-6 Photograph of core NBP99-02 TC/PC 46 . Average grain size data of the logarithmic grain diameter (cm) vs core depth (cm) from calibrated photograph data on right. All measured grain diameters are in black circles, mean diameters for each core depth are in gray square, with standard deviation in light gray line. Dashed line shows linear function for the data.**

Core KC23 has an average of 28% clay, 48% silt, and 24% sand, with the sand content increasing down-core (Figure 4-4). KC23 coarsens down-core. The ratio of very fine sand/total sand remains relatively constant, with an average of 0.24.

Laser grain size data was not collected for core TC/PC 46, as the gravel is too large for this analytical technique. Grain size results are reported in Figure (4-6). Generally, the sediments in this core fine upwards from coarse pebbles at the base of the core up through clay in the trigger core. The sorting also increases up-core.

### **4.3.1.3 Grain Attributes**

#### **4.3.1.3.1 Grain Shape**

Grain shape can be a useful criterion for distinguishing modes of transport and was applied in this study in an attempt to measure the relative influence of glacial transport versus other modes of transport. This was done by comparing grain shapes of samples to those of till, which is used to characterize the glacial source material for the region.

Core KC04 from Outer PIB was used to characterize the till. The till has roughness values of 0.226 for fine-to-medium sand and 0.137 for very fine sand (Figure 4-4). These roughness values in both size fractions fall within the range of values typical of subunits 1A and subunit 1B in this core. The till sample has the highest elongation value among the very-fine sand fraction of any sample analyzed in PIB and is generally characterized as increasing in grain elongation down-core. The sand fraction shows

several spikes in elongation, however this is not mirrored in the very-fine sand-sized particles.

Core KC 10 shows a slight decrease in roughness values down-core and a decrease in elongation at the subunit boundary between subunit1B and subunit1A, seen more prominently in the medium sand. The increase in roughness values, particularly of the sand, coincides with an increase in the proportion of sand in the core.

Roughness values for interior PIB core PC52 are lowest in subunit 1A, as compared to lower subunits within this core (Figure 4-4). A trend of increased roughness and decreased elongation down-core in PC52 is seen in both size fractions. Subunit 1A in PC52 has both the lowest roughness and highest elongation in this core. There is a decrease in elongation in the sand-sized fraction coincident with a slight increase in elongation in the silt-sized fraction within subunit 1C. An increase in roughness is noted within Subunit 1C.

The median roughness values measured at every interval in each of our cores correspond to the highest values reported in the literature, which are all from glacial environments (Table 4-1). This suggests that the sediment deposited in PIB cores was influenced by glacial processes and not altered significantly by any subsequent transport. This is compared to wind-transported quartz silts, with a harmonic 19 range of 0.0042-0.0026 (Mazzullo et al.,1992); coarse silts on south Texas shelf 0.0035 (Mazzullo and Withers, 1984); grus 0.008-0.0093, and glacial flour 0.0068-0.0072 (Dowdeswell, 1982). The trends in roughness and elongation tend to mirror one another. Grain shape roughness coefficients and elongation values do not display any visible trends associated

with their location or subunits of Unit 1. From this we can infer either that the transport mechanisms operating in all locations were the same throughout the deposition of Unit 1, or that these transport mechanisms do not cause there to be a measurable difference in these parameters. The material in all cores appears to be derived glacially with no measurable change in grain shape due to fluvial or eolian transport.

Unit	Reference	Average Roughness [harmonic 19]	Average Elongation [harmonic 2]
PIB Subunit 1A	This Study	0.0073	7.32
PIB Subunit 1B	This Study	0.0084	8.75
PIB Subunit 1C	This Study	0.0080	12.60
PIB Unit 1	This Study	0.0079	9.06
PIB Till	This Study	0.0077	10.97
Wind-Transported Silts	Mazzullo et al., 1992	0.0042-0.0026	nm
South Texas Shelf Silts	Mazzullo and Withers, 1984	0.0035	nm
Grus	Dowdeswell, 1982	0.008-0.0093	nm
Glacial Flour	Dowdeswell, 1982	0.0068-0.0072	nm

**Table 4-1 Average roughness and elongation values yielded by Fourier analysis of grain shapes for Pine Island Bay sediments.**

**Roughness values of sediments transported by various mechanisms are provided for comparison. nm- not measured**

#### 4.3.1.3.2 Micromorphology

Four cores were examined for micromorphology to measure glacial influence versus other modes of sediment transport. Sample intervals were spaced to analyze different subfacies within a single core. Seven intervals were analyzed in Unit 1 throughout PIB in cores PC52, KC23, KC04, and KC10. A till was examined in one core (KC04). Features were counted on over 100 individual quartz grains (Figure 4-7).

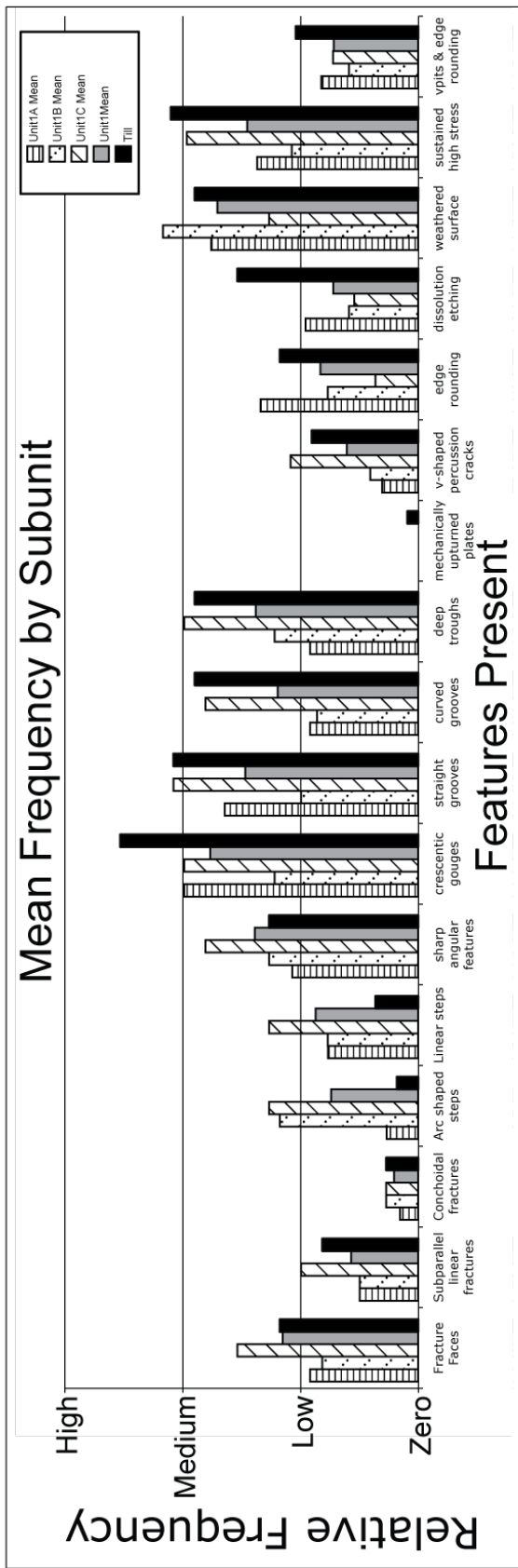


**Figure 4-7 Relative frequency of microtextures observed on over 100 quartz grains. Features were counted as either high, medium, low or zero abundances.**

Sustained high stress microtextures of crescentic gouges, straight and curved grooves and deep troughs are a relict of glacial transport (Sweet and Soreghan, 2010; Kirshner and Anderson, 2011). The till sample in core KC04 has a medium-high abundance of crescentic gouges and a medium abundance of both straight and curved grooves and deep troughs (Figure 4-7). Subunit 1A has a medium abundance of crescentic gouges, low-medium abundance of straight grooves and a low abundance of both curved grooves and deep troughs. Subunit 1B has a low abundance of all sustained high stress microtextures. Subunit 1C has a medium abundance of all sustained high stress microtextures. All of Unit 1 has a medium abundance of crescentic gouges and a low-medium abundance of straight grooves, curved grooves and deep troughs. The till sample has a medium abundance of averaged all sustained high stress microtextures. Unit 1 has a low-medium abundance of all sustained high stress microtextures.

Textures with origins in percussion during fluvial transport include V-shaped percussion cracks and edge rounding. Subunit 1A and subunit 1B have a zero abundance of v-shaped percussion cracks (Figure 4-7). V-shaped percussion cracks are most prevalent in samples from subunit 1C, occurring in low abundance. On average, Unit 1 has a zero-low abundance of v-cracks. The till sample from KC04 has a low abundance of v-shaped percussion cracks. The frequency of edge rounding within Unit 1 decreases from subunit 1A to subunit 1B to subunit 1C. The average of all of Unit 1 is a low abundance. Edge rounding is higher in the till sample than an average of Unit 1. The till



sample has a low abundance of edge rounding. All percussion features (v-pits and edge rounding), remain constant throughout Unit 1, with all samples having a low abundance. The till sample has a slightly higher, but similar abundance of percussion textures, at low abundance.

#### **4.3.1.4 Bulk Composition**

X-ray diffraction (XRD) data was collected in a down core profile for core NBP99-02 TC/PC46 to characterize the provenance, and to determine whether the source had changed through its depositional history based on a change in color (Figure 4-6, Table 4-2). Nine samples were analyzed in Unit 1 and one sample from a rip-up clast lower in the section. All samples in Unit 1 have an average weight percentage abundances of ~16 wt% smectite, ~46 wt% illite and mica, ~25 wt% kaolinite, and ~14 wt% chlorite. There is a lithologic color boundary from brown to gray at 12 cm core depth. The kaolinite content is the highest in the top, brown section of the core (26-30 wt%), decreasing slightly but remaining high in the lower, gray section (20-23 wt%). The weight percentage abundance of the rip-up clast is very similar to those in the uppermost Unit 1. The compositional similarities verify that this sample is indeed a rip up clast of the same Unit 1 material, and that there is a consistent source of material for the entire deposition of Unit 1 in this core.

Reference <sup>1</sup>	Cruise	Sample ID	Depth in core		Description	Latitude (°S)	Longitude (°W)	Water Depth (m)	R0 M-L-I/S (80-90S) <sup>3</sup>		Illite & Mica		Kaolinite	Chlorite
			core top [cm]	bottom [cm]					R0 M-L-I/S	R0 M-L-I/S	Mica	Illite &		
This Study	NBP99-02	TC46	1.0	2.0	Unit 1	-74.214	-106.346	855	15.0	42.9	29.7	12.4		
This Study	NBP99-02	TC46	3.0	4.0	Unit 1	-74.214	-106.346	855	12.9	45.1	27.3	15.2		
This Study	NBP99-02	TC46	8.0	9.0	Unit 1	-74.214	-106.346	855	14.7	43.6	28.0	13.5		
This Study	NBP99-02	TC46	10.0	11.0	Unit 1	-74.214	-106.346	855	16.2	45.0	26.3	12.6		
This Study	NBP99-02	TC46	13.0	14.0	Unit 1	-74.214	-106.346	855	15.9	48.8	19.5	16.0		
This Study	NBP99-02	TC46	17.5	18.5	Unit 1	-74.214	-106.346	855	19.0	44.1	23.3	13.6		
This Study	NBP99-02	TC46	21.5	22.5	Unit 1	-74.214	-106.346	855	18.7	45.2	22.6	13.2		
This Study	NBP99-02	TC46	24.0	25.0	Unit 1	-74.214	-106.346	855	17.8	44.9	21.9	15.3		
This Study	NBP99-02	TC46	60.0	61.0	RipUp Clast Cl	-74.214	-106.346	855	21.5	42.4	23.4	12.2		
Lowe and Anderson, 2002	NBP99-02	PC40	3	3	BC	-73.79	-106.05	953	39.9	39.5	12.8	7.9		
Lowe and Anderson, 2002	NBP99-02	PC40	30	30	BS	-73.79	-106.05	953	37.6	40.5	10.6	11.3		
Lowe and Anderson, 2002	NBP99-02	PC40	45	45	OGC	-73.79	-106.05	953	36.7	40.7	14.5	8.1		
Lowe and Anderson, 2002	NBP99-02	TC45	15	15	BC	-74.173	-106.546	1242	39.9	37.4	15.7	7		
Lowe and Anderson, 2002	NBP99-02	TC45	60	60	BC	-74.173	-106.546	1242	36.2	41.7	16.4	5.6		
Lowe and Anderson, 2002	NBP99-02	PC45	5	5	OGC	-74.173	-106.546	1242	40.2	38.7	14.9	6.2		
Lowe and Anderson, 2002	NBP99-02	PC45	50	50	BS	-74.173	-106.546	1242	41.5	40.6	10.6	7.3		
Lowe and Anderson, 2002	NBP99-02	PC45	138	138	BC	-74.173	-106.546	1242	35.6	45	12	7.4		
Lowe and Anderson, 2002	NBP99-02	PC53	5	5	OGC	-74.667	-104.337	1386	41.9	38.4	12.8	6.8		
Lowe and Anderson, 2002	NBP99-02	PC53	63	63	BS	-74.667	-104.337	1386	27.2	46.7	14.8	11.3		

**Table 4-2 X-ray diffraction data for select cores within Pine Island Bay.**

<sup>1</sup>Samples from Ehrmann et al., (2011) are not included in this table, as the weight percentages and mineral compositions were measured differently in terms of mixed layer clays. All data for that study can be found in Ehrmann et al., (2011). <sup>2</sup>R0 M-L I/S 90S - Randomly oriented Mixed-Layer Illite/Smectite with 90% Smectite layers for This Study. <sup>3</sup>R0 M-L I/S (80-90S) from (Lowe and Anderson, 2002).

The entire Amundsen Sea Embayment has been identified as an area of elevated kaolinite abundances (Lowe and Anderson, 2002; Ehrmann et al., 2011). The region in front of the Pine Island and Thwaites Glacier has kaolinite abundances of 16-22 wt%. The occurrence of kaolinite is particularly diagnostic as it is unable to form under glacial conditions, requiring the presence of pre-glacial sediments beneath the ice. The source for these sediments have yet to be identified, with both the Byrd and Bentley subglacial basins as potential sources. Geophysical evidence in both regions have imaged ~500 m of unconsolidated sediments of an unknown age and composition (Winberry & Anandakrishnan 2004, LeMasurier 2008). The presence of kaolinite and the geophysical evidence implies the presence of subglacial sedimentary strata, which has profound implications for glacial sliding and stability (e.g. Alley et al.,1986).

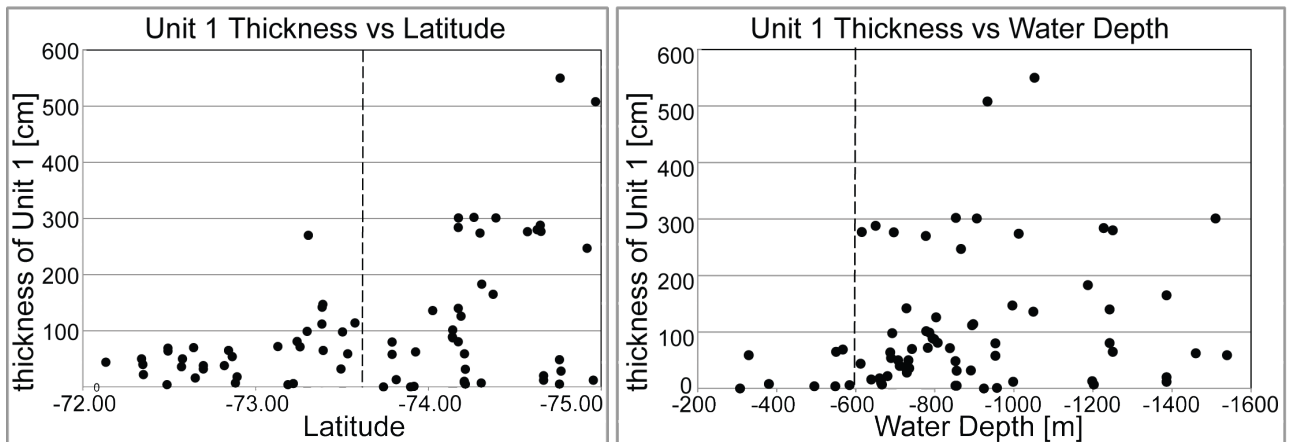


**Figure 4-8 A. Thickness of Unit 1 in centimeters versus core latitude.**

**The dashed line indicates the latitude of the transition between crystalline basement (right of dashed line) to sedimentary substrate (left of line) at ~73.5 °S. B. Thickness of Unit 1 in centimeters versus core water depth. The dashed line is at 615 m water depth, an average shelf depth.**

### 4.3.2 Thickness of Unit 1

Unit 1 is imaged as a thin drape throughout PIB based on geophysical seismic and chirp sub-bottom data (Anderson et al., 2010, Nitsche et al., 2012). This includes PARASOUND data indicating thicknesses up to 20-40 m within minibasins in interior PIB (Nitsche et al., 2012). It is characterized by parallel layering within bathymetric lows.

Unit 1 is present in all cores collected in PIB except for two piston cores, with its absence likely due to loss of surface sediments in these cores. Sediment cores contained 102 cm average thickness of Unit 1 (Figure 4-8). The thickness increases towards the modern Pine Island Glacier front to over 5 m thick (Lowe and Anderson., 2002). In general, thickness decreases seaward from the modern grounding line (Figure 4-8). Cores from the crystalline bedrock region of inner PIB (south of -73.5°S) sampled an average of 133 cm thick Unit 1, over two times the average thickness of outer PIB (north of -73.5°S). Cores taken at all water depths sampled Unit 1. Cores collected at water depths deeper than 615 m recovered on average 116 cm of Unit 1, 4.5 times thicker than cores collected at shallower water depths (Figure 4-8). Unit 1 is the thickest in cores collected

proximal to the modern Pine Island Glacier front (south) and at deeper water depths. In summary, Unit 1 thickness increases toward the glacier front and with increasing water depth.

### **4.3.3 Bathymetric Data Analysis**

Pine Island Bay is characterized as having an intricate drainage network carved into bedrock within the inner portion of the bay (south of  $\sim 73.5^{\circ}\text{S}$  latitude) (Lowe and Anderson, 2002; 2003; Nitsche et al., 2012). Our analysis focuses on evaluating the potential for water storage, pathways for transport, and connectivity of cavities where water could be stored.

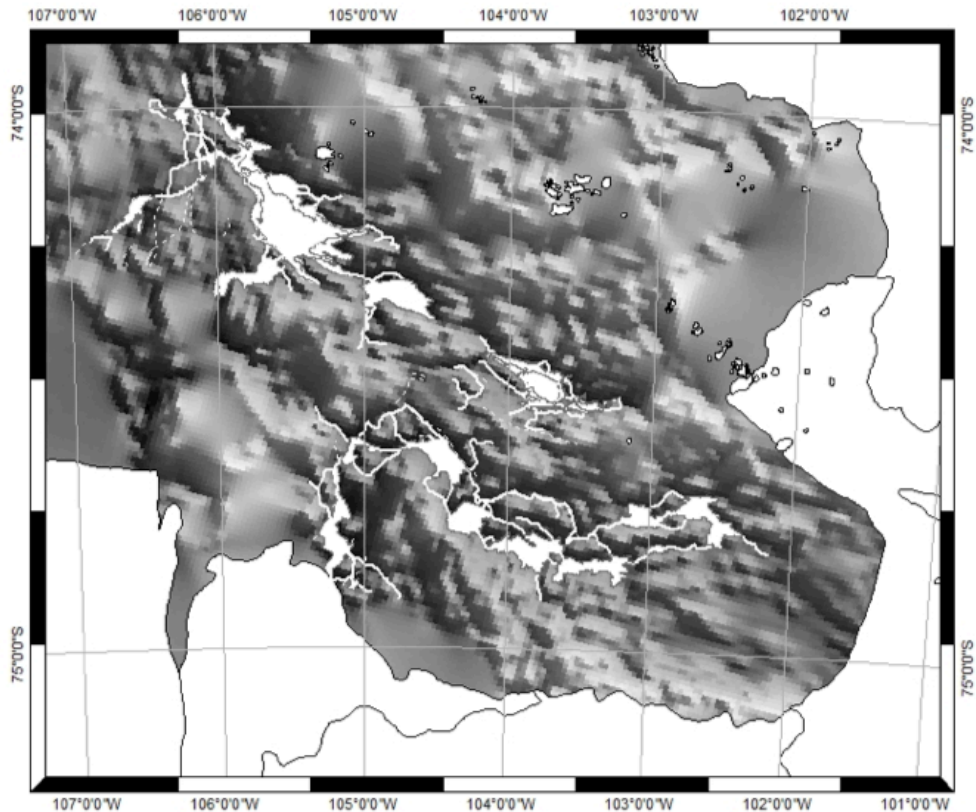


**Figure 4-9 Meltwater depressions and channels in inner PIB.**  
**Channels on which geomorphic analyses were conducted are marked by a solid white line; others for which there is a geomorphic signature are dashed. Hypothesized subglacial water flow is from southeast to northwest.**

#### 4.3.3.1 Subglacial Water Storage and Capacity

The dominant features within inner PIB are steep-sided basins up to 1650 m deep. The basins shown in Figure (4-9) largely coincide with those interpreted by Nitsche et al., (2012). Drumlins and streamlined features at the floor of these depressions are evidence for grounded ice and flowing water in the subglacial environment of inner PIB (Lowe and Anderson 2002; 2003; Nitsche et al. 2012). These basins could potentially have stored

great volumes of meltwater during times when the ice sheet was grounded on the shallower portions of the sea floor. If filled to the level of interconnecting channels between these basins, we calculate that the combined basins could potentially store between 800 and 1200 km<sup>3</sup> of water.

Grounding Position <sup>1</sup>	Meltwater Volume [km <sup>3</sup> ]	
	Kamb Ice Stream <sup>2</sup>	Thwaites Glacier <sup>2</sup>
1	25.42	70.91
2	1.47	36.73
3	3.59	40.94
4	0.47	4.04

**Table 4-3 Total volume of water stored in cavities on the inner shelf as delineated in Figure 4-10 for each of 4 grounding line positions and two end member ice sheet profiles. <sup>1</sup> Grounding positions correspond to locations in Figure 4-10. <sup>2</sup> Volumes calculated using hypothetical ice profiles for two end member modern ice streams. See text for more information.**

To assess how much water may have actually occupied the basins, a hydraulic analysis was conducted. Where there is a gradient in hydraulic head, it is expected that water flows with the gradient. When spatial variability in the hydraulic gradient is very low, we assume that the subglacial water is not moving. The perimeters of subglacial lakes generated by Carter's lake identification algorithm are shown for different ice sheet scenarios (Figure 4-10). These regions of no-flow substantially correlate with the geomorphically identified basins. The hydraulic gradients generated from the two end-member profiles indicate that these depressions were not filled completely. The quantity of stored water within these basins under the two end-member ice profiles is

approximately 70 km<sup>3</sup> (Table 4-3). This calculation represents a minimum quantity of water available for sediment transport or temporarily stored subglacially in PIB, as we did not compute distributed meltwater outside of these large basins.

#### **4.3.3.2 Organization of Channel Systems**

Here we hypothesize that flow between the basins occurred through channels connecting them. Seventy channels running to and between basins were identified. These channels range in length from 1 to 37 km, with a mean length of 8.9 km and highly variable gradients, including uphill gradients (Figure 4-9). Uphill flow is common in subglacial water systems, which are driven by the pressure distribution beneath the ice sheet. Which of these channels was occupied by water at any given time is a function of how much resistance to flow is offered by the channel and the pressure distribution beneath the ice. A more detailed exploration of flow paths can be made through the analysis of specific channels (Figure 4-9).

By examining end-member ice profiles for different grounding line positions of Pine Island Glacier, we observe how changes in hydraulic potential reorganize the subglacial water system. Since water is stored in regions of sufficiently low hydraulic potential gradient, the basins of water storage may be altered by changes in hydraulic potential. Under the scenarios we investigate, water storage occurs within the basins identified independently based on bathymetric data, and the volume of water stored in these basins changes (Figure 4-10). This necessitates water flow between basins, and the observed channels provide the connectivity to enable this flow. Fig (4-9) displays the expected direction of flow based on the topography. Based on the observed



geomorphology, it appears that subglacial water has the potential to remain channelized to the sedimentary-crystalline boundary.



**Figure 4-10 Hydraulic analysis of Pine Island Glacier.**

**A) Grey lines are 200 m bathymetric contours. Black lines denote four hypothesized grounding line positions. B,C) Lake perimeters generated by the lake identification algorithm are shown in shades of grey corresponding to grounding line positions in A. Bathymetric contours (black) are 30m from -800 to -2000m. (B) depicts lakes under a steep ice sheet profile, Thwaites Glacier. (C) depicts lakes under a shallow ice sheet profile, Kamb Ice Stream.**

Hydraulic potential changes occur naturally as the ice sheet profile changes and as water is supplied to the bed. Given these hydraulic potential changes during ice stream retreat and the observed connectivity of basins, it can be inferred that water did indeed flow subglacially.

#### 4.3.4 Age Constraints and Rate of deposition of Unit 1

Here we combine traditional radiocarbon data from previous work (Kirshner et al., 2012 and Lowe and Anderson, 2002) with short-lived radioisotopes ( $^{210}\text{Pb}$ ) measurements from this study to measure Unit 1 accumulation rates. These data are used to evaluate timing as well as calculate sediment flux for Unit 1. We do not calculate rate data from Hillenbrand et al. (2013) as the radiocarbon ages from that study were taken from cores noted as being disturbed by icebergs and mass flow processes. However, Hillenbrand et al., (2013) do provide an upper limit on the age for a similar silt facies as ~8.6 k cal yr BP in core PS75/214, and an upper age limit of glacial retreat as ~11.6 k cal yr BP for a unit that is noted as a gravity flow or turbidite deposit from the same core in inner PIB.

Core PC52, which was collected directly seaward of the modern Pine Island Glacier floating terminus, sampled 120 cm of soft (water-saturated) sediment with no excess  $^{210}\text{Pb}$  (Table 4-4). This implies high accumulation rates and dilution of excess  $^{210}\text{Pb}$ .

Core TC49 was collected seaward of Core PC52 in 852 m water depth (Figure 4-1). This core yielded a well-defined  $^{210}\text{Pb}$  decay profile (Figure 4-4; Table4-4). The  $^{137}\text{Cs}$

activities were also measured in all cores, but are below detection limit. The sediment/water interface is preserved in this core, containing a mixed layer from 3-4 cm thick. The apparent sediment accumulation rate is  $\sim 0.086$  cm/yr for the top 7 cm of the core (Figure 4-4). Radiocarbon age constraints from a foraminifera date at 25 cm is  $1,292 \pm 1,291$  cal yr BP in Core TC49; this date has an exceptionally large error due to small sample sizes and analytical imprecision (Lowe and Anderson, 2002). Thus, the rate of deposition based on radiocarbon data is an average of 0.02 cm/yr, with a minimum rate of 0.001 cm/yr and a maximum rate that could be extremely rapid (up to 25 cm/yr). This radiocarbon-derived sedimentation rate is likely slower than the  $^{210}\text{Pb}$  rate, but due to the large error it is difficult to verify. At core depths of 8 to 12 cm the profile exhibits lowered  $^{210}\text{Pb}$  activities that corresponds to a decrease in the amount of very fine sand in the core. This decrease occurred  $\sim 70$  years ago. A first order assumption based on extrapolating measured rates over the entire thickness of subunit 1A yields an onset age for subunit 1A of  $\sim 560$  cal yrs BP.

The  $^{210}\text{Pb}$  profile of Core TC49 is similar to that of a typical core collected in shallow water. This may suggest relatively fast scavenging of the isotope in the water column and sedimentation. If we can exclude erosion events at the core locations, then the uppermost sediments may be recording an order of magnitude increase in sediment accumulation rate similar to that observed in Svalbard fjords (Szczuciński).

Core KC23 was collected seaward of Core TC49, in Outer PIB in 660 m water depth (Figure 4-1) and records excess  $^{210}\text{Pb}$  only in the uppermost 2 cm of the core, although the data exhibit a classic decay profile (Table 4-4). This indicates an apparent

accumulation rate of 0.02 cm/yr for uppermost Subunit 1A. There are no radiocarbon constraints for Unit 1 in this core. By extrapolating accumulation rates for the thickness of subunit 1A, deposition began ~250 years ago.

Core KC04 was collected seaward of Core KC23, in a deep basin at 729 m water depth, in front of a prominent grounding zone wedge in Outer PIB (Figure 4-1). It has excess  $^{210}\text{Pb}$  in the upper 7 cm of the core (Table 4-4). The apparent sediment accumulation rate is between 0.04 and 0.11 cm/yr, depending on the accepted slope of regression. A single radiocarbon date from planktonic foraminifera in subunit 1B at 14-16 cm core depth yielded an age of  $\sim 6165 \pm 246$  cal yr BP. This yields a long-term accumulation rate of  $\sim 0.0025$  cm/yr for Unit 1. An alternative interpretation for the drop of  $^{210}\text{Pb}$  activities below 1 cm may suggest that the activities measured below may be due to bioturbation (there are hints of bioturbation in X-ray data). However, if the upper cm was deposited within the last 100 years, the accumulation is on the order of 0.01 cm/yr, still an order of magnitude higher than long-term accumulation rates for Unit 1 based on radiocarbon data. By extrapolating the accumulation rates, deposition of subunit 1A began  $\sim 40$ -112 years ago.

The most basinward Core KC10 was collected in 687 m water depth (Figure 4-1). It has an apparent sediment accumulation rate of  $\sim 0.03$  cm/yr based on  $^{210}\text{Pb}$  analysis (Table 4-4). The excess  $^{210}\text{Pb}$  activity is constrained to the upper 3 cm of the core with a classic decay curve. This corresponds to a lithologic boundary of the base of subunit 1A at 3 cm. There are two radiocarbon dates from planktonic foraminifera in subunit 1B, one from 4-6 cm of  $4,701 \pm 322$  cal yr BP and the other from 14-16 cm that is  $6,094 \pm 180$  cal

yr BP. Based on these dates, the sediment accumulation rate for subunit 1B is  $0.007 \pm 0.001$  cm/yr, over an order of magnitude slower than observed for subunit 1A. Based on accumulation rate data, it is likely that subunit 1A began deposition less than 100 years ago.

The  $^{210}\text{Pb}$  analyses indicate that subunit 1A was rapidly deposited and at a rate that is about an order of magnitude faster than subunit 1B. The highest rate,  $\sim 0.086$  cm/yr in Core TC49, occurs close to the modern glacier terminus. This excludes the most proximal Core PC52, which did not record excess  $^{210}\text{Pb}$ , perhaps due to rapid accumulation, which is consistent with thickness increase observed in sub-bottom profiler data. The estimated  $^{210}\text{Pb}$  sediment accumulation rate for the three cores collected in more distal locations within PIB are  $\sim 0.02$  cm/yr (KC23),  $\sim 0.04 - 0.11$  cm/yr (KC04), and  $\sim 0.03$  cm/yr (KC10). All cores yielded a similar order of magnitude sediment accumulation rate. The long-term rates for all of Unit 1 derived from radiocarbon ages are  $\sim 0.0025$  cm/yr (KC04),  $\sim 0.001$  cm/yr and  $\sim 0.0025$  cm/yr (KC10), which is an order of magnitude slower than the short-term ( $^{210}\text{Pb}$ ) rates. Of additional note is the  $\sim 6.1$  ka dates from similar depths in cores KC10 and KC04 that indicate accumulation rates over this time interval of  $\sim 0.0025$  cm/yr.

#### 4.3.5 Sediment Flux in Pine Island Bay

Unit 1 is observed as blanketing all of PIB. Based on this style of sedimentation, the interpolated volume of Unit 1 is approximately  $120 \text{ km}^3$ . The flux rate for Unit 1 is  $0.018 \text{ km}^3/\text{yr}$  based on a 7,000 year onset age (Kirshner et al., 2012) to  $0.014 \text{ km}^3/\text{yr}$  based on a 8,660 year onset age for a similar silt facies (Hillenbrand et al., 2013). We

calculate the volume of sediments that comprise subunit 1A as  $23.8 \text{ km}^3$ . Flux rates for subunit 1A may have been as high as  $0.60 \text{ km}^3/\text{yr}$  to as low as  $0.04 \text{ km}^3/\text{yr}$ , based on end member onsets of subunit 1A deposition (40 years before present from Core KC04 to 560 years before present from Core TC49). A more likely flux for subunit 1A is  $0.11 \text{ km}^3/\text{yr}$ , based on an average onset of subunit 1A from all dated cores as 213 years before present. These flux rates indicate that sediment delivery was approximately an order of magnitude greater for the deposition of subunit 1A than for Unit 1, regardless of whether the earlier or later onset age of Unit 1 is used for flux calculations.

Reference	Cruise	Core	Depth [cm]	Lab Number	Duration [s] (live)	<sup>210</sup> Pb [Bq/g]	error error	ex <sup>210</sup> Pb	<sup>40</sup> K	error
This Study	OSO0910	KC10	0.5	IG0385	167438.8	2.06E-01	3.60E-02			
This Study	OSO0910	KC10	1.5	IG0386	167922	1.39E-01	2.95E-02			
This Study	OSO0910	KC10	2.5	IG0387	181721.7	1.04E-01	2.74E-02			
This Study	OSO0910	KC10	3.5	IG0388	189778.4	1.08E-01	2.58E-02			
This Study	OSO0910	KC04	0.5	IG0375	176761.7	1.78E-01	3.76E-02	9.65E-02		
This Study	OSO0910	KC04	1.5	IG0382	174572.7	1.11E-01	3.34E-02	2.97E-02		
This Study	OSO0910	KC04	2.5	IG0381	150496.8	1.04E-01	3.32E-02	2.20E-02		
This Study	OSO0910	KC04	3.5	IG0384	157395.5	1.32E-01	3.52E-02	5.04E-02		
This Study	OSO0910	KC04	4.5	IG0383	191628.5	1.14E-01	4.07E-02	3.24E-02		
This Study	OSO0910	KC04	5.5	IG0376	251395.8	9.16E-02	2.81E-02	1.00E-02		
This Study	OSO0910	KC04	7.5	IG0377	166049.5	8.78E-02	2.99E-02	6.22E-03		
This Study	OSO0910	KC04	9.5	IG0378	164635.3	6.89E-02	2.36E-02	0.00E+00		
This Study	OSO0910	KC04	11.5	IG0379	182815.1	8.24E-02	2.69E-02	8.24E-04		
This Study	OSO0910	KC04	13.5	IG0380	162985	8.71E-02	3.18E-02	5.53E-03		
This Study	OSO0910	KC23	0.5			0.1331495	0.02852862			
This Study	OSO0910	KC23	1.5			0.0915402	0.02323287			
This Study	OSO0910	KC23	2.5			0.07561594	0.02231069			
This Study	OSO0910	KC23	3.5			0.07357612	0.0225418			
This Study	OSO0910	KC23	4.5			0.07677083	0.0224847			
This Study	OSO0910	KC23	5.5			0.06351364	0.02346141			
This Study	OSO0910	KC23	6.5			0.07379304	0.02633263			
This Study	OSO0910	KC23	7.5			0.07476353	0.02047875			
This Study	OSO0910	KC23	8.5			0.07441116	0.02441914			
This Study	OSO0910	KC23	10.5			0.03808999	0.01758158			
This Study	OSO0910	KC23	15.5			0.05305072	0.01534752			
This Study	NBP99-02	PC52	2.5							
This Study	NBP99-02	PC52	6							
This Study	NBP99-02	PC52	11							
This Study	NBP99-02	PC52	27							
This Study	NBP99-02	TC49	0.5	IG0227	337348.5	0.2437585	5.46E-02			
This Study	NBP99-02	TC49	1.5	IG0236	245145	0.221539	5.34E-02		1.163543	0.09059513
This Study	NBP99-02	TC49	2.5	IG0230	256575.9	0.2690158	0.059394		1.547791	0.1004566
This Study	NBP99-02	TC49	3.5	IG0233	276981.3	0.243267	0.05389313		1.628476	0.1044465
This Study	NBP99-02	TC49	4.5	IG0228	271574.9	0.1834295	0.04892747		1.607827	0.1086347
This Study	NBP99-02	TC49	5.5	IG0237	243259.7	0.1646699	0.04198833		1.577454	0.1073864
This Study	NBP99-02	TC49	6.5	IG0238	243709.8	0.1409157	0.04260092		1.454752	0.09886462
This Study	NBP99-02	TC49	7.5	IG0239	273182.8	0.1301807	0.03901505		1.565215	0.1060174
This Study	NBP99-02	TC49	8.5	IG0234	240474.3	0.08808277	0.04400753		1.491754	0.09995761
This Study	NBP99-02	TC49	9.5	IG0229	536653.4	0.1114526	0.03123446		1.714554	0.1090726
This Study	NBP99-02	TC49	10.5	IG0235	262802.3	0.08093463	0.03505891		1.063002	0.07485552
This Study	NBP99-02	TC49	11.5	IG0240	254024.8	0.1053054	0.04013306		1.560017	0.103779
This Study	NBP99-02	TC49	12.5	IG0232	257189.8	0.1292365	0.04009473		1.649919	0.1106702
This Study	NBP99-02	TC49	13.5	IG0241	251396.5	0.1229667	0.04203076		1.046297	0.0825951
This Study	NBP99-02	TC49	14.5	IG0242	260448.6	0.1398726	0.04152059		1.633172	0.1104909
This Study	NBP99-02	TC49	15.5	IG0231	342280.4	0.07576802	0.02732075		1.695328	0.1130085
This Study	NBP99-02	TC49	16.5	IG0243	254620.9	0.1197585	0.03998361		0.9867376	0.07750764

**Table 4-4 Table of excess <sup>210</sup>Pb measured on sediment cores from within Pine Island Bay.**

**All samples were analyzed at the Institute of Geology, Adam Mickiewicz University in Poznan, Poland.**

## **4.4 Discussion**

### **4.4.1 Sediment and Facies Analysis**

#### **4.4.1.1 Sedimentology, Deposition, and Transport**

Grain size distributions between individual units in Pine Island Bay are markedly different, with an increased degree of sorting up-section (Kirshner et al., 2012). Relative to other terrigenous sediment facies that occur on the Antarctic continental shelf, Unit 1 represents an extreme end member in terms of sorting (Anderson, 1999), (Figure 4-5). The degree of sorting is in fact quite impressive when one considers that the ultimate source material for terrigenous sediments on the continental shelf is of glacial origin. The virtually unsorted till that was sampled in cores from PIB is representative of that glacial source that has not experienced any sorting by marine processes and provides a basis for estimating the magnitude of marine influence. Considerable sorting is required to produce Unit 1 silts from the unsorted source material.

Winnowing of poorly sorted glacial marine sediments by marine currents results in gravelly sands and sandy gravels (residual glacial marine sediments of Anderson et al., 1984). Associated with these deposits are well-sorted sands that indicate bedload transport of the sand. This process occurs on more shallow parts of the continental shelf where wind-driven currents influence the seafloor and on the continental shelf margin and upper slope where strong boundary currents exist (Anderson, 1999; Rodriguez and Anderson, 2004). Sediment cores from the PIB study area have not sampled residual glacial marine sediments or current transported sand. Thus, there is no evidence in the PIB



study area of strong winnowing by marine currents, certainly not to the degree necessary to produce such a widespread deposit as Unit 1.

Given the above arguments and its widespread distribution, Unit 1 is interpreted to have been derived through suspension transport from a subglacial source. Modern oceanographic measurements from Pine Island Bay, in particular from the AutoSub mission beneath the modern Pine Island ice shelf, support the presence of suspended sediments as well as marine currents capable of fine-grained sediment suspension and transport (Jenkins et al., 2010). Autosub observations revealed two plumes in the inner part of PIB. One is a cyclonic gyre of a buoyant plume of melt-laden, deep-water that outflows in front of the modern Pine Island Glacier (Mankoff et al., 2012). The other is a less buoyant plume that occurs well below the sea surface (Hellmer et al., 1998; Jenkins et al., 2010; Mankoff et al., 2012). Tidal forces have been noted as contributing to mixing and circulation within the sub ice-shelf cavity (Robertson, 2010). Plume dynamics in PIB have been modeled as influenced by both the Coriolis effect and sub-shelf topography (Payne et al., 2007).

#### **4.4.1.2 Grain Characteristics as an Indication of Transport**

Our hypothesis was that significant fluvial transport of sediments within the observed subglacial drainage network would result in an increase in percussion features from hydraulic transport on quartz grains within Unit 1, and that these features would overprint high stress microtextures resulting from glacial transport. This, however, was not observed. Percussion microtextures from fluvial transport are rare. Indeed, Unit 1

samples are very similar to the till samples in terms of grain microtexture, indicating that it is a glacially produced deposit.

The trends in grain roughness and elongation tend to mirror one another. This correspondence is expected given that with increased weathering quartz grains will both become more rounded and smoother (Kuhn 1993). Values for roughness are in the range of glacial flour as reported by Dowdeswell (1982) and indicate formation by glacial abrasion and little or no modification by fluvial or marine processes. Grain-grain and grain-bed contact were not sufficient to reduce the surface roughness, decrease angularity and impart non-glacial microtextures. This suggests either low flow energy, low suspended load concentrations, short transport distances, brief transport times, or all of the above.

Finally, the similarities in both the grain shapes and textures of Unit 1 to the till sample indicates that the sorting for Unit 1 is not inherited from some pre-existing sedimentary deposit, although its clay mineralogy does indicate contribution of clay minerals from a non-glacial source.

#### **4.4.1.3 Sediment Composition and Source Region**

The Amundsen Sea Embayment is characterized as a region of elevated kaolinite (Lowe and Anderson, 2002; Ehrmann et al., 2011), which has been further supported by this study. Kaolinite is a clay that cannot form under polar conditions, and is characteristic of moist, temperate to tropical environments. However, it is resistant to physical weathering and is recyclable. The high abundance of kaolinite in Unit 1 implies

a pre-glacial kaolinite-bearing sedimentary source for this material (Anderson et al., 2010; Ehrmann et al., 2011). A rip-up clast within the graded deposits in core NBP99-02 TC/PC46 has the same composition as Unit 1, which indicates that deposition occurred during or after deposition of Unit 1. Potential source areas for Unit 1 are the Byrd Subglacial Basin and Bentley Subglacial Troughs.

#### **4.4.2 Bathymetry**

The Pine Island Bay system contains an intricate drainage network with many bedrock carved glacial morphological features (Lowe and Anderson, 2002; 2003; Nitsche et al., 2012). This study demonstrates that there is potential for storage of significant volumes of water within basins in inner PIB, on the order of 800-1200 km<sup>3</sup>, with up to 70 km<sup>3</sup> of stagnant, non-flowing water. There is adequate channel connectivity between these depressions for the water to be released in response to a changing ice profile or a shallowing of the grounding line, reaching a critical level in the hydraulic potential.

#### **4.4.3 Style of Deposition**

Unit 1 was deposited in one of three fashions; 1. steady-state, constant deposition over the past 7-8 ka; 2. stepwise deposition in which there were times of higher and lower fluxes; or 3. punctuated deposition in discrete, perhaps catastrophic, events.

Sedimentation rates from both <sup>210</sup>Pb and radiocarbon dating reveal that Unit 1 was deposited at varying rates during the past ~7-8 ka and that modern accumulation rates far exceed long-term rates. Thus, Unit 1 was not deposited in a steady state for this entire length of deposition.

An alternate mode of sedimentation is suggestive of a “leaky faucet”, with times of higher outflow alternating with periods of lower flow. Unit 1 contains three different subunits, suggestive of three episodes of increased flow and sedimentation. The rates of deposition vary between subunit 1A and subunit 1B by an order of magnitude. Although not measured, it is likely that subunit 1C may differ as well. There is also variation in ice-rafted sand abundances between the three subunits, another line of evidence for a change in the rate of deposition. It is unlikely that there were times of non-deposition, as this typically results in a layer of concentrated ice-rafted sand and gravel, which is not observed. Unit 1 lacks bedforms and sedimentary structures that may be associated with turbidite deposition.

It has been suggested that graded sands and gravels are deposited in hyper-concentrated flows associated with catastrophic discharges of water from meltwater plumes (Domack and Williams, 1990; Powell, 1990; Ó Cofaigh, 1996; Cutler et al., 2002; Fisher and Taylor, 2002). Evidence for high energy deposition comes from the isolated occurrence of graded gravels and sands in core NBP99-02 TC/PC 46. Poor recovery and scratched core barrels that recovered only loose gravels were noted at a number of locals in inner PIB and may record similar gravelly deposits (Lowe and Anderson, 2002; 2003). Alternatively, the graded sequence in core TC/PC 46 could be a turbidite deposit, although the relatively short run out distance (down slope distance) is considered unfavorable for converting unsorted glacial sediments into such well sorted, graded deposits by this process.

#### 4.4.4 Transport Mechanism

Unit 1 is present in all cores in Pine Island Bay, at a wide range of water depths, with similar thicknesses at water depths ranging from ~300 m to 1200 m. To blanket such a rugged topography, suspended sediment must have traveled at a relatively high level in the water column. This suggests transport within the ISW water mass, which occurs from ~100-450 m in the water column and is known to contain sub-glacially derived-ice shelf meltwater mixed with CDW (Jacobs et al., 2011; Mankoff et al., 2012). The density differences between ISW and underlying CDW is a very sensitive and dynamic balance, a function of temperature, salinity and the amount of sediment in the subglacially derived-meltwater. Suspension within the ISW mass provides a first order approximation of sediment concentration, requiring it initially to be less dense than the CDW layer.

Interflow and overflow deposits often form delta-like deposits, losing traction when entering the marine realm. This is observed in the distribution pattern of Unit 1, as the thickest deposits occur near the modern grounding line where there is a seismically imaged wedge of sediment that thickens towards the modern Pine Island Glacier front. This is also the area of highest measured accumulation rates in sediment core PC52, which recovered 120 cm of soft (water-saturated) sediment that exhibits no  $^{210}\text{Pb}$  decay and is assumed to be a modern deposit. Seaward of this, the sediment dispersal occurred at a relatively high level in the water column. Thus, we interpret Unit 1 as a plumite deposit.

Observed circulation in the sub-ice shelf cavity in PIB (Mankoff et al., 2012) likely contributes to sediment sorting. In addition, Unit 1 may have been sorted during

subglacial transport. Subglacial sorting requires large amounts of water, which we propose does indeed exist. We are unable to differentiate between the two mechanisms as there are no cores from beneath the modern ice shelf and the sorting is quite homogenous throughout the bay. However, it is likely that both processes were influential in sorting Unit 1.

#### **4.4.5 Sediment Delivery**

Sediment flux from the grounding line is an order of magnitude greater for subunit 1A than Unit 1. This could be due to either a change in sediment source, sediment production, or in the mode of delivery. We discount the possibility that this could simply be a change in source, as sediment characteristics indicate that there is a constant, glacially derived source with elevated kaolinite for all of Unit 1. It is unlikely that sediment production rates varied by an order of magnitude as necessitated in the changes in flux, as this would correspond to a large increase in denudation rates, virtually impossible in a polar setting and unobserved. Increased flux of sediment can be explained by hydraulic potential changes in the subglacial environment, resulting in differences in meltwater expulsion and thus sediment delivery. We propose that the glacially sculpted basins within PIB serve as reservoirs for storage of sediment-laden meltwater. Hydraulic potential changes reorganize meltwater storage and mobilize sediment reserves within these basins. Channels within PIB serve as conduits for subglacial, sediment-laden water to the grounding line and beyond. Thus, stored subglacial sediments can be rapidly discharged into PIB. Changes of the ice sheet profile can cause changes in storage potential at a range of magnitudes, as revealed by our hydraulic analysis. A low flux of

background sediments may constantly reach the basins, which would be overprinted with intervals of higher flux during reorganization events.

The similarities in sediment characteristics of subunits 1A, 1B and 1C imply similar modes of transport and flux. Total volumes of Unit 1 eliminate the possibility that subunits 1B and 1C accumulated at the same rate as subunit 1A continuously for the past ~7-8 ka. Rather, the three units represent successive depositional events over the last 7-8 ka. This "leaky capacitor" model for Unit 1 calls for slow, steady release of sediments, punctuated by large fluxes of sediment-laden meltwater outflow.

#### **4.4.6 Pine Island Bay compared to other glacial systems**

Anderson and Fretwell (2008) recognized a drainage network including bedrock carved channels and basins within the inner part of Marguerite Bay. Prior to this discovery, Kennedy and Anderson (1989) introduced the possibility of a sub-ice shelf, meltwater origin for a sorted silt unit that occurs stratigraphically above till and below diatomaceous glaciomarine sediments in the inner part of the bay. Their interpretation was based on a lack of ice-rafted sand or pebbles and a lack of biogenic material. Diatomaceous sediments reflect the onset of open marine conditions and termination of terrigenous silt deposition since ~9.3 k cal yr BP (Kilfeather et al., 2011).

In the Amundsen Sea, seaward of the Getz A, Getz B and Dotson Ice Streams, are meltwater channels cut into crystalline basement (Figure 4-1) (Smith et al., 2009). There are no meltwater deposits in cores collected in this region (Smith et al., 2009). Additionally, deformation till has been sampled within one of the channels, indicating

that it has been overridden by an ice sheet (Smith et al., 2009). Thus, these relict channels survived an advance of the ice sheet, retaining similar dimensions as recently active channels (Smith et al., 2009).

Thwaites Glacier was confluent with the Pine Island Glacier during the last glacial maximum, and as recently as ~10.6 ka, based on ice sheet reconstructions in the region (Figure 4-1) (Kirshner et al., 2012). It is one of the most rapidly changing and largest glaciers on Earth (Chen et al., 2009; Rignot et al., 2011). It has a similar configuration to the Pine Island Glacier, a landward sloping bed extending to the interior of the WAIS (Holt et al., 2006). Recent advances in airborne ice-penetrating radar data collection and processing on a catchment-wide scale has revealed tributaries underlain by ice-flow-aligned sedimentary bedforms beneath Thwaites Glacier. These features transition seaward into exposed crystalline bedrock ~50 km upstream of the modern grounding line. This configuration, as well as the scale of the bedforms, are similar to the Holocene configuration in front of the Pine Island Glacier (Schroeder et al., in review). Thwaites Glacier has steep surface slopes over this region, allowing for high hydrologic gradients. This suggests that the modern configuration of Thwaites Glacier may be short-lived and poised for a similar meltwater-intensive retreat as the Holocene Pine Island Glacier.

## **4.5 Conclusions**

The inner part of Pine Island Bay contains several basins that are linked by channels. These basins have a combined storage capacity on the order of 1000 km<sup>3</sup> of water and sediment. The distribution of subglacial water is dynamically driven by



changes in grounding line position and hydraulic gradient. An extensive plumite deposit (Unit 1) records an episode of meltwater discharge, which occurred during the late stages of ice sheet retreat  $\sim 7\text{-}8.6$  k cal yr BP. This is a draping deposit that overlies proximal glacial marine sediments and thickens towards the modern grounding line. Similarities in both the grain shape and microtextures of Unit 1 relative to till indicates a glacial origin for Unit 1 with no measureable fluvial alteration of grains. High kaolinite content indicates a sedimentary source for clays.

Unit 1 was deposited from sediment-laden plumes emanating from beneath the Pine Island ice shelf. It was subsequently transported as either an interflow or overflow within the ISW layer. Age constraints indicate that subunit 1A, the youngest subunit, is a modern deposit that coincides with recent rapid retreat of the grounding line. This modern subunit has an order of magnitude greater flux relative to the entire Unit 1 deposit. This is attributed to episodic sedimentation of Unit 1. Thus, Unit 1 is interpreted as a product of non-steady-state processes where low background sedimentation alternates with sediment sequestration and purging caused by changes in hydraulic potential and glacial reorganization.

This study demonstrates that meltwater-intensive glacial retreat occurred on at least three occasions throughout the Holocene, including the current event. These events record episodes of glacial reorganization and associated meltwater release. Similar meltwater-intensive retreat occurred in Marguerite Bay during the early Holocene (Kennedy and Anderson, 1989; Kilfeather et al., 2011) and culminated in virtual loss of the ice shelf (Bentley et al., 2011). The Thwaites Glacier area currently displays a

configuration similar to that of Pine Island Glacier in the Holocene, suggesting that it may be poised for a meltwater-intensive retreat.

## Conclusions

The main conclusions of my thesis corroborate other findings that the cryosphere is a dynamic portion of the earth system.

I added new radiocarbon and  $^{210}\text{Pb}$  dates, sedimentary facies analysis, and bathymetric data. I reconstructed the post-Last Glacial Maximum deglacial history in Pine Island Bay for a better understanding of the causes of ice sheet retreat. I constructed the first detailed facies model in the region, adding robustness to the analysis. My results record a clear retreat stratigraphy in PIB of terrigenous sandy silt (plumite), pebbly sandy mud (ice-proximal glacimarine), and till. My reconstructed glacial history includes, initial retreat from the outer continental shelf shortly after the LGM and before 16.4 k cal yr BP, in response to rising sea level. I observed a sub-ice shelf facies in central PIB that spans ~12.3–10.6 k cal yr BP. Widespread impingement of warm water onto the continental shelf caused an abrupt change from sub-ice shelf sedimentation to distal glacimarine

sedimentation dominated by dispersal of terrigenous silt between 7.8 and 7.0 k cal yr BP. The uppermost sediments in PIB were hydrodynamically sorted by meltwater plumes. The most recent release of sediment coincides with rapid retreat of the grounding line, and has an order of magnitude greater flux relative to the entire unit, indicating episodic sedimentation. This is the first identification of a meltwater-derived deposit in Antarctica and demonstrates that punctuated meltwater-intensive glacial retreat occurred at least three times throughout the Holocene in this region.

Additionally, I examined quartz sand grains to conduct an analysis of mode of transport for sediments in the Antarctic Peninsula region from the Eocene to present to record the onset of glaciation. The sand grain analysis was consistent with other proxies on the same samples, which demonstrated progressive cooling since the Eocene. The northern Antarctic Peninsula Ice Sheet was present from the Pliocene onwards.

These results have contributed to the field of paleo-ice sheet reconstructions by adding data for the long time-scale as well as post-LGM retreat history. I have contributed to the field of sedimentology by providing a detailed facies model within Pine Island Bay. Lastly, I have contributed broadly to glaciology by providing sedimentary evidence for a meltwater-intensive retreat.

## References

- Abramoff, M. D., Magalhaes, P. J., and Ram, S. J. (2004). Image processing with ImageJ. *Biophotonics International* **11**, 36-42.
- Alley, R. B. (1989). Water-Pressure Coupling of Sliding and Bed Deformation .2. Velocity-Depth Profiles. *Journal of Glaciology* **35**, 119-129.
- Alley, R. B., Blankenship, D. D., and Bentley, C. R. (1986). Deformation of till beneath ice stream B, West Antarctica. *Nature*.
- Anandakrishnan, S., and Alley, R. B. (1997). Stagnation of ice stream C, West Antarctica by water piracy. *Geophysical Research Letters* **24**, 265-268.
- Anderson, J. B. (1999). "Antarctic marine geology." Cambridge University Press, Cambridge ; New York.
- Anderson, J. B., Brake, C. F., and Myers, N. C. (1984). Sedimentation on the Ross Sea Continental-Shelf, Antarctica. *Marine Geology* **57**, 295-333.
- Anderson, J. B., and Fretwell, L. O. (2008). Geomorphology of the onset area of a paleo-ice stream , Marguerite Bay , Antarctic Peninsula. **512**, 503-512.
- Anderson, J. B., Jakobsson, M., and Party, O. S. (2010). Oden Southern Ocean 0910 OSO0910 Cruise Report. In "Cruise Report." University of Stockholm, Stockholm.

- Anderson, J. B., Kennedy, D. S., Smith, M. J., and Domack, E. W. (1991). Sedimentary facies associated with Antarctica's floating ice masses. *In* "Glacial marine sedimentation; Paleoclimatic significance." (J. B. Anderson, and G. M. Ashley, Eds.). The Geological Society of America, Boulder, CO.
- Anderson, J. B., Kirshner, A. E., and Simms, A. R. (in review). Antarctica's Contribution to Post-LGM Sea-level Rise. *Geological Society of London Special Publication Antarctic Palaeoenvironmental Evolution* **editor Hambrey and others.**
- Anderson, J. B., Kurtz, D. D., Domack, E. W., and Balshaw, K. M. (1980). Glacial and Glacial Marine-Sediments of the Antarctic Continental-Shelf. *Journal of Geology* **88**, 399-414.
- Anderson, J. B., and Thomas, M. A. (1991). Marine Ice-Sheet Decoupling as a Mechanism for Rapid, Episodic Sea-Level Change - the Record of Such Events and Their Influence on Sedimentation. *Sedimentary Geology* **70**, 87-104.
- Anderson, J. B., Warny, S., Askin, R. A., Wellner, J. S., Bohaty, S. M., Kirshner, A. E., Livsey, D. N., Simms, A. R., Smith, T. R., Ehrmann, W., Lawver, L. A., Barbeau, D., Wise, S. W., Kulhanek, D. K., Weaver, F. M., and Majewski, W. (2011). Progressive Cenozoic cooling and the demise of Antarctica's last refugium. *Proceedings of the National Academy of Sciences of the United States of America* **108**, 11356-11360.
- Andrews, J. T., Domack, E. W., Cunningham, W. L., Leventer, A., Licht, K. J., Jull, A. J. T., DeMaster, D. J., and Jennings, A. E. (1999). Problems and possible solutions

concerning radiocarbon dating of surface marine sediments, Ross Sea, Antarctica.  
*Quaternary Research* **52**, 206-216.

Bard, E., Hamelin, B., Arnold, M., Montaggioni, L., Cabioch, G., Faure, G., and Rougerie, F. (1996). Deglacial sea-level record from Tahiti corals and the timing of global meltwater discharge. *Nature* **382**, 241-244.

Bentley, M. J., Johnson, J. S., Hodgson, D. A., Dunai, T., Freeman, S. P. H. T., and Ó Cofaigh, C. (2011). Rapid deglaciation of Marguerite Bay, western Antarctic Peninsula in the Early Holocene. *Quaternary Science Reviews* **30**, 3338-3349.

Berkman, P. A., and Forman, S. L. (1996). Pre-bomb radiocarbon and the reservoir correction for calcareous marine species in the Southern Ocean. *Geophysical Research Letters* **23**, 363-366.

Bindschadler, R. a. (2002). History of lower Pine Island Glacier, West Antarctica, from Landsat imagery. *Journal of Glaciology* **48**, 536-544.

Bohaty, S. M., Kulhanek, D. K., Wise, S., Jemison, K., Warny, S., and Sjunneskog, C. (2011). Age Assessment of Eocene–Pliocene Cores Recovered on the SHALDRIL II Expedition, Antarctic Peninsula. In "Tectonic, Climatic and Cryospheric Evolution of the Antarctic Peninsula " (J. B. Anderson, and J. S. Wellner, Eds.). American Geophysical Union, Washington D.C.

Boudier, T., and Tupper, B. (2011). Shape Analysis by Fourier Descriptors computation. In "ImageJ Documentation Wiki."

- Bull, P. A. (1981). Environmental reconstruction by electron microscopy. *Progress in physical geography* **5**.
- Carter, S. P., Blankenship, D. D., Peters, M. E., Young, D. A., Holt, J. W., and Morse, D. L. (2007). Radar-based subglacial lake classification in Antarctica. *Geochemistry Geophysics Geosystems* **8**.
- Carter, S. P., Blankenship, D. D., Young, D. A., Peters, M. E., Holt, J. W., and Siegert, M. J. (2009). Dynamic distributed drainage implied by the flow evolution of the 1996-1998 Adventure Trench subglacial lake discharge. *Earth and Planetary Science Letters* **283**, 24-37.
- Chen, J. L., Wilson, C. R., Blankenship, D., and Tapley, B. D. (2009). Accelerated Antarctic ice loss from satellite gravity measurements. *Nature Geoscience* **2**, 859-862.
- Clark, P. U., Dyke, A. S., Shakun, J. D., Carlson, A. E., Clark, J., Wohlfarth, B., Mitrovica, J. X., Hostetler, S. W., and McCabe, A. M. (2009). The Last Glacial Maximum. *Science* **325**, 710-714.
- Curren, M. G. (1999). Descriptions of Sediment Recovered by the R/V Nathaniel B. Palmer, United States Antarctic Program, Cruis 02, 1999. In "Antarctic Marine Geology Research Facility." Florida State University, Tallahassee, Fl.
- Cutler, P. M., Colgan, P. M., and Mickelson, D. M. (2002). Sedimentologic evidence for outburst floods from the Laurentide Ice Sheet margin in Wisconsin, USA: implications for tunnel-channel formation. *Quaternary International* **90**, 23-40.



Denton, G. H., and Hughes, T. J. (1981). The Arctic Ice Sheet: an outrageous hypothesis.

*In "The Last Great Ice Sheets." pp. 437-467. Wiley-Interscience, New York.*

Denton, G. H., and Sugden, D. E. (2005). Meltwater features that suggest Miocene ice-sheet overriding of the Transantarctic Mountains in Victoria Land, Antarctica.

*Geografiska Annaler Series a-Physical Geography* **87A**, 67-85.

Domack, E., Duran, D., Leventer, A., Ishman, S., Doane, S., McCallum, S., Amblas, D.,

Ring, J., Gilbert, R., and Prentice, M. (2005). Stability of the Larsen B ice shelf on the Antarctic Peninsula during the Holocene epoch. *Nature* **436**, 681-685.

Domack, E., Leventer, A., Dunbar, R., Taylor, F., Brachfeld, S., Sjunneskog, C., and

Party, O. L. S. (2001). Chronology of the Palmer Deep site, Antarctic Peninsula: a Holocene palaeoenvironmental reference for the circum-Antarctic. *Holocene* **11**, 1-9.

Domack, E. W., Jacobson, E. A., Shipp, S., and Anderson, J. B. (1999). Late Pleistocene-

Holocene retreat of the West Antarctic Ice-Sheet system in the Ross Sea: Part 2 - Sedimentologic and stratigraphic signature. *Geological Society of America*

*Bulletin* **111**, 1517-1536.

Domack, E. W., and Williams, C. (1990). Fine structure and suspended sediment

transport in three Antarctic fjords. *Antarctic Research Series* **50**, 71-89.

Dowdeswell, J. A. (1982). Scanning Electron-Micrographs of Quartz Sand Grains from

Cold Environments Examined Using Fourier Shape-Analysis. *Journal of*

*Sedimentary Petrology* **52**, 1315-1323.

- Dowdeswell, J. A. (1986). The Distribution and Character of Sediments in a Tidewater Glacier, Southern Baffin-Island, Nwt, Canada. *Arctic and Alpine Research* **18**, 45-56.
- Dowdeswell, J. A., Evans, J., O Cofaigh, C., and Anderson, J. B. (2006). Morphology and sedimentary processes on the continental slope off Pine Island Bay, Amundsen Sea, West Antarctica. *Geological Society of America Bulletin* **118**, 606-619.
- Dowdeswell, J. A., Osterman, L. E., and Andrews, J. T. (1985). Quartz Sand Grain Shape and Other Criteria Used to Distinguish Glacial and Non-Glacial Events in a Marine Core from Frobisher Bay, Baffin Island, Nwt, Canada. *Sedimentology* **32**, 119-132.
- Ehrlich, R., and Weinberg, B. (1970). An Exact Method for Characterization of Grain Shape. *Journal of Sedimentary Petrology* **40**, 205-&.
- Ehrmann, W., Hillenbrand, C. D., Smith, J. A., Graham, A. G. C., Kuhn, G., and Larter, R. D. (2011). Provenance changes between recent and glacial-time sediments in the Amundsen Sea embayment, West Antarctica: clay mineral assemblage evidence. *Antarctic Science* **23**, 471-486.
- Evans, J., Dowdeswell, J. A., Cofaigh, C., Benham, T. J., and Anderson, J. B. (2006). Extent and dynamics of the West Antarctic Ice Sheet on the outer continental shelf of Pine Island Bay during the last glaciation. *Marine Geology* **230**, 53-72.

- Evans, J., and Pudsey, C. J. (2002). Sedimentation associated with Antarctic Peninsula ice shelves: implications for palaeoenvironmental reconstructions of glacimarine sediments. *Journal of the Geological Society* **159**, 233-237.
- Fairbanks, R. G. (1989). A 17,000-year glacio-eustatic sea level record: influence of glacial melting rates on the Younger Dryas event and deep-ocean circulation. *Nature* **342**.
- Fedele, J. J., and Garcia, M. H. (2009). Laboratory experiments on the formation of subaqueous depositional gullies by turbidity currents. *Marine Geology* **258**, 48-59.
- Fisher, T. G., and Taylor, L. D. (2002). Sedimentary and stratigraphic evidence for subglacial flooding, south-central Michigan, USA. *Quaternary International* **90**, 87-115.
- Folk, R. L., and Ward, W. C. (1957). Brazos River bar [Texas]; a study in the significance of grain size parameters *Journal of Sedimentary Research* **27**, 3-26.
- Fowler, A. C. (1987). Sliding with Cavity Formation. *Journal of Glaciology* **33**, 255-267.
- Fricker, H. A., Scambos, T., Bindschadler, R., and Padman, L. (2007). An active subglacial water system in West Antarctica mapped from space. *Science* **315**, 1544-1548.
- Graham, A. G. C., Larter, R. D., Gohl, K., Dowdeswell, J. A., Hillenbrand, C. D., Smith, J. A., Evans, J., Kuhn, G., and Deen, T. (2010). Flow and retreat of the Late

Quaternary Pine Island-Thwaites palaeo-ice stream, West Antarctica. *Journal of Geophysical Research-Earth Surface* **115**, -.

Graham, A. G. C., Larter, R. D., Gohl, K., Hillenbrand, C.-d., Smith, J. A., and Kuhn, G. (2009). Bedform signature of a West Antarctic palaeo-ice stream reveals a multi-temporal record of flow and substrate control. **28**, 2774-2793.

Gray, L. (2005). Evidence for subglacial water transport in the West Antarctic Ice Sheet through three-dimensional satellite radar interferometry. *Geophysical Research Letters* **32**, 2-5.

Haines, J., and Mazzullo, J. (1988). The Original Shapes of Quartz Silt Grains - a Test of the Validity of the Use of Quartz Grain Shape-Analysis to Determine the Sources of Terrigenous Silt in Marine Sedimentary Deposits. *Marine Geology* **78**, 227-240.

Harden, S. L., Demaster, D. J., and Nittrouer, C. A. (1992). Developing Sediment Geochronologies for High-Latitude Continental-Shelf Deposits - a Radiochemical Approach. *Marine Geology* **103**, 69-97.

Hellmer, H. H., Jacobs, S., S., and Jenkins, A. (1998). "Oceanic erosion of a floating Antarctic glacier in the Amundsen Sea." American Geophysical Union.

Hemer, M. A., Post, A. L., O'Brien, P. E., Craven, M., Truswell, E. M., Roberts, D., and Harris, P. T. (2007). Sedimentological signatures of the sub-Amery Ice Shelf circulation. *Antarctic Science* **19**, 497-506.

- Heroy, D. C., and Anderson, J. B. (2005). Ice-sheet extent of the Antarctic Peninsula region during the Last Glacial Maximum (LGM), Insights from glacial geomorphology. *Geological Society of America Bulletin* **117**, 1497-1497.
- Heroy, D. C., and Anderson, J. B. (2007). Radiocarbon constraints on Antarctic Peninsula Ice Sheet retreat following the Last Glacial Maximum (LGM). *Quaternary Science Reviews* **26**, 3286-3297.
- Hesse, R., Khodabakhsh, S., Klaucke, I., and Ryan, W. B. F. (1997). Asymmetrical turbid surface-plume deposition near ice-outlets of the Pleistocene Laurentide ice sheet in the Labrador sea. *Geo-Marine Letters* **17**, 179-187.
- Hillenbrand, C. D., Kuhn, G., Smith, J. A., Gohl, K., Graham, A. G. C., Larter, R. D., Klages, J. P., Downey, R., Moreton, S. G., Forwick, M., and Vaughan, D. G. (2013). Grounding-line retreat of the West Antarctic Ice Sheet from inner Pine Island Bay. *Geology* **41**, 35-38.
- Hillenbrand, C. D., Smith, J. A., Kuhn, G., Esper, O., Gersonde, R., Larter, R. D., Maher, B., Moreton, S. G., Shimmield, T. M., and Korte, M. (2010). Age assignment of a diatomaceous ooze deposited in the western Amundsen Sea Embayment after the Last Glacial Maximum. *Journal of Quaternary Science* **25**, 280-295.
- Holt, J. W., Blankenship, D. D., Morse, D. L., Young, D. A., Peters, M. E., Kempf, S. D., Richter, T. G., Vaughan, D. G., and Corr, H. F. J. (2006). New boundary conditions for the West Antarctic Ice Sheet: Subglacial topography of the Thwaites and Smith glacier catchments. *Geophysical Research Letters* **33**, -.

- Hughes, T. (1977). West Antarctic Ice Streams. *Reviews of Geophysics* **15**, 1-46.
- Hughes, T. (1998). "Ice Sheets." Oxford University Press, New York.
- Hughes, T. (2002). Calving bays. *Quaternary Science Reviews* **21**, 267-282.
- Hughes, T. (2011). A simple holistic hypothesis for the self-destruction of ice sheets. *Quaternary Science Reviews* **30**, 1829-1845.
- Hughes, T. J. (1981). The weak underbelly of the West Antarctic ice sheet. *Journal of Glaciology* **27**, 518-525.
- Jacobs, S. S., Hellmer, H. H., and Jenkins, A. (1996). Antarctic ice sheet melting in the Southeast Pacific. *Geophysical Research Letters* **23**, 957-960.
- Jacobs, S. S., Jenkins, A., Giulivi, C. F., and Dutrieux, P. (2011). Stronger ocean circulation and increased melting under Pine Island Glacier ice shelf. *Nature Geoscience* **4**, 519-523.
- Jakobsson, M., Anderson, J. B., Nitsche, F. O., Dowdeswell, J. A., Gyllencreutz, R., Kirschner, N., Mohammad, R., O'Regan, M., Alley, R., Anandakrishnan, S., Eriksson, B., Kirshner, A. E., Fernandez, R., Stolldorf, T., Minzoni, R., and Majewski, W. (2011). Geological Record of Ice Shelf Break-up and Grounding Line Retreat, Pine Island Bay, West Antarctica. *Geology*.
- Jakobsson, M., Anderson, J. B., Nitsche, F. O., Gyllencreutz, R., Kirshner, A. E., Kirchner, N., O'Regan, M., Mohammad, R., and Eriksson, B. (2012). Ice sheet

retreat dynamics inferred from glacial morphology of the central Pine Island Bay Trough, West Antarctica. *Quaternary Science Reviews* **38**, 1-10.

Jamieson, S., Vieli, A., Livingstone, S., Stokes, C., O Cofaigh, C., and Hillenbrand, C. D. (2011). The controls on the post-LGM retreat of Marguerite Bay palaeo ice-stream, Antarctic Peninsula: highresolution

mapping constrains numerical modelling, Edinburgh, Scotland.

Jenkins, A., Dutrieux, P., Jacobs, S. S., McPhail, S. D., Perrett, J. R., Webb, A. T., and White, D. (2010). Observations beneath Pine Island Glacier in West Antarctica and implications for its retreat. *Nature Geoscience* **3**, 468-472.

Jenkins, A., Vaughan, D. G., Jacobs, S. S., Hellmer, H. H., and Keys, J. R. (1997). Glaciological and oceanographic evidence of high melt rates beneath Pine island glacier, west Antarctica. *Journal of Glaciology* **43**, 114-121.

Johnson, J. S., Bentley, M. J., and Gohl, K. (2008). First exposure ages from the Amundsen Sea Embayment , West Antarctica : The Late Quaternary context for recent thinning of Pine Island , Smith , and Pope Glaciers.

Joughin, I., Tulaczyk, S., Bamber, J. L., Blankenship, D., Holt, J. W., Scambos, T., and Vaughan, D. G. (2009). Basal conditions for Pine Island and Thwaites Glaciers, West Antarctica, determined using satellite and airborne data. *Journal of Glaciology* **55**, 245-257.

- Kamb, B. (1987). Glacier Surge Mechanism Based on Linked Cavity Configuration of the Basal Water Conduit System. *Journal of Geophysical Research-Solid Earth and Planets* **92**, 9083-9100.
- Kamb, B., Raymond, C. F., Harrison, W. D., Endlehardt, H., Echelmeyer, K. A., Humphrey, N., Brugman, M. M., and Pfeffer, T. (1985). Glacier surge mechanism: 1982–1983 surge of Variegated Glacier, Alaska. *Science* **227**, 469-479.
- Katz, R. F., and Worster, M. G. (2010). Stability of ice-sheet grounding lines. *Proceedings of the Royal Society a-Mathematical Physical and Engineering Sciences* **466**, 1597-1620.
- Kennedy, D. S., and Anderson, J. B. (1989). Glacial-Marine Sedimentation and Quaternary Glacial History of Marguerite Bay, Antarctic Peninsula. *Quaternary Research* **31**, 255-276.
- Kilfeather, A. A., Cofaigh, C. O., Lloyd, J. M., Dowdeswell, J. A., Xu, S., and Moreton, S. G. (2011). Ice-stream retreat and ice-shelf history in Marguerite Trough, Antarctic Peninsula: Sedimentological and foraminiferal signatures. *Geological Society of America Bulletin* **123**, 997-1015.
- Kirshner, A. E., and Anderson, J. B. (2011). Cenozoic Glacial History of the Northern Antarctic Peninsula: A Micromorphological Investigation of Quartz Sand Grains. *In "Tectonic, Climatic, and Cryospheric Evolution of the Antarctic Peninsula." (J.*



B. Anderson, and J. S. Wellner, Eds.), pp. 153-166. American Geophysical Union, Washington D.C.

Kirshner, A. E., Anderson, J. B., Jakobsson, M., O'Regan, M., Majewski, W., and Nitsche, F. O. (2012). Post-LGM deglaciation in Pine Island Bay, West Antarctica. *Quaternary Science Reviews* **38**, 11-26.

Krinsley, D., and Margolis, S. (1969). A Study of Quartz Sand Grain Surface Textures with Scanning Electron Microscope. *Transactions of the New York Academy of Sciences* **31**, 457-&.

Krinsley, D. H., and Doornkamp, J. C. (1973). "Atlas of quartz sand surface textures." University Press, Cambridge [Eng.].

Krumbein, W. C., and Pettijohn, F. J. (1938). "Manual of Sedimentary Petrography."

Kuhn, G., Melles, M., Ehrmann, W. U., Hambrey, M. J., and Schmiedl, G. (1993). Character of Clasts in Glaciomarine Sediments as an Indicator of Transport and Depositional Processes, Weddell and Lazarev Seas, Antarctica. *Journal of Sedimentary Petrology* **63**, 477-487.

Lambeck, K., and Chappell, J. (2001). Sea level change through the last glacial cycle. *Science* **292**, 679-686.

Lees, G. (1964). A New Method for Determining the Angularity of Particles. *Sedimentology* **3**, 2-21.

- LeMasurier, W. E. (2008). Neogene extension and basin deepening in the West Antarctic rift inferred from comparisons with the East African rift and other analogs. *Geology* **36**, 247-250.
- Lewis, A. R., Marchant, D. R., Kowalewski, D. E., Baldwin, S. L., and Webb, L. E. (2006). The age and origin of the Labyrinth, western Dry Valleys, Antarctica: Evidence for extensive middle Miocene subglacial floods and freshwater discharge to the Southern Ocean. *Geology* **34**, 513-516.
- Livingstone, S. J., Ó Cofaigh, C., Stokes, C. R., Hillenbrand, C.-D., Vieli, A., and Jamieson, S. S. R. (2012). Antarctic palaeo-ice streams. *Earth-Science Reviews* **111**, 90-128.
- Lowe, a., and Anderson, J. (2002). Reconstruction of the West Antarctic ice sheet in Pine Island Bay during the Last Glacial Maximum and its subsequent retreat history. *Quaternary Science Reviews* **21**, 1879-1897.
- Lowe, A. L., and Anderson, J. B. (2003). Evidence for abundant subglacial meltwater beneath the paleo-ice sheet in Pine Island Bay, Antarctica. *Journal of Glaciology* **49**, 125-138.
- Lythe, M. B., Vaughan, D. G., and Consortium, B. (2001). BEDMAP: A new ice thickness and subglacial topographic model of Antarctica. *Journal of Geophysical Research-Solid Earth* **106**, 11335-11351.
- Macayeal, D. R. (1992a). Irregular Oscillations of the West Antarctic Ice-Sheet. *Nature* **359**, 29-32.

- MacAyeal, D. R. (1992b). The Basal Stress-Distribution of Ice Stream-E, Antarctica, Inferred by Control Methods. *Journal of Geophysical Research-Solid Earth* **97**, 595-603.
- MacAyeal, D. R., Scambos, T. A., Hulbe, C. L., and Fahnestock, M. A. (2003). Catastrophic ice-shelf break-up by an ice-shelf-fragment-capsize mechanism. *Journal of Glaciology* **49**, 22-36.
- Mahaney, W. C. (2002). "Atlas of sand grain surface textures and applications." Oxford University Press, Oxford [England] ; New York.
- Mahaney, W. C., Claridge, G., and Campbell, I. (1996). Microtextures on quartz grains in tills from Antarctica. *Palaeogeography Palaeoclimatology Palaeoecology* **121**, 89-103.
- Mahaney, W. C., and Kalm, V. (1995). Scanning Electron-Microscopy of Pleistocene Tills in Estonia. *Boreas* **24**, 13-29.
- Mahaney, W. C., and Kalm, V. (2000). Comparative scanning electron microscopy study of oriented till blocks, glacial grains and Devonian sands in Estonia and Latvia. *Boreas* **29**, 35-51.
- Mahaney, W. C., Vortisch, W., and Julig, P. (1988). Relative Differences between Glacially Crushed Quartz Transported by Mountain and Continental Ice - Some Examples from North-America and East-Africa. *American Journal of Science* **288**, 810-826.

- Maldonado, A., Barnolas, A., Bohoyo, F., Escutia, C., Galindo-Zaldivar, J., Hernandez-Molina, J., Jabaloy, A., Lobo, F. J., Nelson, C. H., Rodriguez-Fernandez, J., Somoza, L., and Vazquez, J. T. (2005). Miocene to Recent contourite drifts development in the northern Weddell Sea (Antarctica). *Global and Planetary Change* **45**, 99-129.
- Mankoff, K. D., Jacobs, S. S., Tulaczyk, S. M., and Stammerjohn, S. E. (2012). The role of Pine Island Glacier ice shelf basal channels in deep-water upwelling, polynyas and ocean circulation in Pine Island Bay, Antarctica. *Annals of Glaciology* **53**, 123-128.
- Marensi, S. A., Net, L. I., and Santillana, S. N. (2002). Provenance, environmental and paleogeographic controls on sandstone composition in an incised-valley system: the Eocene La Meseta Formation, Seymour Island, Antarctica. *Sedimentary Geology* **150**, 301-321.
- Marshall, J. R. (1987). "Clastic particles : scanning electron microscopy and shape analysis of sedimentary and volcanic clasts." Van Nostrand Reinhold Co., New York.
- Mazzullo, J., Alexander, A., Tieh, T., and Ding, M. L. (1992). The Effects of Wind Transport on the Shapes of Quartz Silt Grains. *Journal of Sedimentary Petrology* **62**, 961-971.
- Mazzullo, J., and Ritter, C. (1991). Influence of Sediment Source on the Shapes and Surface Textures of Glacial Quartz Sand Grains. *Geology* **19**, 384-388.

- Mazzullo, J., and Withers, K. D. (1984). Sources, Distribution, and Mixing of Late Pleistocene and Holocene Sands on the South Texas Continental-Shelf. *Journal of Sedimentary Petrology* **54**, 1319-1334.
- Mccave, I. N., Bryant, R. J., Cook, H. F., and Coughanowr, C. A. (1986). Evaluation of a Laser-Diffraction-Size Analyzer for Use with Natural Sediments. *Journal of Sedimentary Petrology* **56**, 561-564.
- Mercer, J. H. (1978). West Antarctic Ice Sheet and Co<sub>2</sub> Greenhouse Effect - Threat of Disaster. *Nature* **271**, 321-325.
- Miller, K. G., Kominz, M. A., Browning, J. V., Wright, J. D., Mountain, G. S., Katz, M. E., Sugarman, P. J., Cramer, B. S., Christie-Blick, N., and Pekar, S. F. (2005). The phanerozoic record of global sea-level change. *Science* **310**, 1293-1298.
- Mosola, A. B., and Anderson, J. B. (2006). Expansion and rapid retreat of the West Antarctic Ice Sheet in eastern Ross Sea: possible consequence of over-extended ice streams? *Quaternary Science Reviews* **25**, 2177-2196.
- Nitsche, F. O., Gohl, K., Larter, R. D., Hillenbrand, C. D., Kuhn, G., Smith, J., Jacobs, S., Anderson, J. B., and Jakobsson, M. (2012). Paleo ice flow and subglacial meltwater dynamics in Pine Island Bay, West Antarctica. *The Cryosphere Discussions* **6**, 4267-4304.
- Nitsche, F. O., Jacobs, S. S., Larter, R. D., and Gohl, K. (2007). Bathymetry of the Amundsen Sea continental shelf: Implications for geology, oceanography, and glaciology. *Geochemistry Geophysics Geosystems* **8**, -.

- Ó Cofaigh, C. (1996). Tunnel valley genesis. *Progress in Physical Geography* **20**, 1-19.
- Ó Cofaigh, C., and Dowdeswell, J. A. (2001). Laminated sediments in glacimarine environments : diagnostic criteria for their interpretation. **20**.
- Ó Cofaigh, C., Dowdeswell, J. A., Evans, J., and Larter, R. D. (2008). Geological constraints on Antarctic palaeo-ice-stream retreat. **525**, 513-525.
- Payne, A. J., Holland, P. R., Shepherd, A. P., Rutt, I. C., Jenkins, A., and Joughin, I. (2007). Numerical modeling of ocean-ice interactions under Pine Island Bay's ice shelf. *Journal of Geophysical Research-Oceans* **112**.
- Powell, R. D. (1990). Glacimarine processes at grounding-line fans and their growth to ice-contact deltas. *Geological Society, London, Special Publications* **53**, 53-73.
- Pratson, L. F., Nittrouer, C. A., Wiberg, P. L., Steckler, M. S., Swenson, J. B., Cacchione, D. A., Karson, J. A., Murray, A. B., Wolinsky, M. A., Gerber, T. P., Mullenbach, B. L., Spinelli, G. A., Fulthorpe, C. S., O'Grady, D. B., Parker, G., Driscoll, N. W., Burger, R. L., Paola, C., Orange, D. L., Field, M. E., Friedrichs, C. T., and Fedele, J. J. (2007). Seascape Evolution on Clastic Continental Shelves and Slopes. *In "Continental Margin Sedimentation."* pp. 339-380. Blackwell Publishing Ltd.
- Pritchard, H. D., Ligtenberg, S. R. M., Fricker, H. A., Vaughan, D. G., van den Broeke, M. R., and Padman, L. (2012). Antarctic ice-sheet loss driven by basal melting of ice shelves. *Nature* **484**, 502-505.

- Rasband, W. S. (1989). Image Version 1.21, User's Guide. PB90-123308. National Institutes of Health, Bethesda, MD.
- Reimer, P. J., Baillie, M. G. L., Bard, E., Bayliss, A., Beck, J. W., Blackwell, P. G., Ramsey, C. B., Buck, C. E., Burr, G. S., Edwards, R. L., Friedrich, M., Grootes, P. M., Guilderson, T. P., Hajdas, I., Heaton, T. J., Hogg, A. G., Hughen, K. A., Kaiser, K. F., Kromer, B., McCormac, F. G., Manning, S. W., Reimer, R. W., Richards, D. A., Southon, J. R., Talamo, S., Turney, C. S. M., van der Plicht, J., and Weyhenmeyer, C. E. (2009). Intcal09 and Marine09 Radiocarbon Age Calibration Curves, 0-50,000 Years Cal Bp. *Radiocarbon* **51**, 1111-1150.
- Rignot, E. (2006). Changes in ice dynamics and mass balance of the Antarctic ice sheet. *Philosophical Transactions of the Royal Society a-Mathematical Physical and Engineering Sciences* **364**, 1637-1655.
- Rignot, E., Bamber, J. L., Van Den Broeke, M. R., Davis, C., Li, Y. H., Van De Berg, W. J., and Van Meijgaard, E. (2008). Recent Antarctic ice mass loss from radar interferometry and regional climate modelling. *Nature Geoscience* **1**, 106-110.
- Rignot, E., Vaughan, D. G., Schmelz, M., Dupont, T. K., and MacAyeal, D. (2002). Acceleration of Pine Island and Thwaites Glaciers, West Antarctica. *Annals of Glaciology* **34**, 189-194.
- Rignot, E., Velicogna, I., van den Broeke, M. R., Monaghan, A., and Lenaerts, J. (2011). Acceleration of the contribution of the Greenland and Antarctic ice sheets to sea level rise. *Geophysical Research Letters* **38**.

- Rignot, E. J. (1998). Fast recession of a West Antarctic glacier. *Science* **281**, 549-551.
- Rittenhouse, G. (1943). Measuring intercept sphericity of sand grains. *American Journal of Science* **241**, 109-116.
- Robertson, R. (2010). Tides, the PIG, and. In "IOP Conference Series: Earth and Environmental Science ", pp. 012002. IOP Publishing.
- Rodriguez, A. B., and Anderson, J. B. (2004). Contourite origin for shelf and upper slope sand sheet, offshore Antarctica. *Sedimentology* **51**, 699-711.
- Schoof, C. (2007a). Ice sheet grounding line dynamics: Steady states, stability, and hysteresis. *Journal of Geophysical Research-Earth Surface* **112**, -.
- Schoof, C. (2007b). Marine ice-sheet dynamics. Part 1. The case of rapid sliding. *Journal of Fluid Mechanics* **573**, 27-55.
- Schroeder, D. M., Blankenship, D. D., Young, D. A., Kirshner, A. E., and Anderson, J. B. (submitted). Subglacial bedforms suggest Thwaites Glacier, West Antarctica is poised for a melt-water intensive retreat *Geology*.
- Sharpe, D. R. (1988). Late Glacial Landforms of Wollaston Peninsula, Victoria-Island, Northwest-Territories - Product of Ice-Marginal Retreat, Surge, and Mass Stagnation. *Canadian Journal of Earth Sciences* **25**, 262-279.
- Shepherd, A., Wingham, D., and Rignot, E. (2004). Warm ocean is eroding West Antarctic Ice Sheet. *Geophysical Research Letters* **31**, 4.



- Shepherd, A., Wingham, D. J., Mansley, J. A. D., and Corr, H. F. J. (2001). Inland thinning of Pine Island Glacier, West Antarctica. *Science* **291**, 862-864.
- Smith, J. a., Hillenbrand, C.-D., Larter, R. D., Graham, A. G. C., and Kuhn, G. (2009). The sediment infill of subglacial meltwater channels on the West Antarctic continental shelf. *Quaternary Research* **71**, 190-200.
- Smith, J. A., Hillenbrand, C. D., Kuhn, G., Larter, R. D., Graham, A. G. C., Ehrmann, W., Moreton, S. G., and Forwick, M. (2011). Deglacial history of the West Antarctic Ice Sheet in the western Amundsen Sea Embayment. *Quaternary Science Reviews* **30**, 488-505.
- Smith, R. T., and Anderson, J. B. (2009). Ice-sheet evolution in James Ross Basin, Weddell Sea margin of the Antarctic Peninsula: The seismic stratigraphic record. *Geological Society of America Bulletin* **122**, 830-842.
- Smith, R. T., and Anderson, J. B. (2011). Seismic stratigraphic results from SHALDRIL II: implications for glacial evolution of the northern Antarctic Peninsula. In "Tectonic, Climatic and Cryospheric Evolution of the Antarctic Peninsula " (J. B. Anderson, and J. S. Wellner, Eds.). American Geophysical Union, Washington D.C.
- Stearns, L. A., Smith, B. E., and Hamilton, G. S. (2008). Increased flow speed on a large East Antarctic outlet glacier caused by subglacial floods. *Nature Geoscience* **1**, 827-831.

- Stickley, C. E., St John, K., Koc, N., Jordan, R. W., Passchier, S., Pearce, R. B., and Kearns, L. E. (2009). Evidence for middle Eocene Arctic sea ice from diatoms and ice-rafted debris. *Nature* **460**, 376-U88.
- Sugden, D. E., Denton, G. H., and Marchant, D. R. (1991). Subglacial Meltwater Channel Systems and Ice Sheet Overriding, Asgard Range, Antarctica. *Geografiska Annaler. Series A. Physical Geography* **73**, 109-121.
- Sweet, D. E., and Soreghan, G. S. (2010). Application of Quartz Sand Microtextural Analysis to Infer Cold-Climate Weathering for the Equatorial Fountain Formation (Pennsylvanian-Permian, Colorado, USA). *Journal of Sedimentary Research* **80**, 666-677.
- Thoma, M., Jenkins, A., Holland, D., and Jacobs, S. (2008). Modelling Circumpolar Deep Water intrusions on the Amundsen Sea continental shelf, Antarctica. **35**, 1-6.
- Thomas, R., Rignot, E., Casassa, G., Kanagaratnam, R., Acuña, C., Akins, T., Brecher, H., Frederick, E., Gogineni, P., Krabill, W., Manizade, S., Ramamoorthy, H., Rivera, A., Russell, R., Sonntag, J., Swift, R., Yungel, J., and Zwally, J. (2004). Accelerated Sea-Level Rise from West Antarctica. *Science* **306**.
- Thomas, R. H. (1977). Calving bay dynamics and ice sheet retreat up the St. Lawrence valley system. *Géographie Physique et Quaternaire* **31**, 347-356.

U.S. Department of Commerce, N. O. a. A. A., National Geophysical Data Center.

(2001). 2-minute Gridded Global Relief Data (ETOPO2).

Uenzelmann-Neben, G., Gohl, K., Larter, R. D., and Schluter, P. (2007). Differences in ice retreat across Pine Island Bay, West Antarctica, since the Last Glacial Maximum: Indications from multichannel seismic reflection data. US Geological Survey Open-File Report.

Vaughan, D. G. (2008). West Antarctic Ice Sheet collapse - the fall and rise of a paradigm. *Climatic Change* **91**, 65-79.

Vaughan, D. G., Corr, H. F. J., Ferraccioli, F., Frearson, N., Hare, A. O., Mach, D., Holt, J. W., Blankenship, D. D., Morse, D. L., and Young, D. A. (2006). New boundary conditions for the West Antarctic ice sheet : Subglacial topography beneath Pine Island Glacier. **33**, 2-5.

Vaughan, D. G., and al., e. (2001). "A review of Pine Island Glacier, West Antarctica: Hypotheses of instability vs. observations of change ".

Walder, J. S., and Fowler, A. (1994). Channelized Subglacial Drainage over a Deformable Bed. *Journal of Glaciology* **40**, 3-15.

Walsh, J. P., and Nittrouer, C. A. (1999). Observations of sediment flux to the Eel continental slope, northern California. *Marine Geology* **154**, 55-68.

Warny, S., and Askin, R. (2011a). Last Remnants of Cenozoic Vegetation and Organic-Walled Phytoplankton in the Antarctic Peninsula's Icehouse World. *In* "Tectonic,

Climatic, and Cryospheric Evolution of the Antarctic Peninsula." pp. 167-192.  
Spec. Publ. AGU, Washington, DC.

Warny, S., and Askin, R. (2011b). Vegetation and Organic-Walled Phytoplankton at the End of the Antarctic Greenhouse World: Latest Eocene Cooling Events. *In* "Tectonic, Climatic, and Cryospheric Evolution of the Antarctic Peninsula." pp. 193-210. Spec. Publ. AGU, Washington, DC.

Weertman, J. (1976). Glaciology's Grand Unsolved Problem. *Nature* **260**, 284-286.

Wellner, J. S., Anderson, J. B., Ehrmann, W., Weaver, F. M., Kirshner, A., Livsey, D., and Simms, A. R. (2011). History of an Evolving Ice Sheet as Recorded in SHALDRIL Cores From the Northwestern Weddell Sea, Antarctica. *In* "Tectonic, Climatic, and Cryospheric Evolution of the Antarctic Peninsula." pp. 131-151. Spec. Publ. AGU, Washington, DC.

Winberry, J. P., and Anandakrishnan, S. (2004). Crustal structure of the West Antarctic rift system and Marie Byrd Land hotspot. *Geology* **32**, 977-980.

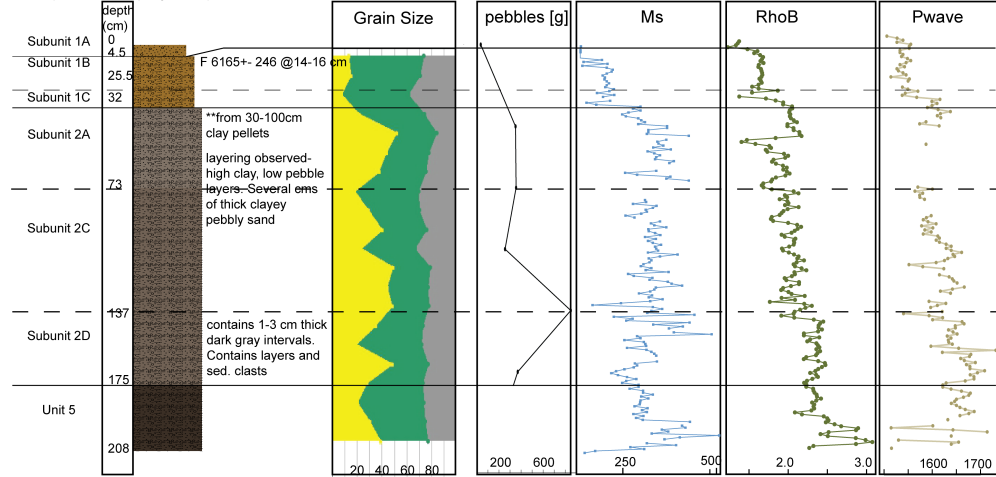
Wingham, D. J., Siegert, M. J., Shepherd, A., and Muir, A. S. (2006). Rapid discharge connects Antarctic subglacial lakes. *Nature* **440**, 1033-6.

Wingham, D. J., Wallis, D. W., and Shepherd, A. (2009). Spatial and temporal evolution of Pine Island Glacier thinning, 1995-2006. *Geophysical Research Letters* **36**, -.

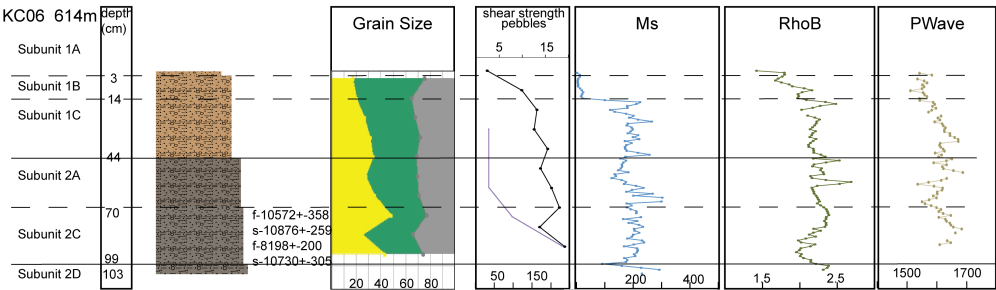
Zachos, J., Pagani, M., Sloan, L., Thomas, E., and Billups, K. (2001). Trends, rhythms, and aberrations in global climate 65 Ma to present. *Science* **292**, 686-693.

# Appendix A

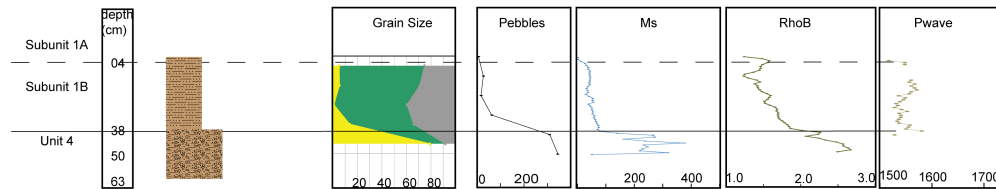
KC04 (KC05 redeployment) 729 m



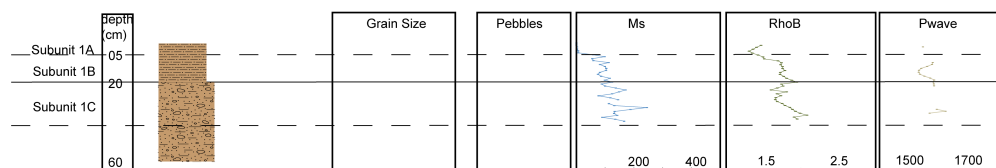
KC06 614m



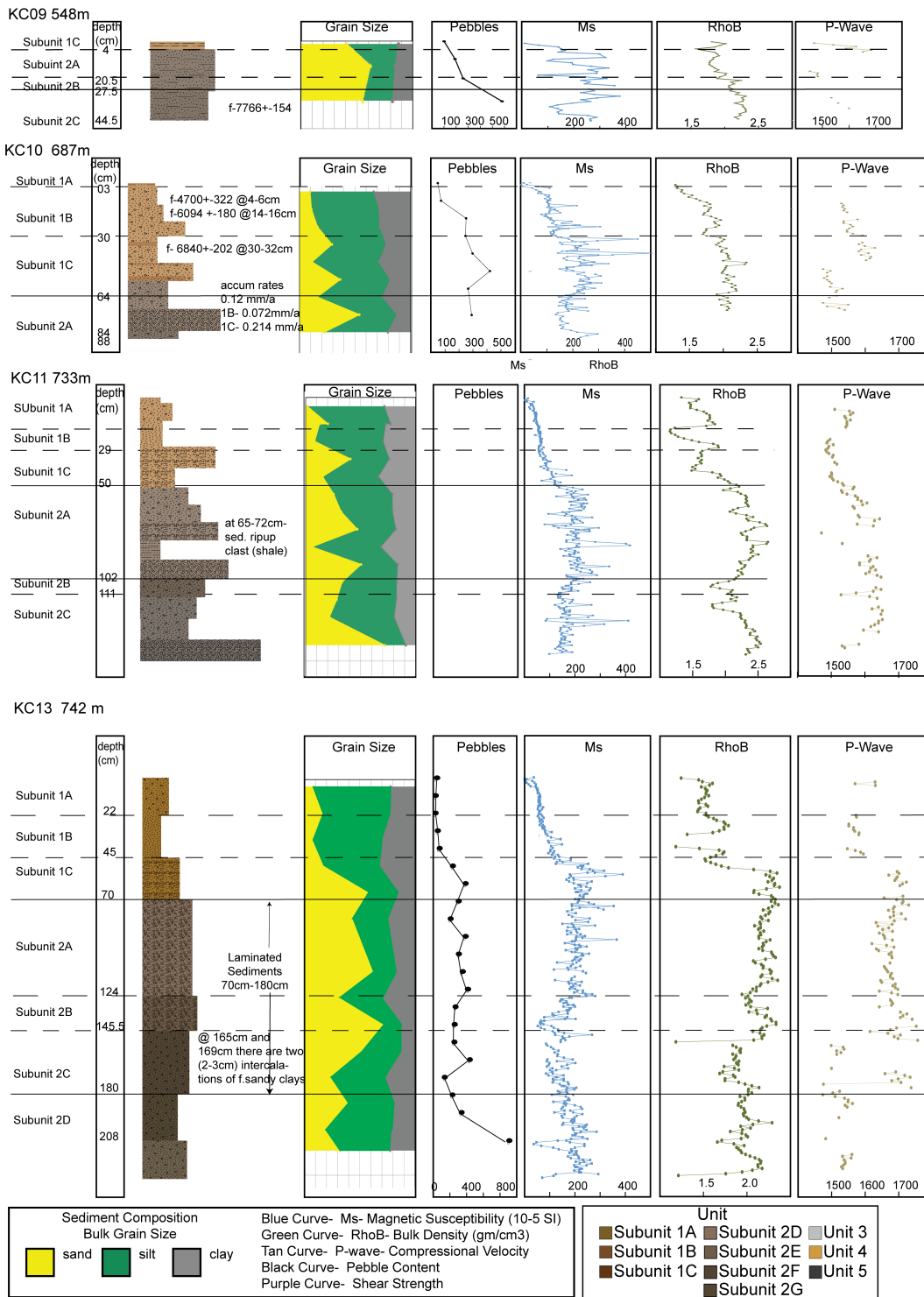
KC07 707m



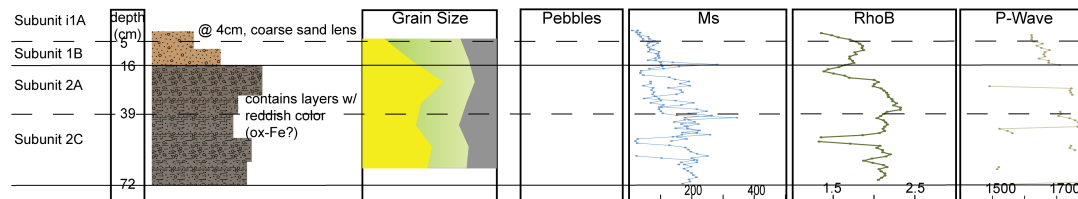
KC08 711m



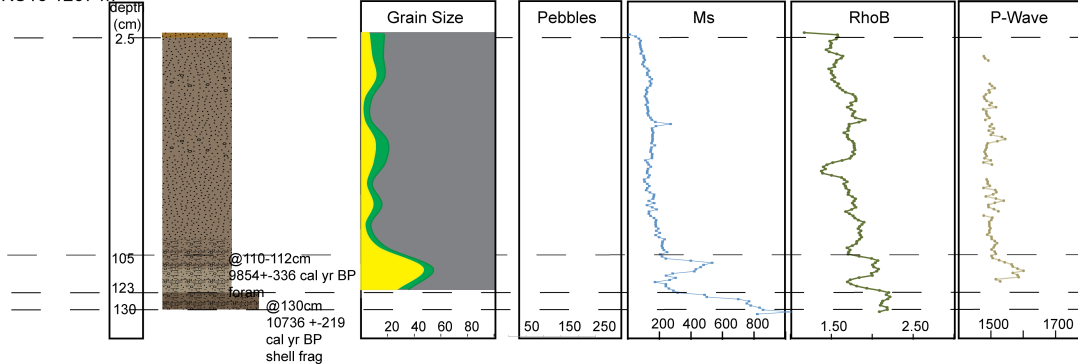
Sediment Composition			Blue Curve- Ms- Magnetic Susceptibility (10 <sup>-5</sup> SI)		Unit		
Bulk Grain Size			Green Curve- RhoB- Bulk Density (gm/cm <sup>3</sup> )		Subunit 1A		
Yellow	Green	Grey	Tan Curve- P-wave- Compressional Velocity		Subunit 2D		
			Black Curve- Pebble Content		Subunit 1B		
			Purple Curve- Shear Strength		Subunit 2E		
					Subunit 1C		
					Subunit 2F		
					Unit 3		
					Unit 4		
					Unit 5		
					Subunit 2G		



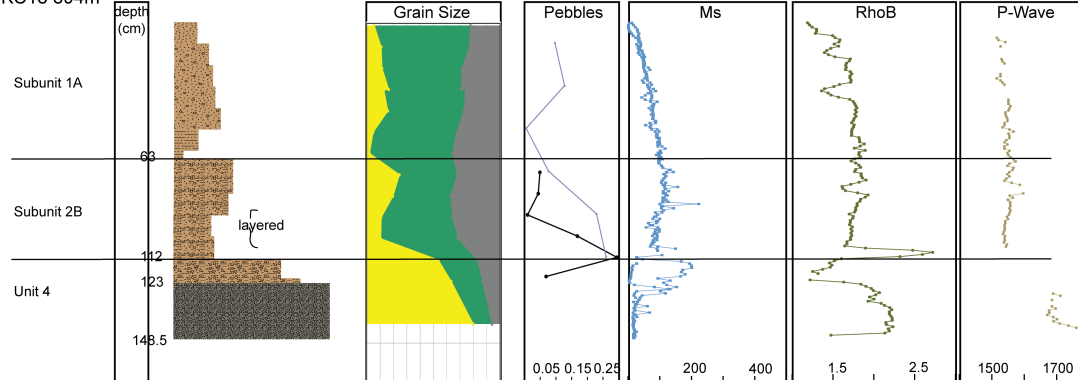
KC14 639m



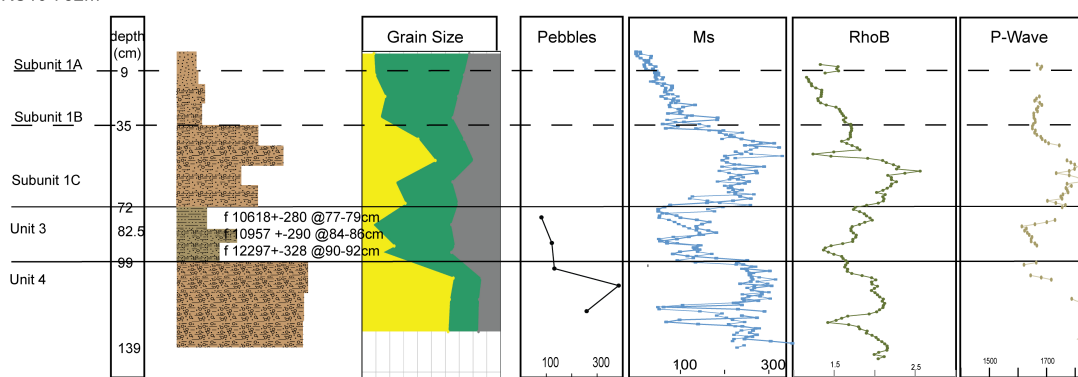
KC15 1257 m



KC18 894m

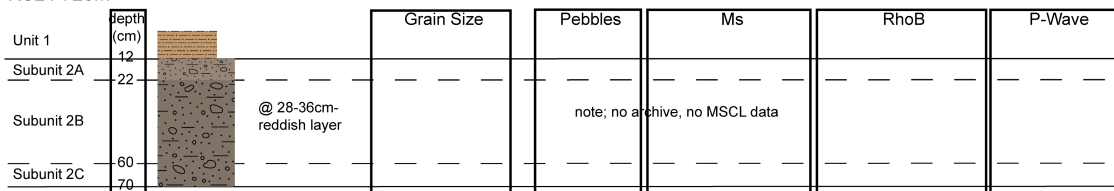


KC19 782m

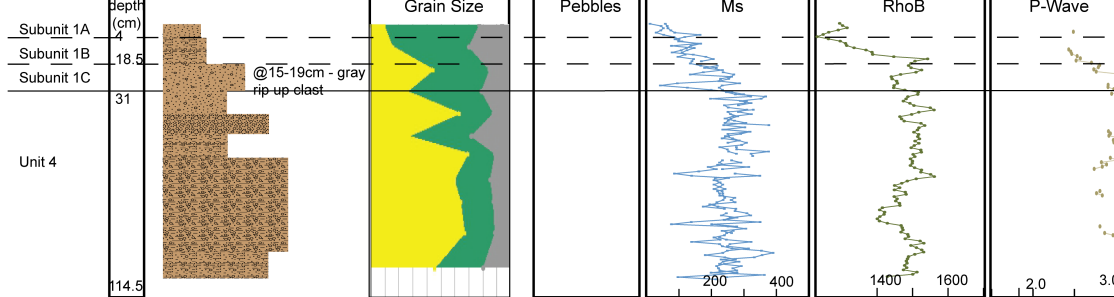


Sediment Composition			Blue Curve- Ms- Magnetic Susceptibility (10 <sup>-5</sup> SI)	Unit		
Bulk Grain Size			Green Curve- RhoB- Bulk Density (gm/cm <sup>3</sup> )	Subunit 1A	Subunit 2D	Unit 3
Yellow	Green	Grey	Tan Curve- P-wave- Compressional Velocity	Subunit 1B	Subunit 2E	Unit 4
			Black Curve- Pebble Content	Subunit 1C	Subunit 2F	Unit 5
			Purple Curve- Shear Strength		Subunit 2G	

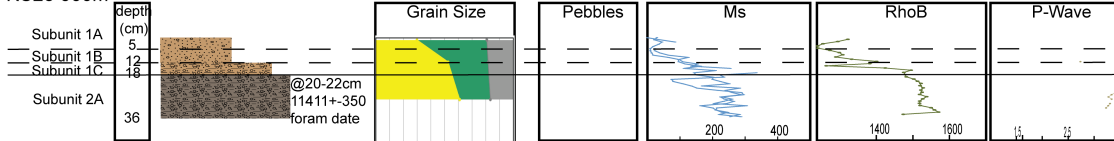
KC21 728m



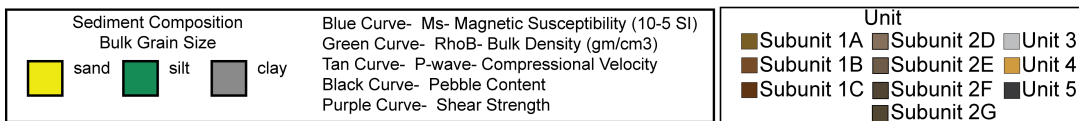
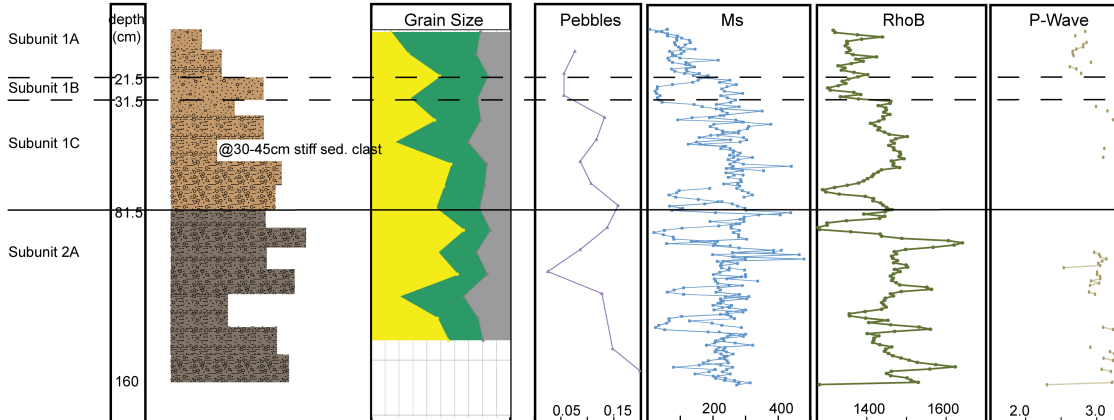
KC22 724m



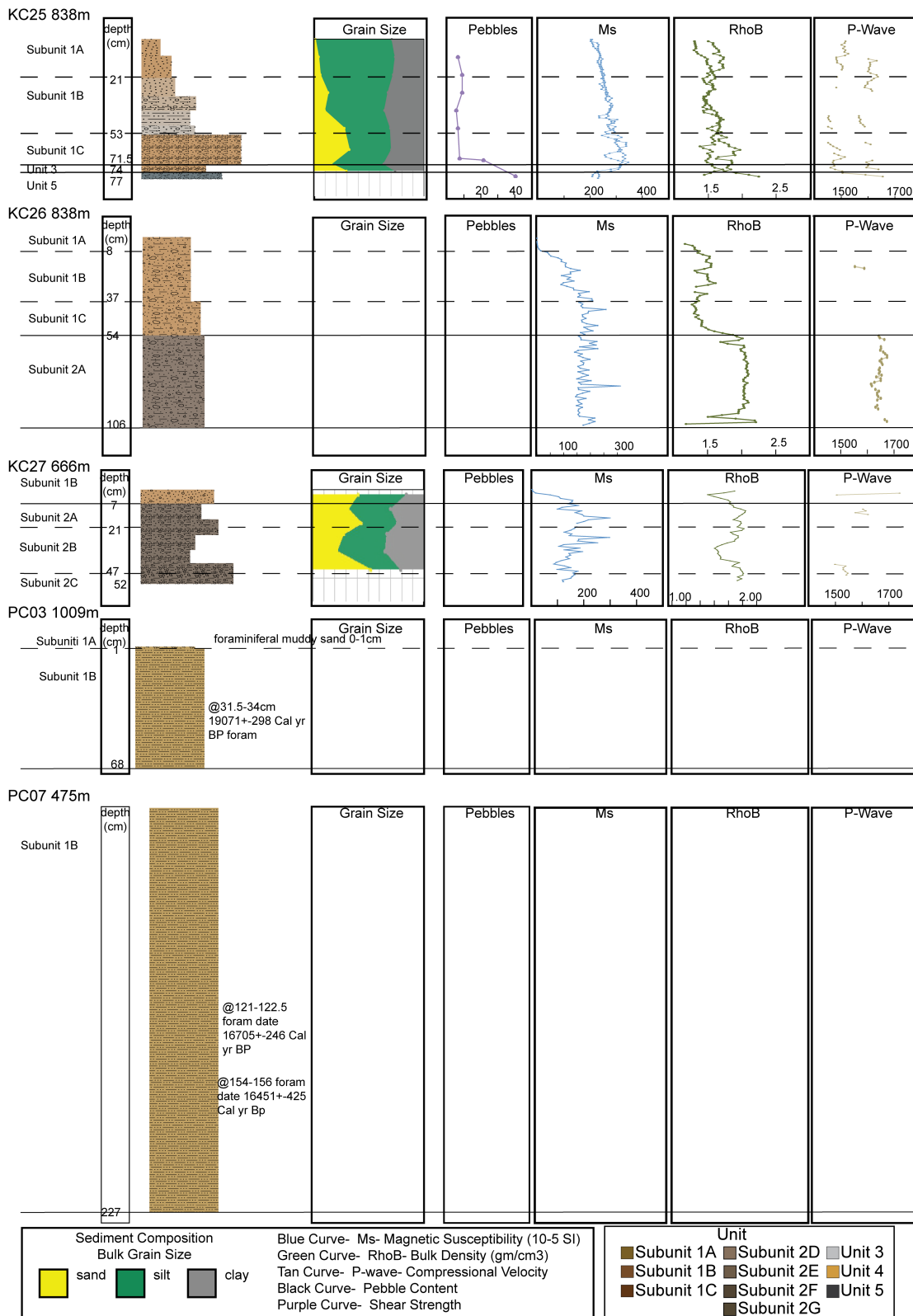
KC23 660m



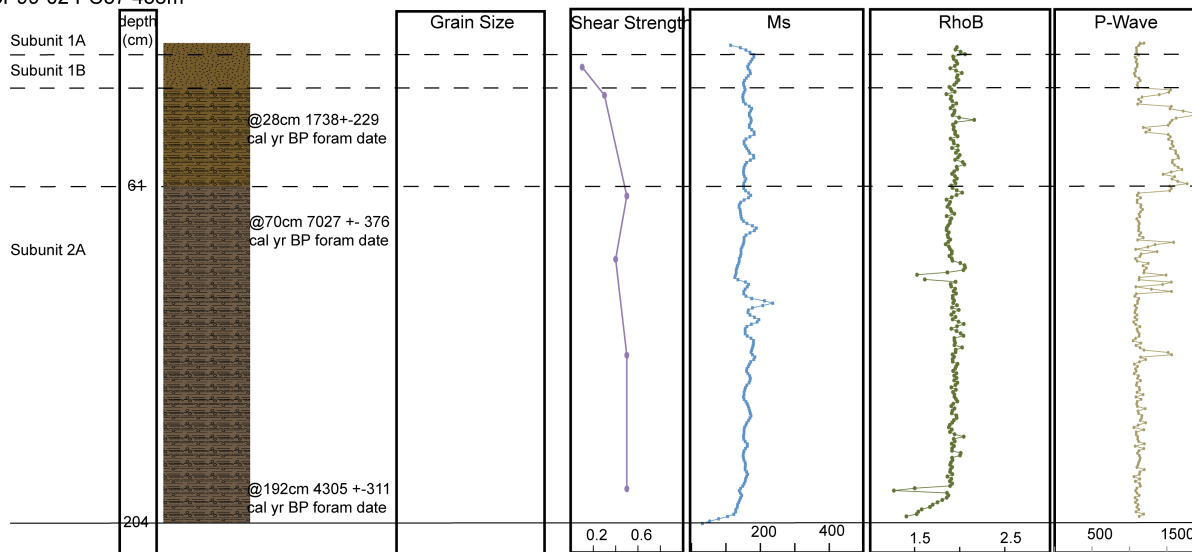
KC24 807m



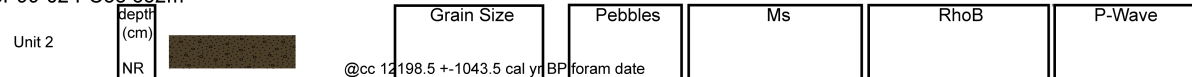




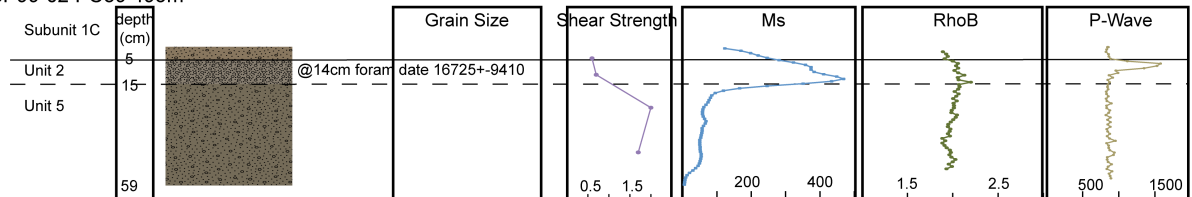
NBP99-02 PC37 438m



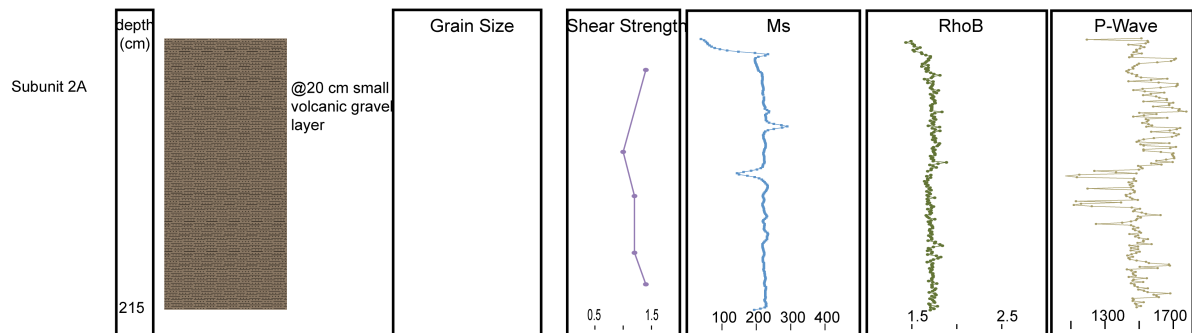
NBP99-02 PC38 652m



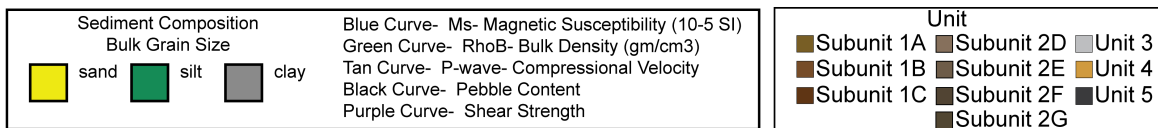
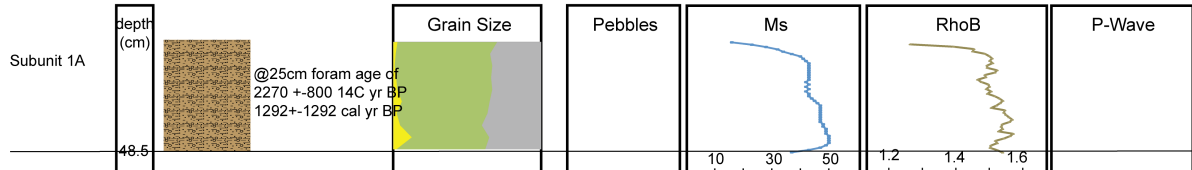
NBP99-02 PC39 495m



NBP99-02 PC41 957m



NBP99-02 TC49 852m



## Appendix B

Grains were deflocculated using sodium metaphosphate in deionized water for 24 hours. The sediment was then gently stirred into suspension and filtered through a coarse-weave paper filter by vacuum. The quartz grains were isolated using a Frantz magnetic separator.

Individual grains were digitally imaged using a Zeiss SteREO Microscope at a resolution of 3.6 microns per pixel, spanning the full range of silt particles. The two-dimensional boundaries of the grains were traced using Matlab's Image Processing toolbox™. Composite grains were excluded from the count. Each sample interval yielded between 50 grains and 400 grains for analysis. The digitally calibrated diameters of these grains were used to group them into very fine-to fine-sand and fine-to medium-sand classes for analysis. Dowdeswell (1985) cautions against comparing grains of different sizes after an analysis of medium sand and very fine sand produced statistically different roughness values. The division between size classes was adjusted downward from this study because there is very little medium sand in these samples. A minimum of 50 points along the grain boundary were used to calculate the first 24 harmonic coefficients for each grain. The calculation was done by the Fourier plugin for ImageJ™ developed by Boudier and Tupper (2011; see also Rasband, W.S., 1989; Abramoff et al., 2004).

Fourier shape analysis is a valuable tool in the interpretation of glacial marine sediments, particularly in distal sedimentary environments as transport mechanism is often convoluted. In combination with grain size data, it can be used to

differentiate grains likely transported by meltwater streams from grains melted out from basal debris-rich ice or grains of eolian origin (Dowdeswell, 1986). Introduced by Ehrlich and Weinburg (1970), the Fourier technique uses harmonics to characterize grain shape by calculating their fit to the grain perimeter. The harmonic amplitudes ( $C_n$ ) increase with the positive degree of fit.

Second harmonic is used as a proxy for the vertical elongation of the grains. Haines and Mazzullo (1988) identified a very good inverse correlation between the second harmonic amplitude and Rittenhouse sphericity values (1943). High harmonics contain more lobes equally distributed radially.